DEVELOPMENT OF ANTIMICROBIAL EDIBLE FILMS USING LOBSTER SHELL-WASTE DERIVED CRUDE CHITOSAN

by

Abhinav Jain

Submitted in partial fulfilment of the requirements
for the degree of Master of Applied Science

at

Dalhousie University
Halifax, Nova Scotia
August 2021

In the memory of my beloved mother,
Late Smt. Neelam Jain

TABLE OF CONTENTS

LIST OF TABLES

LIST OF FIGURES

ABSTRACT

This thesis explored Atlantic lobster (*Homarus americanus*) shell-waste as a chitosan (LCh) source for developing antimicrobial edible films for food packaging applications. The study focused on improving the physicochemical properties of the films by blending fish gelatin (Ge) and sunflower oil (O) with LCh and evaluating the effect of plasticizer, polymer concentration (1-2%LCh w/v) and drying temperatures (37/60/80 °C) on these films. FT-IR, XRD and TGA analysis revealed excellent intermolecular interactions between film components; however, high-temperature drying adversely affected these interactions. The formulations of LCh-Ge-O composite films were optimized using Response Surface Methodology, and the obtained models allowed films to be tailored to a wide range of functionalities for niche packing applications. Regarding their antimicrobial activity against *E. coli*, neat LCh films presented a high degree of inhibition (77-83%), but composite films showed significantly reduced activity. Overall, LCh-Ge-O films demonstrated excellent potential as an eco-friendly alternative to conventional plastic films.

Keywords: *lobster shells, chitosan, fish gelatin, edible packaging, antimicrobial films, response surface methodology.*

LIST OF ABBREVIATIONS AND SYMBOLS USED

β_i – Linear coefficients of a regression model

β_{ij} – Interaction coefficients of a regression model

β_o – Quadratic coefficients of a regression model

σ – Mechanical stress

ε – Mechanical strain

ε_n – Error associated with RSM prediction model for a response parameter

λ – Wavelength

θ – Light scattering angle

R^2 – Coefficient of determination

R^2_{adj} – Adjusted coefficient of determination

R^2_{pred} – Predicted coefficient of determination

Δw – Weight loss / Change in weight

Δt – Change in time

A_c – Area under the crystalline regions of XRD diffractograms

A_a – Area under the amorphous regions of XRD thermograms

A – Absorbance

AA – Acetic acid

ANOVA – Analysis of variance

APB – Acid-producing bacteria

Ar – Exposed area of the film

ATR – Attenuated total refection

BG – Bovine hide gelatin

C_p – Protein conversion coefficient

C_q – Chitin conversion coefficient

$CaCO_3$ – Calcium carbonate

CA – Contact angle

CCh – Commercially available crab-shell chitosan

CFU – Colony-forming unit

Ch – Chitosan

CrI – Crystallinity Index

d_n – Individual desirability function for a response parameter

D – Overall desirability function

DA – Degree of acetylation

db – Dry matter basis

DD – Degree of deacetylation

DM – Demineralized

DP - Deproteinized

DS – Degree of swelling

DSC – Differential scanning calorimetry

DTGA – Differential thermogravimetric analysis

EAB – Elongation at break

EM – Elastic modulus

EMC – Equillibrated moisture content

FAO – Food and Agriculture Organization of the United Nations

FBGU – Fungal beta-glucanase units

FFS – Film-forming solution

FT – Film thickness

FT-IR – Fourier transform infrared spectroscopy

Ge – Fish gelatin

Gly – Glycerol

GPC – Gel-permeation chromatography

GRAS – Generally recognized as safe

HCh – Analytical grade high molecular weight chitosan (Sigma-Aldrich)

HCl – Hydrochloric acid

HDPE – High-density polyethylene

HSD – Honest significant difference

IR – Infrared

K – Sum of non-nitrogen compounds

LCh – Lobster shell-waste derived crude chitosan

LDPE – Low-density polyethylene

LLCh – Low molecular weight lobster shell-derived chitosan

LPIs – Lobster processing industries

LS – Light scattering

m – Weight or mass

M_P – Peak molecular weight

M_W – Weight average molecular weight

M_N – Number average molecular weight

M_V – Viscosity average molecular weight

MW – Molecular weight

MWCO – Molecular weight cut-off

N_t – Total elemental nitrogen

NaOH – Sodium hydroxide

- NH_2 – Amino group

- OH – Hydroxyl group

O – Sunflower oil

OP_{UV} – Opacity in the ultraviolet (UV) spectrum

OP_{VIS} – Opacity in the visible spectrum

P_{Sat} – Saturation vapour pressure

PDI – Polydispersity index

PEC – Polyelectrolytic complex

PP – Polypropylene

RH – Relative humidity

RI – Refractive index

RSM – Response Surface Methodology

RT – Room temperature

T_d – Peak thermal degradation temperature

TG – Tuna skin gelatin

TGA – Thermogravimetric analysis

TS – Tensile strength

UNEP – United Nations Environmental Program

USFDA – United States Food and Drug Administration

v/v – Volume by volume

VS - Viscometric

w/v – Weight by volume

w/w – Weight by weight

W – Weight or mass

WCA – Water contact angle

WS – Water solubility

WVP – Water vapour permeability

WVTR – Water vapour transmission rate

X_i – Independent variables

XRD – X-ray diffraction

Y_n – Predicted response parameter

ACKNOWLEDGEMENTS

CHAPTER 1

INTRODUCTION

Shellfish processing and consumption generate thousands of tonnes of shell-waste and by-products globally each year. Most of this waste is either unsustainably discarded in landfills and seas, causing land and coastal pollution concerns or ends up in low-value applications as fertilizers, animal feed or energy recovery through incineration (Archer & Russel, 2008; Hülsey, 2018; Kaur & Dhillon, 2015). However, if optimally utilized, these by-products can be a valuable bioresource as they are generally rich in various high-value nutritional or bioactive compounds such as complex carbohydrates, proteins, lipids, minerals and carotenoids (Chen et al., 2016; Hülsey, 2018). Chitin, a unique biopolymer, is one of such compounds found abundantly in crustacean shells and has attracted significant scientific interest in the recent past due to its remarkable properties and distinct derivatives (Chen et al., 2016).

Atlantic-Canada is the largest producer and exporter of live and processed American/Atlantic lobsters (*Homarus americanus*) worldwide, accounting for more than 58% of the global production (FAO, 2020). In 2019, Canada landed 103,917 tonnes of American lobster, valuing more than 1.5 billion CAD, indicating the significance of lobster processing industries (LPIs) in the region (Fisheries and Oceans Canada, 2019b, 2019c). However, lobsters have a low portion of consumable meat, and up to 75% of the lobster mass can be discarded during its processing, generating large amounts of shell waste and other by-products (Ilangumaran, 2014; Nguyen, Barber, Corbin, et al., 2017). Hence, the sheer abundance of this lobster-originated shell waste opens up prospects for its utilization as an economical and sustainable chitin source.

Chitin and its derivatives are exceptional biomolecules with various novel and well-established applications in tissue engineering, drug-delivery, waste-water treatment, plant disease management, and industrial production of several valuable chemicals as platform compounds (Chen et al., 2016; Hülsey, 2018; Ilangumaran et al., 2017; Nguyen, Barber, Corbin, et al., 2017; Yang, 2011). Among these applications, the potential of acid-soluble deacetylated chitin-derivatives, i.e. chitosan and chitooligosaccharides, as critical components of active, biodegradable

or edible food packaging systems are noteworthy (Elsabee, 2015; Fernández-de Castro et al., 2016; Hamed et al., 2016).

In the past few decades, the unsustainable and uncontrolled disposal of single-use fossil-fuel-based non-biodegradable plastic packaging waste, primarily originating from food packaging, has resulted in extensive land and oceanic pollution, causing detrimental effects on the natural environment (Marsh & Bugusu, 2007; Rhodes, 2018). Moreover, the continued rapid depletion of the earth's fossil fuel reserves has raised serious concerns regarding the future of plastic-based packaging systems (Leceta, Guerrero, Cabezudo, et al., 2013). As a result, in recent years, the scientific community has made significant strides toward finding eco-friendly and sustainable food packaging alternatives that can either partially or fully replace fossil-fuel-based plastics.

Chitosan-based packaging films are of particular interest in this regard due to their biodegradable, biocompatible, edible and antimicrobial nature, along with their renewable biological origin (chitosan source) and thus can offer numerous environmental and functional benefits over conventional plastic films in specific food packaging and preservation applications (Dutta et al., 2009; Elsabee, 2015; Leceta, Guerrero, Cabezudo, et al., 2013). However, the challenges associated with pure chitosan films such as their inherent hydrophilic nature, high rigidity, poor thermal processibility, high dependence on environmental humidity, limited technology for their industrial processing and possible costs associated with the chitosan production have severely limited their applications in the food industry (Aider, 2010; Elsabee, 2015; Khouri, 2019).

In order to address these deficiencies and improve the physicochemical properties and overall functionality of chitosan films, continuous efforts have been made over the last two decades to optimize the process conditions (Singh et al., 2015; Srinivasa et al., 2007), incorporate plasticizers & functional additives (Cerqueira et al., 2012b; Elsabee, 2015) and blend chitosan with other biopolymers such as starch, alginate, or zein protein (Cazón & Vázquez, 2020; Santacruz et al., 2015; Zhang et al., 2019). Fish gelatin is one of such blending biopolymers with excellent compatibility with chitosan and the ability to enhance film flexibility and elasticity (Hosseini et al., 2013; Yao et al., 2017). It is also reasonably cheap and can be sustainably sourced from the processing of abundantly available fish waste (skin, bones and fins) (Avena-Bustillos et al., 2006;

Hosseini et al., 2013). On the other hand, hydrophobic compounds like oils mixed with chitosan in small proportions can significantly enhance the hydrophobicity and water vapour barrier properties of the resultant films (Elsabee, 2015; Ojagh et al., 2010).

However, despite the recent advancements in the field, there are still considerable gaps in the production, processing and applicability of chitosan-based edible films in the food packaging industry. In addition to the utilized solvents, additives and processing parameters, the physicochemical properties and behaviour of chitosan, and its interaction with other film components (solvent acid, plasticizers and copolymers), are highly influenced by its purity and structural characteristics (MW and %DD), which in turn are dependent on its source and extraction procedure (Ansorena et al., 2018; Elsabee, 2015; Khouri, 2019; Nadarajah, 2005; Nunthanid et al., 2001; Park et al., 2002). Unfortunately, most of the available literature on the production and properties of chitosan or composite films is based on analytical grade or high purity chitosan, with no reports made to this day on utilization of chitosan derived from the shell-waste of Atlantic lobsters for edible film applications. Moreover, several variations and inconsistencies have been reported throughout the literature regarding the effect of various factors on the physicochemical properties of chitosan films, leading to extreme difficulties in predicting and controlling their behaviour as a packaging material, thus limiting their commercial applicability.

The present study addresses some of these gaps by evaluating the applicability of low-cost crude chitosan procured from abundantly available Atlantic lobster-shell waste in the production of solvent cast edible films. The study investigates the effect of various factors such as polymer and plasticizer concentrations, drying temperatures, chitosan molecular weight and incorporation of fish-gelatin and sunflower oil on the physicochemical properties of the lobster-shell derived chitosan films. Moreover, the study develops optimized procedures and formulations for tailoring physicochemical properties of lobster-shell chitosan – fish gelatin – sunflower oil composite films based on their desired applications in various food preservation and containment functions.

1.1 SCOPE AND RESEARCH OBJECTIVES

The overall goal of this study was to utilize lobster shell-waste as an accessible and cheap source of chitosan for developing functional edible films with the potential to substitute single-use plastic packaging and modify these films according to different food packaging applications. To achieve this goal, the defined research objectives of this thesis were:

1. To characterize and compare lobster shell-waste derived crude chitosan (LCh) with commercially available chitosan by evaluating the physicochemical behaviour of their solvent cast films.

2. To evaluate the effect of incorporating fish gelatin (Ge) and sunflower oil (O) in LCh films when prepared at different film drying temperatures.

3. To optimize the formulations of lobster-shell chitosan – fish gelatin – sunflower oil (LCh-Ge-O) composite films using Response Surface Methodology for different film functionalities according to niche packaging applications.

4. To investigate the antimicrobial properties of optimized LCh-Ge-O composite films and to examine the effect of replacing LCh with enzymatically hydrolyzed low molecular weight LCh.

1.2 THESIS LAYOUT AND ORGANIZATION

Chapter 2 provides the background information and a review of the available literature regarding the various facets of this project and utilized materials, including the prospects of Atlantic lobster shell-waste as a potential chitosan source and the critical aspects of chitosan as a film-forming biopolymer.

The overall experimental work reported in this thesis is divided into three distinct chapters (Chapter 3, 4 and 5), with each chapter being a follow-up study on the observations of the previous chapters.

Chapter 3 is a preliminary study for evaluating the applicability of crude chitosan obtained from lobster-shell waste in the preparation of edible films. This chapter presents the extraction procedure, characteristics of extracted LCh and the procedure for preparing chitosan-based edible films. It also compares the physicochemical properties of LCh films with films obtained from commercially available crab-shell chitosan and high molecular weight analytical grade chitosan.

Chapter 4 is an investigative study on the preparation and characterization of LCh composite films incorporated with fish gelatin and sunflower oil. The study also presents the effect of different film drying temperatures on the physicochemical, structural and thermal properties of neat and composite LCh films.

Chapter 5 is an optimization study for LCh-Ge-O composite film formulations and provides regression equations for predicting various physical, mechanical, optical and barrier properties for these films depending on their composition. The study also presents some optimized formulations of composite films depending on their intended functionality in different food packaging applications. Finally, the effect of replacing LCh with enzymatically hydrolyzed low molecular weight LCh on the physicochemical and antimicrobial properties of optimized films has also been reported in this chapter.

In the end, **Chapter 6** summarizes the major findings from all three experimental chapters and provides concluding remarks on the contributions of this study to the field and suggestions for future work.

CHAPTER 2

LITERATURE REVIEW

2.1 CANADIAN LOBSTER INDUSTRY AND LOBSTER SHELL-WASTE

Atlantic or American lobsters (*Homarus americanus*) are arguably the most economically significant seafood commodity in Canada, owing to their premium pricing and high demand across the globe (Fisheries and Oceans Canada, 2019a; Lobster Council of Canada, 2010). As the largest producer and exporter of live and processed Atlantic lobsters worldwide, Canada occupies more than 58% of the global share, indicating the importance of lobster production and processing industries in the country (FAO, 2020; Lobster Council of Canada, 2010). In 2019, Canada landed over 103 thousand tonnes of Atlantic lobsters, 93% of which were exported with a trade value of about 2.6 billion CAD, a significant chunk of the country's total marine product export revenue (Fisheries and Oceans Canada, 2018, 2019a, 2019c). Although the Covid-19 pandemic has significantly impacted the production, processing and export of lobsters in 2020, the industry is expected to return to normalcy and grow in the following years (FAO, 2021).

The majority of Canadian lobster production comes from three Atlantic provinces, i.e., Nova Scotia, New Brunswick, and Prince Edward Island (Lobster Council of Canada, 2010; Thériault et al., 2013). The aggregate commercial value of lobsters landed in 2019 by these three provinces was 1411.8 million CAD against the country's total of 1596.6 million CAD (Fisheries and Oceans Canada, 2019c). Moreover, approximately 55% of it was contributed by Nova Scotia alone (Figure 2.1).
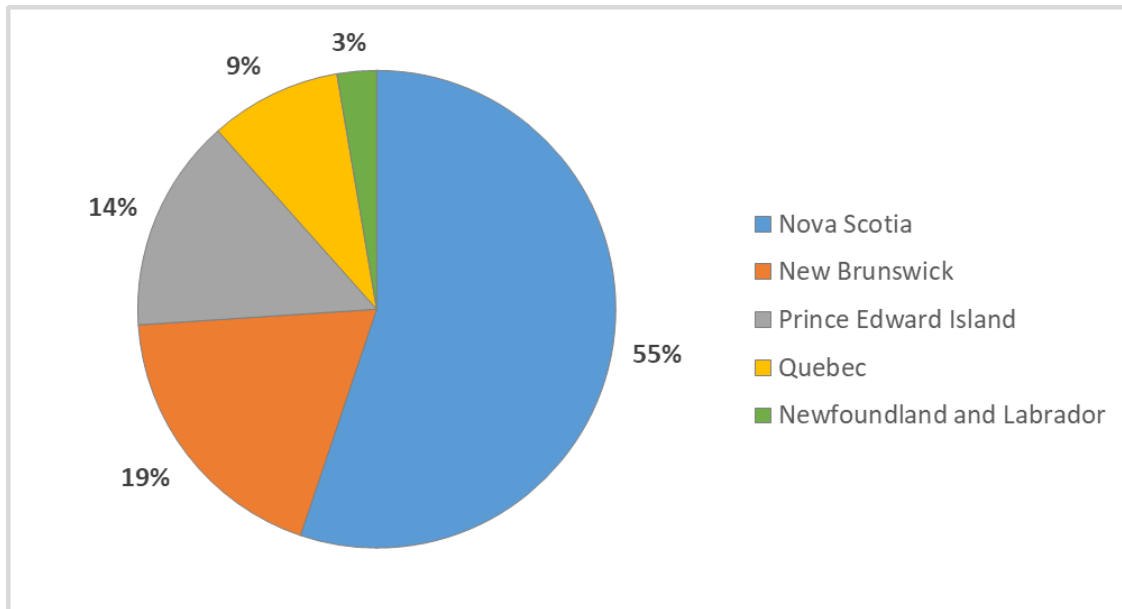
Figure 2.1: Canadian lobster landing values in 2019 (produced using data from Fisheries and Oceans Canada, (2019b)).

Canadian lobster market and sales are broadly categorized into two groups: live and processed (frozen and canned) (Thériault et al., 2013). Although live lobsters are preferred by the consumers and fetch a higher price, the constraints of domestic/international trade & logistics of live produce and demand for increased shelf-life and convenience have given rise to a massive food processing sector for lobster processing in Atlantic Canada (Nguyen, Barber, Corbin, et al., 2017; Thériault et al., 2013). According to a government report in 2013, over 55% of total lobster landing in Canada was processed into various frozen or canned products, and lobster processing industries (LPIs) are estimated to grow significantly in the next few decades (Thériault et al., 2013). Unfortunately, due to the low portions of consumable meat in lobsters (20-30% by weight), LPIs generate enormous quantities of shell waste and by-products (> 40,000 tonnes/year), which is primarily discarded in dumpsites, landfills and oceans, contributing to land and coastal pollution due to their high resistance to biodegradation (Healy et al., 1994; Nguyen, Barber, Corbin, et al., 2017). In addition, LPIs incur huge costs associated with the transportation and disposal of this waste, compelling them to shift towards more sustainable and cost-effecting alternatives (Kerton et al., 2013; Nguyen, Barber, Corbin, et al., 2017).

Apart from their inorganic matrix, crustacean shells are composed of high-value biomolecules, i.e., proteins (20-40% db), chitin (15-40% db), unsaturated lipids (5-10% db) and significantly high amounts of astaxanthin, making a convincing argument towards their utilization as a potential renewable bioresource (Chen et al., 2016; Kerton et al., 2013). In recent years, crustacean shells have found some commercial applications as low-value animal feed supplements and organic fertilizers or their utilization as a feed source for chitin extraction that can be further converted to high-value chitosan (Archer & Russel, 2008; Hülsey, 2018; Kaur & Dhillon, 2015; Xu, 2017). However, at present, only a tiny fraction of lobster shell-waste generated in Atlantic Canada is utilized for these applications (Schaer, 2021; Xu, 2017).

2.2 BACKGROUND ON CHITOSAN

Chitosan is an artificially modified biodegradable and edible polysaccharide derived from chitin, a structural biopolymer readily found in the exoskeletons of arthropods such as crustaceans, arachnids and insects, and the cell walls of fungi and some algal species (Lizardi-Mendoza et al., 2016). Chitin is the second most prevalent biopolymer in nature after cellulose and is also structurally very similar to cellulose, and thus is often termed as a nitrogenated cellulose derivative (Ioelovich, 2017). It is a homopolymer of N-acetyl-D-glucosamine (GlcNAc) monomers connected linearly through β (1–4) glycosidic linkages. However, in nature, it is found as a random copolymer of GlcNAc and D-glucosamine (GlcN) subunits, with the prior being predominate in the polymer chain (Figure 2.2) (Arnold et al., 2020; Kumari & Kishor, 2020).

Chitin is usually highly resistant to physical and chemical degradation and is insoluble in aqueous and most organic solvents due to its excessive intra and intermolecular hydrogen bonding and hydrophobic acetyl groups, which significantly restricts its commercial applications to a few specialized fields (Annu et al., 2017; Lizardi-Mendoza et al., 2016). However, with a decrease in its degree of N-acetylation (DA%), its hydrophobic nature significantly decreases due to the increased availability of hydrophilic free amine groups (NH_2) in its structure, providing it with a net positive charge in water (Kumari & Kishor, 2020). Therefore, partially deacetylated chitin with DA less than 30-40% becomes readily soluble in dilute acidic aqueous mediums and is referred to as chitosan (Figure 2.2) (Khouri, 2019). Chitosan is a unique, non-toxic biopolymer offering

8

excellent biodegradability, biocompatibility, high adsorption capacity and activity against microorganisms, and with its increased solubility, it can also be easily processed into edible films and coatings (Chen et al., 2016; Hahn et al., 2020; Zhang et al., 2013).
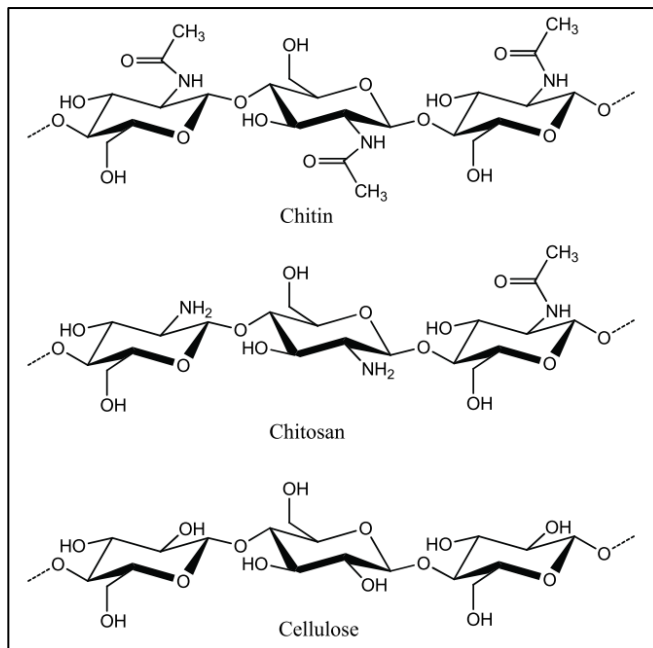
Figure 2.2: Structure of chitin, chitosan and cellulose (adapted from Alvarenga (2011)).

2.3 SOURCES, PRODUCTION AND APPLICATIONS OF CHITOSAN

Chitin exists in three different polymorphic forms in nature, i.e., α, β and γ-forms, depending on the orientation of polymer chains (Figure 2.3) (Ioelovich, 2017; Kumari & Kishor, 2020). α-chitin, being the most abundant one, is usually isolated from crustaceans, insects and fungi and comprises anti-parallel chains that significantly increase its thermodynamic stability caused by strong intermolecular hydrogen bonding (Chen et al., 2016). On the other hand, the β-polymorph consists of parallel chain arrangements and can be found in squid pens and tube worms. Finally, in γ-chitin, every third chain is arranged in the opposite direction and can be isolated from cuttlefish and insect cocoons (Ioelovich, 2017). Both β and γ-forms, however, are structurally quite unstable, have high sensitivity to swelling and are relatively rare to find (Annu et al., 2017).

9
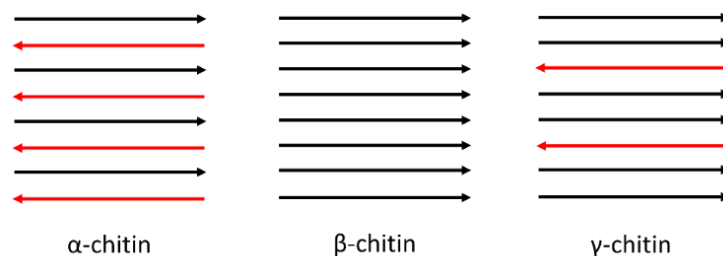
Figure 2.3: Orientation of polymer chains in different allomorphs of chitin.

Even with such widespread availability in nature, chitin and therefore chitosan is only obtained commercially from the exoskeletal shells of crustaceans, i.e., shrimps, crabs, crayfish, and krill, due to their high chitin content (15-40%) and availability as a low-cost food processing by-product (Chen et al., 2016; Nadarajah, 2005).

2.3.1 Chitosan Production

Characteristics of chitosan such as its purity, molecular weight, degree of deacetylation, and polydispersity index are critically influenced by its source and extraction conditions (Yadav et al., 2019). Chitosan can be isolated from crustacean shells using either harsh acid-alkali chemical extraction procedures or biological procedures (enzymatic or fermentative methods) and usually involves four basic steps: demineralization, deproteinization, deacetylation, and depigmentation (Annu et al., 2017). Demineralization of shells is achieved by dissolving inorganic salts in low pH conditions by either adding strong mineral acids like HCl or by acid-producing bacterial (APB) fermentation (Arbia et al., 2013; Kerton et al., 2013). During deproteinization, shell proteins are disintegrated and dissolved in hot alkaline conditions or are enzymatically hydrolyzed using proteolytic bacterial fermentation or directly treating with proteolytic enzymes (Annu et al., 2017; Arbia et al., 2013). Next, the resultant substrate is deacetylated to produce chitosan by again treating it with concentrated alkali solutions at high temperatures or using the chitin deacetylase enzyme (Kumari & Kishor, 2020). Finally, the extracted chitosan is purified by removing residual pigments like carotenoids using oxidizing agents or solvent extraction (Kerton et al., 2013).

While chemical extraction procedures have high extraction efficiencies and short processing times, they adversely affect the physicochemical properties of chitosan and are considered unsustainable and uneconomical due to their high energy and freshwater requirements and the use of corrosive chemicals (Kumari & Kishor, 2020; Xu, 2017). On the other hand, biological procedures are eco-friendly, energy-efficient and produce a reproducible product with desired properties (Yadav et al., 2019). However, they are slow, have low product yield and are limited to laboratory-scale studies (Arbia et al., 2013; Kumari & Kishor, 2020). Therefore, the majority of commercial chitosan production relies on chemical extraction procedures, which consequently increases the cost of chitosan procurement despite the cheap and abundant availability of its source material (crustacean shell-waste).

2.3.2 Functional Properties of Chitosan

The distinct chemical and structural characteristics of chitosan provide it with unique functional properties that can be utilized in various industrial and medical applications, making chitosan a highly attractive and valuable biopolymer (Yadav et al., 2019). While the acetylated units of chitosan can form hydrogen bonds and hydrophobic interactions contributing to its molecular stability and structural rigidity (Lizardi-Mendoza et al., 2016), most of its exceptional properties are associated with the free amino groups of its deacetylated units that give chitosan its polycationic nature and solubility in dilute acidic mediums (Annu et al., 2017; Kumari & Kishor, 2020). Additionally, the reactive hydroxyl and amino groups of chitosan permit diverse interactions with organic and inorganic compounds, which can modify and enhance chitosan's physical and solution properties (Lizardi-Mendoza et al., 2016).

2.3.3 Commercially Relevant Applications of Chitosan

One of the leading commercial applications of chitosan is for the adsorption and removal of pollutants from industrial and municipal wastewater due to its positive charge and reactive functional groups ($-NH_2$ and $-OH$) that result in excellent metal chelating ability and high affinity towards negatively charged organic compounds such as lipids, proteins, phenolic compounds and industrial dyes (Hahn & Zibek, 2018; Kumari & Kishor, 2020; Liu et al., 2013; Nechita, 2017; Varma et al., 2004; Wydro et al., 2007). As well, an evergrowing list of biological and bioactive

properties of chitosan and its derivatives, including biocompatibility, hemocompatibility, anti-tumour activity, anti-inflammatory activity, has made the use of chitosan increasingly applicable in various biomedical fields (Arya et al., 2017; Kumari & Kishor, 2020; Zhao et al., 2018). The biodegradable and non-toxic nature of chitosan, along with its biocidal activity, has also made it suitable for several agricultural applications as eco-friendly anti-bacterial and anti-fungal agents for plant disease management or as encapsulating agents in the controlled delivery and release of drugs (pesticides, herbicides and insecticides) and micronutrients to the crops (Majeed et al., 2017; Malerba & Cerana, 2018; Orzali et al., 2017). Moreover, the activity of chitosan and its oligomers as a bio-stimulant has also been widely applied for enhanced seed germination and eliciting disease resistance in plants (Ilangumaran, 2014; Majeed et al., 2017; Malerba & Cerana, 2018).

In addition to the above-mentioned unique properties of chitosan, its recognition as a generally safe (GRAS) food additive, dietary supplement, and functional ingredient by the USFDA has made it commercially relevant in a wide range of food processing and preservation applications as well (Morin-Crini et al., 2019). For instance, several reports have been published on successful applications of chitosan as a natural antioxidant and antimicrobial agent to enhance the quality and shelf-life of fresh produce, processed products and beverages in the form of solutions, powders, and coatings (Friedman & Juneja, 2010; No et al., 2007). As well, chitosan has also found applications as an effective coagulant and flocculant for clarification of fruit juices, beers and wines and as a health supplement and nutraceutical for its nutritional value and functional benefits as a prebiotic and hypocholesterolemic agent (Gutiérrez, 2017; Morin-Crini et al., 2019; Xu, 2017).

In recent years, chitosan has also attracted much scientific interest as a film-forming biopolymer for the development of biodegradable and edible films and coatings for food packaging and preservation applications due to their several functional and environmental benefits over conventional plastic packaging (Khouri, 2019; Leceta, Guerrero, Cabezudo, et al., 2013; Nadarajah, 2005). This will be discussed in more detail in the following sections of this literature review.

2.4 EDIBLE PACKAGING

Single-use non-biodegradable food packaging is one of the most significant contributors to plastic waste and associated land and oceanic pollution. According to the United Nations Environmental Program (UNEP), in 2015, more than 140 million tons of single-use plastic packaging waste was globally generated, most of which comprises food packaging waste (Marsh & Bugusu, 2007; UNEP, 2018). Unfortunately, only about 20% of this plastic waste is either recycled or incinerated, while the rest ends up in landfills, or the oceans, causing detrimental effects on the natural environment and accumulation of microplastics in the food chain (Rhodes, 2018; UNEP, 2018). Moreover, the production of conventional plastics is highly reliant on non-renewable petroleum-based raw materials, and with the unavoidable depletion of fossil fuels, there has been a growing urgency and push towards developing novel packaging systems with low environmental impact (Leceta, Guerrero, Ibarburu, et al., 2013; Rajpal, 2007; Rhodes, 2018).

Biodegradable packaging materials primarily based on renewable and compostable constituents originating from marine, agricultural or bacterial sources can provide a partial solution to the environmental and sustainability issues of plastic packaging (Aguirre-Joya et al., 2018; Angelo et al., 2017; Rajpal, 2007). Edible packaging is a subset of biodegradable packaging and can be defined as a thin membrane or a coat composed of polysaccharides, proteins, lipids or composites that acts as a protective covering for food products and is in itself safely consumable along with the product (Khouri, 2019). Edible packaging can be described as either a coating, where a film-forming solution is directly applied and dried on the surface of the product (via immersion, brushing or spray) or as a separately cast or extruded film that can be wrapped around or contain the product (Falguera et al., 2011; Wang et al., 2017). In addition to the low environmental impact associated with their biodegradable nature, edible films and coatings can offer an array of functional advantages over conventional packaging in terms of food preservation and shelf-life extension, quality and texture enhancement, esthetics, and delivery of nutritional and functional additives (Han, 2014; Pavlath & Orts, 2009).

Several biomaterials related to proteins, polysaccharides (carbohydrates and gums) and lipids, such as casein, soy protein, gelatin, methylated derivatives of cellulose, starch, chitosan, alginate, carrageenan, and certain waxes have been identified in the last two decades as potential

film-forming materials with desired physical and chemical properties (Aguirre-Joya et al., 2018; Han, 2014). In general, polysaccharide and protein-based films and coatings offer good structural integrity and mechanical properties along with excellent resistance against O_2, CO_2 and ethylene gas permeation but are very sensitive to moisture and have poor vapour barrier properties (Aguirre-Joya et al., 2018; Falguera et al., 2011; Pavlath & Orts, 2009). On the other hand, lipids and waxes offer superior resistance against moisture but lack the desired structural stability and are difficult to shape as homogeneous films (Debeaufort & Voilley, 2009; Falguera et al., 2011). Consequently, synergistic combinations of these constituents have often been utilized in recent studies to take advantage of the properties of each component (Ansorena et al., 2018; Souza et al., 2020; Wang et al., 2017).

Over the years, edible coatings have found widespread niche commercial applications in the preservation and shelf life extension of various food products such as fresh horticultural produce, meat & poultry, fish products, confectionery & bakery products, and cheese (Angelo et al., 2017; Han, 2014; Olivas & Barbosa-Cánovas, 2009; Ustunol, 2009). However, coatings do not serve the primary containment function of packaging and do not provide mechanical protection to the product and thus have to be used in conjunction with sturdy outer packaging. On the other hand, edible films can provide the required protection to the contained products against external stresses while also offering other functional benefits such as the delivery and slow release of antioxidants or antimicrobial agents in order to prolong the shelf-life of the contained products (Blanco-Pascual & Gómez-Estaca, 2017). Despite this, in contrast to edible coatings, edible films have not yet seen much commercial success due to their product-specific applicability, higher production costs and direct competition with significantly cheaper conventional thermoplastic films such as low- or high-density polyethylene (LDPE/HDPE) or polypropylene (PP) films (Azeredo et al., 2009; Falguera et al., 2011; Leceta, Guerrero, Cabezudo, et al., 2013). Efforts have more recently been directed towards developing, enhancing and modifying edible films and their physicochemical characteristics to overcome these deficiencies and eventually substitute thermoplastics, which seems achievable in the near future (Angelo et al., 2017; Pavlath & Orts, 2009). Table 2.1 lists some of the commercial edible coatings and films presently available as food packaging alternatives in the marketplace.

Table 2.1: List of some commercially available edible coatings and films (Angelo et al., 2017; Erkmen & Barazi, 2018; Pavlath & Orts, 2009; Prasad et al., 2018).

Company	Product	Film-forming components	Applications
Edible coatings			
AgriCoat NatureSeal Ltd.	Semperfresh™	Sucrose esters, vegetable oils and plant cellulose	Pre- and postharvest protection of fresh fruits, delayed ripening and reduced moisture loss
BASF	FreshSeal®	Not disclosed	Postharvest protection of melons, mangoes and tomatoes
Improveat	BioFruitCoat	Not disclosed	Reduced enzymatic and oxidative degradation of fresh fruits and vegetables
	BioNutriCoat	Blend of vitamins, antioxidants and pre- & probiotics	Increased nutritional value of fresh produce, cheese, meat and bakery products
	BioCheeseCoat	Not disclosed	Reduced microbial spoilage and moisture loss from cheese
	BioMeatCoat	Not disclosed	Reduced microbial spoilage and extended shelf-life of meat products
Caragum International®	Fibrecoat Spray	Vegetable fibres	Reduced oil absorption in fried breaded products
	Fibrecoat Tempura	Seaweed extracts and vegetable fibres	Reduced oil absorption in fried meat products
Mantrose-Haeuser Co., Inc.	Crystalac®	Shellac and vegetable-based proteins	Glaze for confectionary products with increased fat resistance and reduce moisture loss
	Certicoat®	Blend of custom formulated oil and natural wax products	Glaze for hard and soft sugar-shell panned candies with reduced moisture loss
	NatureSeal®	Blend of vitamins and calcium ascorbate	Prevention of oxidative browning in selected fresh-cut fruits and guacamole

Table 2.1: Continued.

Company	Product	Film-forming components	Applications
Fruitsymbiose Inc.	Pürbloom	Algal extracts and calcium ascorbate	Shelf-life extension of fresh-cut fruits and vegetables
De Leye Agro B.V.	Bio-Fresh™	Sucrose esters and Carboxymethylcellulose (CMC)	Postharvest protection of pears and apples, delayed ripening and reduced moisture loss
Nova Chem Ltd.	Nutri-Save™	Carboxymethyl chitosan	Reduced respiration and moisture loss in pleas and avocados
Opta Food Ingredients Inc.	Opta Glaze	Wheat gluten	Reduced microbial spoilage in raw eggs
Mori™	-	Silk Protein	Reduced microbial spoilage, moisture loss and oxidation in several food products
Edible Films			
COGIN®	-	Carrageenan-based films	Packaging of processed meat and poultry products
Kris-Kraft Polymer Inc.	-	Hydroxymethylpropylcellulose (HPMC) based films	Mechanical protection of several foods
BioEnvelop® Agro Inc.	-	Cellulose derivative and starch-based films	Mechanical protection of several foods
MonoSoL LLC	Vivos™ Edible delivery systems	Not disclosed	Water-soluble edible films
Notpla Limited	Ooho	Sodium alginate-based films	Packaging of high moisture and liquid foods
Innovation Utility Vehicle	Columbus' Egg	Not disclosed	Packaging of high moisture and liquid foods

2.5 CHITOSAN-BASED EDIBLE FILMS FOR FOOD PACKAGING APPLICATIONS

Among various reported film-forming biopolymers, chitosan has arguably attracted the most scientific and commercial interest in the recent past due to its abundant availability, inherent antimicrobial nature, and excellent film properties (Ansorena et al., 2018; Gutiérrez, 2017). Moreover, its compatibility and ability to interact with various other biopolymers, biomolecules and inorganic compounds on a molecular level due to its unique cationic nature have also made chitosan a material of interest in the development of composite films with enhanced physicochemical properties (Wang et al., 2017).

Edible films can be prepared by either wet (evaporative solvent casting) or dry (extrusion and thermo-pressing) processing methods (Epure et al., 2011; Nadarajah, 2005). Solvent casting is the most utilized technique for the small-scale production of biopolymer-based films but can also be applied at an industrial scale using continuous casting equipment (Blanco-Pascual & Gómez-Estaca, 2017; Rossman, 2009). Alternatively, thermo-pressing and extrusion are much more feasible in a commercial setting due to their several advantages over solvent casting in terms of processing times, energy efficiency and floor-space requirements (Blanco-Pascual & Gómez-Estaca, 2017; Pelissari et al., 2011; Wang et al., 2017). Extruded edible films based on several proteins and polysaccharides such as casein, gelatin, wheat gluten, starch, pectin and water-soluble cellulose derivatives have been reported in the literature (Dangaran et al., 2009; Hanani et al., 2014; Kocira et al., 2021; Li et al., 2011; Repka et al., 2005). However, because of the excessive hydrogen bonding in its structure, chitosan thermally degrades before melting and cannot be extruded in its native form (Annu et al., 2017; Lizardi-Mendoza et al., 2016). Therefore, chitosan films are primarily prepared by wet processing owing to the high solubility of chitosan in dilute aqueous acid solutions (Cazón & Vázquez, 2020).

Several different procedures and processing parameters have been reported in the literature for preparing chitosan films and coatings (Aider, 2010; Cazón & Vázquez, 2020; Dutta et al., 2009). However, most of them usually involves solubilizing chitosan in an acidic aqueous medium at low concentrations (0.5 - 4% w/v – due to the processing challenges caused by the high viscosity of the solutions) followed by either its direct application on food surfaces by spray-coating, spread-coating or immersion coating, or by casting it in flat containers like Petri dishes or metal trays. The

drying of these aqueous chitosan solutions leaves behind a robust and colourless homogeneous coat on the food surface or a solvent cast film in the container that can be peeled off and further applied in food packaging applications. In recent years, researchers have also been able to produce thermoplastic chitosan by using thermomechanical processing, making extruded chitosan films a possibility (Epure et al., 2011; Grande et al., 2018; Matet et al., 2013). However, the production of thermoplastic chitosan requires large proportions of plasticizers, and the resultant extruded or hot-pressed neat chitosan films usually have inferior physicochemical properties compared to their solvent cast counterparts (Chen, 2015; Epure et al., 2011; Grande et al., 2018; Matet et al., 2013; Wang et al., 2017). Therefore, extruded chitosan-based edible films are almost always produced as a blend in small proportions with other thermoplastic polymers (Mendes et al., 2016; Pelissari et al., 2011, 2012).

2.5.1 Properties of Chitosan Films

The applicability of an edible film as a food packaging material is often assessed by its mechanical (strength, flexibility and elasticity), barrier (permeation of liquids and gases), optical (transparency and colour) and functional properties (Blanco-Pascual & Gómez-Estaca, 2017; Gutiérrez, 2017). In general, solvent cast chitosan films offer high strength and rigidity, excellent resistance to gas and lipid permeability (except for water vapour permeation due to hydrophilic nature), a colourless transparent appearance, and an innate antimicrobial and bivalent mineral chelating ability, making them highly attractive for food packaging and preservation applications (Aider, 2010; Cazón & Vázquez, 2020; Guilbert et al., 1995; Khouri, 2019; Zhang et al., 2013). However, these properties are highly dependent and significantly influenced by several film-forming parameters such as the characteristics of chitosan (purity, MW and %DD), type and concentration of acid solvents and plasticizing agents, functional additives and blending polymers, and the processing and post-processing factors (drying temperature, storage conditions, film neutralization, heat curing, cross-linking etc.) (Ansorena et al., 2018; Cazón & Vázquez, 2020; Elsabee, 2015; Khouri, 2019; Nadarajah, 2005). Moreover, widespread discrepancies can be found throughout the literature regarding the effect of these factors on the specific properties of chitosan films, which is a significant limiting factor for their commercialization.

The antimicrobial nature of chitosan is the flag-bearing property that distinguishes it from other film-forming biopolymers and has been studied and applied in various fields and forms. Past studies have shown the activity of chitosan films against a wide range of microorganisms with the highest sensitivity against yeasts and moulds, followed by gram-positive and gram-negative bacteria (Aider, 2010). Although the complete mechanism behind the inhibitory activity of chitosan is still a topic of debate, it is likely to be associated with the free amino groups of chitosan that interact with the anionic sites on the bacterial or fungal cell walls, disrupting them and leading to the leakage of their cytoplasmic contents (Aider, 2010; Elsabee, 2015; Rajpal, 2007). However, the antimicrobial potency of chitosan films significantly varies with the intrinsic properties of chitosan, the host organism and the conditions of the growth medium (pH and ionic strength) (Dutta et al., 2009; Wang et al., 2017). Attempts have also been made to enhance the antimicrobial efficiency of chitosan films by incorporating other active ingredients like nisin or several essential oils into the film matrix (Aider, 2010; Elsabee, 2015).

The molecular weight (MW) and the deacetylation degree (%DD) of chitosan play a significant role in the molecular arrangement and crystalline structure of the films, which in turn affects most of their physicochemical properties. For instance, Nunthanid et al. (2001) characterized solvent cast films prepared from chitosan of different MW and %DD and observed an increase in the tensile strength (TS) and crystallinity (CrI) and a decrease in % elongation at break (EAB) of the films with an increase in the MW and %DD of chitosan. They attributed these results to the formation of chain entanglement networks in high MW chitosan and a denser packing with increased intermolecular interactions in a highly deacetylated chitosan (small amino groups replacing bulky acetyl groups). They also reported a decrease in the moisture uptake of the films with increasing %DD and decreasing MW of chitosan. Alves et al. (2019) and Park et al. (2002) made similar observations on the effect of MW and %DD of chitosan on the mechanical properties of the films. In addition, Alves et al. (2019) also reported an increased water solubility of the films with an increase in %DD and a decrease in MW. Past studies have also reported the influence of MW and %DD of chitosan on the antimicrobial activity of the films against different bacterial and fungal strains; however, there are inconsistencies in the observed effects (Aider, 2010; Elsabee, 2015).

The type and concentration of acid utilized for solubilizing chitosan and the final pH of the aqueous solvent have also been reported to significantly impact the mechanical, barrier and optical properties of the chitosan films (Cazón & Vázquez, 2020; Park et al., 2002). These effects are generally associated with the structure and size of the acids and their interactions with protonated amino groups as a counter ion, which may influence the inter and intramolecular interactions between the chitosan chains (Bégin et al., 1999; Khouri, 2019; Kim et al., 2006; Nadarajah, 2005). In a study by Kim et al. (2006), chitosan films prepared in different organic acid solutions (formic, acetic, lactic and propionic acid) and at different final solvent pH showed significantly different physicochemical properties. They reported that with an increase in the solvent pH, water vapour permeability (WVP) and water solubility (WS) of the films increased while their tensile strength (TS) decreased. Moreover, they concluded that the films prepared in acetic acid (chitosan-acetate films) showed the best structural integrity with the highest TS and a lower WVP and WS among the tested acid solvents. Similar observations were made by Park et al. (2002) while testing chitosan films prepared in acetic, malic, citric or lactic acid solvents. Due to the high variation observed in the properties of the chitosan films with changing the acid type, they recommended utilizing different acids as solvents to tailor the properties of chitosan films according to the needed functionality. However, most of the available literature for chitosan films is based on acetic acid as a solvent because of its excellent compatibility with chitosan, cheap availability, and relative safety as a food additive (Gutiérrez, 2017; Khouri, 2019).

While neat chitosan-acetate films generally offer very high TS (40 - 150 MPa; higher than most commercial polymer-based films such as low and high-density polyethylene (LDPE/HDPE) and polypropylene (PP) films), they tend to be rigid and brittle with comparatively low stretchability (4 - 50%) (Cazón & Vázquez, 2020; Khouri, 2019; Leceta, Guerrero, Ibarburu, et al., 2013; Nadarajah, 2005; Nunthanid et al., 2001; Park et al., 2002; Ziani et al., 2008). Therefore, plasticizers such as polyols (glycerol, sorbitol and polyethylene glycol) or sugars (glucose and sucrose) are often blended with chitosan to reduce the frictional forces between the polymer chains, resulting in enhanced flexibility and stretchability of the films while compromising on their TS (Ansorena et al., 2018; Cazón & Vázquez, 2020; Santacruz et al., 2015; Vieira et al., 2011). However, the addition of plasticizers (type and proportions) also significantly affects almost all other film properties, including their swelling ability, water solubility and overall hydrophilicity,

but the reported effects are often inconsistent (Alves et al., 2019; Cerqueira et al., 2012b; Leceta, Guerrero, & de la Caba, 2013; Rodríguez-Núñez et al., 2014; Ziani et al., 2008). The most adverse effect is observed on the mass transfer/barrier properties of the films (water vapour/O_2/CO_2) as the incorporation of plasticizers reduces the intermolecular forces and enhances the mobility of polymer chains, resulting in a lesser density of polymer packing and a higher free volume, which in turn increases the overall permeability of the films (Ansorena et al., 2018; Cazón & Vázquez, 2020; Cerqueira et al., 2012b; Leceta, Guerrero, & de la Caba, 2013).

The drying and storage conditions while preparing chitosan films also play a critical role in defining film characteristics. Although temperature, time, and drying methods have been reported to influence the structural arrangement of polymer chains, affecting the film matrix and overall film crystallinity (Fernández-Pan et al., 2010; Homez-Jara et al., 2018; Mayachiew & Devahastin, 2008), the environmental humidity during processing, storage and characterization of chitosan films is considered a far more critical factor. The reason being the hydrophilic nature of chitosan films, because of which they readily absorb moisture from the surroundings as a function of the environmental RH. This absorbed moisture acts as an uncontrolled plasticizer in the films and significantly influences their mechanical and barrier properties, just like a polyol plasticizer (Nadarajah, 2005; Ziani et al., 2008). Therefore, most studies condition chitosan films at a specified RH until an equilibrium is attained prior to their testing and characterization to minimize the variability in the results.

In conjunction with their mechanical properties comparable to other biopolymers, and excellent resistance against lipids, O_2 and CO_2 transfer, the antimicrobial nature of chitosan films make them an ideal choice for food preservation and shelf-life extension applications. However, the high sensitivity of chitosan towards environmental humidity (hygroscopicity) and its high water vapour permeability restrict their direct applications (Ansorena et al., 2018). Therefore, to overcome these issues and enhance the overall functionality of chitosan films, several modification strategies have been proposed over the years, such as film surface neutralization, heat curing, cross-linking, grafting, incorporation of functional or active ingredients and more (Ansorena et al., 2018; Elsabee, 2015; Khouri, 2019). Among these strategies, blending chitosan with other compatible biopolymers and biomaterials to modify specific characteristics of the edible films has been extensively reported in the literature and is briefly discussed in the following section.

2.5.2 Chitosan Blend and Co-polymer Films

Single component edible films usually always have certain disadvantages limiting their functionality (Rajpal, 2007). For instance, they can have good mechanical properties but still offer poor resistance to water vapour permeability due to their hydrophilic nature (most polysaccharide and protein-based films) (Aguirre-Joya et al., 2018; Nieto, 2009; Zhang et al., 2013) or can act as an excellent barrier to moisture but offer inadequate homogeneity and overall film integrity (hydrophobic lipids or wax-based films) (Aguirre-Joya et al., 2018; Debeaufort & Voilley, 2009; Falguera et al., 2011). Therefore, blending biopolymers and additives of different physiological nature is one of the most effective ways to produce edible films with desirable properties while overcoming the limitations offered by single-component-based films (Ansorena et al., 2018; Cazón & Vázquez, 2020). Composite edible films obtained from mixing chitosan with other polysaccharides, or proteins and lipids, have shown promising improvements and better performance in terms of their mechanical, transport and other physicochemical properties compared to stand-alone chitosan films (Ansorena et al., 2018; Cazón & Vázquez, 2020; Elsabee, 2015).

2.5.2.1 *Chitosan-polysaccharide films*

Chitosan generally shows excellent compatibility with anionic polysaccharides containing negatively charged side-chain groups in their structure, such as alginate, carrageenan, CMC and pectin (Nieto, 2009; Park et al., 2001; Wang et al., 2021; Yan et al., 2001). This is often attributed to the electrostatic interactions between these negatively charged groups and the protonated amino groups of chitosan, resulting in the formation of stable polyelectrolytic complexes (PEC) between the two polymers (Ansorena et al., 2018; Elsabee, 2015; Yan et al., 2001). Baron et al. (2017) characterized edible films obtained from the blends of different proportions of chitosan and pectin extracted from blue crab waste and orange peels and reported an increase in the water solubility and moisture content of the films with increasing concentration of pectin. Moreover, the authors observed that chitosan-pectin composite films were more flexible and elastic than their stand-alone counterparts but had no significant effect on their vapour barrier properties, which can be crucial in eliminating the need for plasticizers in chitosan-based films. Ismillayli et al. (2020) developed stable chitosan PEC films complexed with alginate or carrageenan and studied their antimicrobial

potential against *Staphylococcus aureus* and *Escherichia coli*. The authors reported a significantly enhanced inhibitory activity of PEC films (chitosan-alginate and chitosan-carrageenan) against both bacterial strains compared to their original polymers (chitosan, alginate or carrageenan).

Neutral polysaccharides have also shown the potential to modify various properties of chitosan films (Cazón & Vázquez, 2020; Elsabee, 2015). For example, a significant improvement in the mechanical and thermal properties was reported for chitosan films reinforced with a high proportion of nanofibrillated cellulose (Fernandes et al., 2010). On the other hand, a decrease in the water vapour permeability (WVP) along with improved mechanical properties was achieved for chitosan films combined with thermally gelatinized corn starch (Xu et al., 2005).

2.5.2.2 *Chitosan-protein films*

Various animal and plant-based proteins, such as casein, whey protein, collagen, gelatin, soy protein, wheat gluten and corn zein, have been utilized as blending polymers in a wide number of studies to enhance or modify the functionality of chitosan films (Elsabee, 2015; Haghighi et al., 2020). (Pereda et al., 2008, 2009) combined sodium caseinate with chitosan and reported ionic interactions between the two polymers resulting in highly homogeneous composite films with improved tensile strength (TS) while not affecting their % elongation (EAB). In a different study, Valenzuela et al. (2013) reported that composite films of chitosan-quinoa protein presented high flexibility with almost eight times the %EAB observed for neat unplasticized chitosan films without showing any adverse effect on their WVP. However, a significant reduction in the TS and resistance to oxygen transfer was also observed for these films.

Among all reported chitosan-protein blends, chitosan-gelatin composite films are the most studied and reported in the literature. This can be explained by the cheap availability of gelatin and high compatibility between the two polymers providing better functionality to the resultant films (Haghighi et al., 2020; Wang et al., 2021). Chitosan-gelatin composite films are discussed separately in Section 1.5.3.

2.5.2.3 Chitosan-lipid films

A feasible approach to lower the moisture sensitivity of chitosan-based edible films and improve their WVP is to incorporate hydrophobic biomolecules, such as oils and fatty acids, into the film matrix (Cazón & Vázquez, 2020; Pereda et al., 2012). Moreover, utilizing functional hydrophobic compounds like essential oils or vitamin E for this purpose can also promote the antimicrobial and antioxidant capacity of the films (Azarifar et al., 2019; Blanco-Fernandez et al., 2013; Kakaei & Shahbazi, 2016). In some cases, the incorporation of lipids can show plasticizing effects as well, lowering film rigidity and stiffness. However, their increased proportions mostly exhibit detrimental effects on the overall mechanical properties of the films (Cazón & Vázquez, 2020). Shen & Kamdem (2015) studied the effect of different concentrations of citronella essential oil (CEO) and cedarwood oil (CWO) on the physicochemical properties of the chitosan films. They reported a significant concentration-dependent decrease in the moisture uptake and WVP of the films for both CEO and CWO. Additionally, the oils significantly improved the %EAB of the films at low concentrations (10% w/w) without having much effect on their TS. At higher concentrations (30% w/w), however, both TS and %EAB reduced drastically.

Chitosan can also favourably interact with some lipids (electrostatic or hydrophobic interactions) to produce films with enhanced structural integrity, hence improving both TA and %EAB (Ansorena et al., 2018). Pereda et al. (2012) reported such favourable interactions between chitosan and olive oil. They not only obtained an increase in film hydrophobicity (decrease in WVP, equilibrium moisture content, water-solubility and water diffusion coefficient, and an increase in water contact angle) with increasing proportions of olive oil (0-15% w/w) but also observed a significant concentration-dependent increase in their TS, %EAB and elastic modulus. The only drawback of olive oil incorporation was the considerable increase in the opacity of the films.

2.5.3 Chitosan-Gelatin Composite Films

Gelatin, a partially hydrolyzed derivative of collagen, is a water-soluble animal protein usually obtained from fish and animal processing by-products (bones, hides, cartilages, etc.) (Pereda et al., 2011; Wang et al., 2017). It has numerous and widespread commercial applications

in the food industry because of its distinct properties (thickening, gelling, emulsifying and foaming), GRAS status, nutritious amino acid profile and cheap availability (Ansorena et al., 2018; Azarifar et al., 2019; Wang et al., 2021). Additionally, the presence of high contents of proline, glycine and hydroxyproline in the gelatin structure provides it with the ability to form homogeneous, transparent and flexible films with excellent mass transfer resistance against most gases, volatile compounds, oils and ultraviolet radiation (UV) and the potential to be applied as an edible packaging material (Haghighi, Biard, et al., 2019; Pereda et al., 2011; Wang et al., 2021). Unfortunately, just like chitosan, gelatin too is a hydrophilic biopolymer, and thus its resultant films are also susceptible to environmental RH and offer high water vapour permeability (WVP) (Gómez-Estaca et al., 2011; Haghighi, Biard, et al., 2019). Moreover, the proportions of amino acid and molecular weight of gelatin vary significantly with the source and extraction procedure, providing high structural and physicochemical variability in the resultant films (Avena-Bustillos et al., 2006 Gómez-Estaca et al., 2011; Kołodziejska & Piotrowska, 2007).

Chitosan and gelatin show a high affinity towards each other due to their hydrophilic nature and ability to interact electrostatically (Haghighi, Biard, et al., 2019). At a pH below 6.2 but above the iso-electric point of gelatin (4.5-5.2), the protonated amino groups of chitosan form polyelectrolytic complexes (PEC) with the anionic carboxylate groups of gelatin (Wang et al., 2021; Yin et al., 2005). Various authors have previously confirmed the presence of such complexion between chitosan and gelatin using X-ray diffraction, thermogravimetric analysis and FTIR spectroscopy (Hosseini et al., 2013; Pereda et al., 2011; Qiao et al., 2017; Yin et al., 2005). Consequently, chitosan-gelatin composite films have been reported to offer improved mechanical, physical, thermal, optical, and transport properties when compared to their stand-alone counterparts (Gómez-Estaca et al., 2011; Hosseini et al., 2013; Patel et al., 2018; Pereda et al., 2011; Rivero et al., 2009; Rui et al., 2017; Wang et al., 2017, 2021). In addition, due to the thermoplastic nature of gelatin, it can impart poorly explored properties like heat sealability to the composite films, which can be a defining factor for their packaging applications (Prateepchanachai et al., 2019).

Pereda et al. (2011) developed composite films from chitosan (Ch) and bovine-hide gelatin - type B (BG) prepared at 0.8Ch:1BG w/w ratio and compared them against plasticized Ch or BG stand-alone films. Compared to Ch or BG films, the composite films (Ch-BG) showed a significant

reduction in their WVP and equilibrated moisture content and an increase in % elongation (EAB) and antimicrobial activity against *E. coli* and *Listeria monocytogenes*. In addition, the incorporation of gelatin also increased the total soluble matter and transparency of composite films. However, a different study by Rivero et al. (2009) utilizing the same type of gelatin and similar processing conditions reported an increase in WVP and a decrease in TS compared to Ch films with no significant effect on %EAB. The difference in the initial pH of the composite film-forming solutions and proportions of Ch and BG blends utilized in the two studies could explain these contradicting results.

The applicability of mammalian gelatin derived from bovine or porcine waste in food applications is challenged by the associated risk of Bovine Spongiform Encephalopathy outbreaks along with the dietary restrictions posed in some religions (Avena-Bustillos et al., 2006; Hosseini et al., 2013; Wasswa et al., 2007). Gelatin from marine sources (warm or cold water fish skins, bones and fins) is an exciting alternative to mammalian gelatin as it does not have any associated potential safety hazards and is also considered kosher and halal (Avena-Bustillos et al., 2006; Chiou et al., 2009). Furthermore, large quantities of fish-processing waste are generated each year, posing economic and environmental challenges for disposal, and this can be utilized as a cheap, sustainable and eco-friendly source for the commercial production of fish gelatin (Hosseini et al., 2013; Wasswa et al., 2007). Another advantage of fish-gelatin over traditional mammalian gelatin is its increased hydrophobicity due to its significantly lower content of hydrophilic hydroxyproline, which provides better moisture resistance to the resultant films (Avena-Bustillos et al., 2006; Elsabee, 2015).

A study published by Gómez-Estaca et al. (2011) compared chitosan-gelatin composite films prepared from either bovine-hide (BG) or tuna-skin gelatin (TG). The authors reported that TG-Ch composite films were significantly more resistant to water solubility and had higher %EAB compared to BG-Ch and stand-alone Ch films. In addition, both TG-Ch and BG-Ch composite films presented lower WVP and TS than Ch films. However, no significant difference was found for WVP and TS among the two composite films. Contradictory results were found in a different study by Hosseini et al. (2013), who compared the chitosan-fish gelatin composite films with different proportions of gelatin to chitosan (0:100, 60:40, 70:30, 80:20 and 100:0). According to their observations, the hydrophilic nature of composite films significantly increased (water

solubility and WVP) with increasing proportions of fish-gelatin. Also, the %EAB of the composite films with higher gelatin content considerably improved while sacrificing on TS. The reason can be pinned down to a difference in the MW of chitosan, amount of added plasticizer and drying temperature utilized in the two studies.

Some studies have also incorporated additional hydrophobic compounds like essential oils into the chitosan-gelatin composite films in order to improve film hydrophobicity and antimicrobial potential (Haghighi, Biard, et al., 2019; Kakaei & Shahbazi, 2016; Wang et al., 2021; Yao et al., 2017). One such example is a study published by Yao et al. (2017), who incorporated different concentrations of D-limonene (0, 0.25, 0.50, 0.75, and 1.0% w/w film-forming solution) into chitosan-fish gelatin composite films. Along with the concentration-dependent increase in the %EAB and decrease in the TS, D-limonene significantly enhanced the surface hydrophobicity (water contact angle) and antimicrobial activity (against *E. coli*) of the composite films. However, as expected, a considerable increase in the opacity of the films was also observed.

2.5.4 Opportunites for Lobster-based Chitosan Composite Films

Over the years, the literature associated with the description, development, modification and application of chitosan-based biodegradable or edible films has significantly expanded, yet their commercialization in the food packaging industry is still prohibitive due to the high dependency of their properties on an excessive number of factors, including the source of chitosan, and the high cost of chitosan itself. Nevertheless, some of these issues can be addressed by utilizing low-cost crude chitosan procured from the valorization of abundantly available lobster-shell waste and blending chitosan with other cheap but compatible biopolymers like gelatin. Despite the wealth of research on chitosan and chitosan-based films, crude chitosan extracted from lobster-shell waste has not been explored for edible film application. Moreover, opportunities exist for optimizing and tailoring chitosan or composite films for specific niche packaging applications and standardizing their development procedures.

CHAPTER 3

EXTRACTION AND CHARACTERIZATION OF CHITOSAN FROM LOBSTER SHELL-WASTE AND DEVELOPMENT OF SOLVENT CAST CHITOSAN FILMS

3.1 INTRODUCTION

Sustainable management and valorization of shellfish waste have gained widespread interest in the last two decades owing to the associated economic benefits and increased environmental awareness (Kerton et al., 2013). As discussed in Chapter 2, Atlantic Canada generates enormous quantities of lobster shell-waste, and in order to get rid of it, lobster processing industries (LPIs) incur costs to landfill, incineration or disposal in seas. However, utilizing this shell-waste as a renewable bioresource for producing high-value products such as chitosan has excellent economic prospects.

On the other hand, the abundance of fossil-fuel-based non-biodegradable plastic waste originating from food packaging industries has raised serious environmental concerns and has attracted much-needed attention to the renewable and biodegradable biopolymer-based packaging materials (Leceta, Guerrero, Cabezudo, et al., 2013). Chitosan is an ideal candidate in this regard due to its abundant availability, excellent film-forming ability, biocompatibility and inherent antimicrobial properties (Dutta et al., 2009; Leceta, Guerrero, Cabezudo, et al., 2013). Therefore, producing chitosan from crustacean shell waste and using it to develop edible films for food packaging applications can be a significant step towards addressing these two major waste-related issues at once, in addition to generating significant commercial value.

Extensive research has been done on extraction, characterization and applicability of shell-derived chitosan and chitosan-based edible films in the past (Aider, 2010; Dutta et al., 2009; Elsabee, 2015). However, very limited literature is available on chitosan obtained from the shells of Atlantic lobsters (*Homarus americanus*), and thus its use in the development of edible antimicrobial films has not yet been reported. Therefore, the primary objective of the study presented in this chapter was to characterize and compare lobster-shell derived crude chitosan with

commercially available crab-shell chitosan and analytical grade (high purity) chitosan with regards to the structural and physicochemical properties of their solvent cast films.

3.2 MATERIALS AND METHODS

3.2.1 Materials and Reagents

A homogeneous mix of claw and tail shells of Atlantic lobster (*Homarus americanus*) was obtained from Clearwater Seafoods Inc. (NS, Canada). Crab-shell chitosan was purchased from Tidal Vision (WA, USA), and high molecular weight chitosan was purchased from Sigma-Aldrich (ON, Canada). Unless specified, all reagents utilized in this study were of analytical grade and were purchased from either Sigma-Aldrich (ON, Canada), Fisher Scientific (ON, Canada) or BDH® VWR Chemicals (USA).

3.2.2 Extraction of Chitosan from Lobster Shells

Lobster shells were washed thoroughly with tap water, dried at 60° C for 24 h in a hot-air oven (Hermatherm™, Thermo Fisher Scientific, USA), and ground into smaller pieces using a high-power blender (Model BL660, SharkNinja Operating LLC, USA). The obtained product was stored in sealed containers at room temperature. Crude chitin was extracted from these dried and ground lobster shells using an acid-alkali two-stage chemical extraction procedure, i.e., demineralization followed by deproteinization of the shells as described below. The obtained chitin was then chemically converted to chitosan via alkali-based deacetylation.

3.2.2.1 *Demineralization and deproteinization of dried lobster shells*

Following the procedure described by W. Xu et al. (2020), ground lobster shells were sieved to 2 mm particle size and were added into a 2M hydrochloric acid (HCl) solution at a concentration of 0.1 g/mL. The addition of shells was done over a period of 2 h to prevent excessive foaming. The solution was continuously stirred (250 rpm) for 24 h at room temperature to allow the acid to solubilize minerals from the shell particles. The demineralized (DM) shells were then

washed with distilled water until achieving neutral pH, followed by overnight oven-drying at 60 °C. The dried DM shells were collected the next day, and their weight was recorded.

For deproteinization, the obtained DM shells were ground to a coarse powder using an electric-powered grain mill (WonderMill, Canada) and were added into a 1M sodium hydroxide solution (NaOH) at a concentration of 0.1 g/mL. The alkaline solution was continuously stirred (200 rpm) and heated at 70 °C for 6 h. The solution was then cooled to room temperature, and the residue was collected using vacuum filtration with Whatman filter paper (grade 1). This residue was washed with distilled water to neutrality and oven-dried overnight at 60 °C. The dried product (crude chitin) was collected and weighed the next day, and the extraction yield was calculated using the following equation:

$$Crude\ chitin\ yield\ (\%) = \frac{Weight\ of\ the\ extracted\ chitin\ residue}{Weight\ of\ the\ treated\ dried\ lobster\ shells} \times 100 \quad (Eq.\ 3.1)$$

3.2.2.2 Deacetylation of crude chitin

The chitin obtained from the above procedure was derivatized into chitosan by partially removing its acetyl groups using concentrated alkali solution according to a procedure described by Trung et al. (2006). The extracted chitin was treated with 50% NaOH solution at 60 °C for 20 h with constant stirring (200 rpm) at a concentration of 0.1 g/mL. The treated mixture was cooled, and the residue was collected using vacuum filtration with Whatman filter paper (grade 1). This residue was again washed with distilled water to achieve neutral pH and oven-dried at 60 °C for 48 h. The weight of the dried residue, i.e. crude lobster-shell chitosan (LCh), was recorded, and the % yield was calculated using the following equation:

$$Crude\ chitosan\ yield\ (\%) = \frac{Weight\ of\ the\ extracted\ chitosan\ residue}{Weight\ of\ the\ treated\ chitin} \times 100 \quad (Eq.\ 3.2)$$

3.2.3 Characterization of Extracted Chitin and Chitosan

3.2.3.1 Proximate analysis

The moisture, ash and fat content of dried lobster shells, DM shells, extracted crude chitin, and LCh were determined using the standard methods described by AOAC (1990). Briefly, the moisture content was determined by oven-drying the samples at 105 °C for 24 h. The ash content was measured by charring and burning the samples at 600 °C for 3 h in a muffle furnace (Thermo Fisher Scientific, USA). The total lipid content of the samples was determined using the Soxhlet apparatus (C. Gerhardt UK Ltd, UK) with diethyl-ether as the extraction solvent for 3 h.

The total elemental nitrogen present in lobster shells, DM shells and extracted chitin was measured using elemental analysis (PerkinElmer Inc., USA), and the chitin and protein content of these samples were calculated using the following equations (Díaz-Rojas et al., 2006):

$$\% \ chitin \ content \ (Q) = \frac{\left(\left(N_t \times C_p\right) + K - 100\right) \times C_q}{C_p - C_q} \qquad \text{(Eq. 3.3)}$$

$$\% \ protein \ content \ (P) = \frac{\left(\left(N_t \times C_q\right) + K - 100\right) \times C_p}{C_q - C_p} \qquad \text{(Eq. 3.4)}$$

Here, N_t denotes total elemental nitrogen; C_p denotes protein conversion coefficient (6.25 for marine products); C_q denotes chitin conversion coefficient (14.5 for completely acetylated chitin); K denotes the sum of all non-nitrogen compounds, i.e., % ash content, % lipid content, % moisture content. All measurements were performed in triplicates, and their averages were reported.

3.2.3.2 Fourier-transform infrared (FT-IR) spectroscopy

The structural analysis of dried lobster shells, DM shells, extracted chitin and LCh was performed by FT-IR spectroscopy (Spectrum Two, PerkinElmer, USA) using an attenuated total reflection (ATR) accessory (MIRacle™ Single Reflection ATR, PIKE Technologies, USA) with

a diamond ATR crystal. The measurements were taken using a method described by Nguyen, Barber, Smith, et al. (2017) with slight modifications. Before analysis, the samples were ground into a fine powder using a mortar and pestle. The final spectra for each sample was an aggregate of 32 scans recorded at a resolution of 4 cm^{-1} between 4000 cm^{-1} to 500 cm^{-1}. Additionally, FT-IR spectra were obtained for commercially available crab-shell chitosan (CCh) (Tidal Vision, USA) and analytical grade high molecular weight chitosan (HCh) (Sigma-Aldrich, USA) for comparison with LCh. All measurements were performed in triplicates.

3.2.3.3 Estimation of the degree of acetylation (DA) and deacetylation (DD)

Absorbance results from FT-IR spectroscopy were used for calculating the *DA* for extracted chitin and *DD* for chitosan samples using the following equations (Brugnerotto et al., 2001):

$$DA\ (\%) = 31.92 \times \frac{A_{1320}}{A_{1420}} - 12.20 \qquad \text{(Eq. 3.5)}$$

$$DD\ (\%) = 100 - DA(\%) \qquad \text{(Eq. 3.6)}$$

Here, A_{1320} and A_{1420} denote sample absorbance values at 1320 cm^{-1} and 1420 cm^{-1}, respectively.

3.2.3.4 Molecular weight (MW) analysis for chitosan using gel-permeation chromatography

The molecular weights of LCh, CCh and HCh, were determined using gel-permeation chromatography (GPC) equipped with viscometric (VS), light scattering (LS) and refractive index (RI) detectors (Agilent, 1260 Infinity 2 Multi-Detector GPC/SEC System, US). The samples were prepared in 0.1 M sodium acetate buffer (pH 4.4) at 4 mg/mL concentration. GPC analysis was performed by eluting the samples with 0.1 M sodium acetate buffer through a series of two PL aquagel-OH MIXED-M columns (8 µm, 300 x 7.5 mm, Agilent, US) at a flow rate of 1 mL/min. The samples were filtered through a 0.45 µm syringe filter (Basix^{TM}, Fisher Scientific, US) before injection, and sample volumes of 50, 25 and 10 µL were injected. The calibration curve was

obtained by eluting pullulan polysaccharide narrow standards (GPC/SEC Calibration Kit, Agilent, US) at a concentration of 0.5 mg/mL with peak molecular weights (M_P) ranging from 9.5 kDa to 642 kDa.

3.2.3.5   *Analysis of the thermal behaviour of chitosan*

The thermal behaviour of LCh was evaluated using a simultaneous thermal analyzer (STA 8000, PerkinElmer, USA) in TGA and DSC mode. The samples were heated at 10 °C/min from 30 to 900 °C, under a constant nitrogen gas purge (20 mL/min). The weight of the samples ranged from 14 to 17 mg. The TGA, differential curve of the TGA (DTGA) and DSC curves were obtained. All measurements were performed in triplicates.

3.2.4   Development of Solvent Cast Chitosan Films

A procedure for preparing chitosan-based edible films was developed based on a review of several methods described in the literature (Cerqueira et al., 2012b; Leceta et al., 2015; Singh et al., 2015; Ziani et al., 2008). Firstly, powdered chitosan samples (LCh, CCh or HCh) were dissolved in aqueous acetic acid (1%, v/v) at a concentration of 20 mg/mL. The solutions were then continuously stirred (300 rpm) for three hours at 60 °C and filtered while still hot through a 25 μm wire mesh using vacuum filtration to remove impurities. Finally, the obtained chitosan solutions were de-gassed to prevent the formation of air bubbles in the films either by applying vacuum over the solutions for 15 min or by sonicating the samples using a probe sonicator (VCX 750, Vibra-Cell^{TM}, Sonics and Materials, USA) for 10 mins at 40% amplitude and 15-second pulse. Note here that no plasticizers were added to the chitosan solutions in this stage of film development.

Approximately 0.25 g/cm^2 of each de-gassed chitosan solution was poured into polystyrene Petri dishes (100x15 mm, Fisherbrand^{TM}, USA) and dried at 60 °C for 24 h in the hot-air oven. The dried films were carefully peeled off from the dishes and conditioned at 21 ± 2 °C (room temperature) in a desiccator with a saturated magnesium nitrate solution (52 - 54% RH) for at least three days prior to any analysis.

3.2.5 Characterization of Solvent Cast Chitosan Films

3.2.5.1 *Film thickness*

The thickness of the chitosan films was measured using a digital thickness gauge (Neoteck®, USA) with the least count of 0.001 mm. Ten measurements were taken at randomly distributed points (one at the centre and nine at the outer or inner edges of the film), and the mean value obtained from these measurements was further used for determining the mechanical, barrier and optical properties of the films.

3.2.5.2 *Equilibrated moisture content, Degree of Swelling and Water Solubility*

The equilibrated moisture content (EMC), degree of swelling (DS) and water solubility (WS) for the chitosan films were determined based on a previous method described by Homez-Jara et al. (2018) with slight modifications. Briefly, 10 mm diameter circles were punched out of the films using a wad punch set (Boehm®, Hoffmann Group, USA) and weighed (W_I) with a precision of 0.1 mg. Next, the film samples were dried at 103 °C in the hot-air oven for 24 h, and their dry matter weight was recorded (W_D). The dried film samples were then put into 20 mL glass scintillation vials containing 15 mL distilled water for swelling, placed on an orbital shaker (KS 130 control, IKA® Works, USA) and agitated for 24 h (320 rpm) at room temperature (RT). The extra water on the surface of the swollen films was gently removed using Kimwipes, and subsequently, the weight of the swollen samples was measured (W_{SW}). Finally, the swollen samples were again dried at 103 °C for 24 h, and their final weight was recorded (W_F). Average values from triplicates for each film type were reported.

The values for percentage *EMC*, *DS* and *WS* for the film samples were calculated using the following equations –

$$EMC\ (\%) = \frac{W_I - W_D}{W_D} \times 100 \qquad\qquad\qquad \text{(Eq. 3.7)}$$

$$DS\ (\%) = \frac{W_{SW} - W_D}{W_D} \times 100 \qquad\qquad\qquad (Eq.\ 3.8)$$

$$WS\ (\%) = \frac{W_D - W_F}{W_D} \times 100 \qquad\qquad\qquad (Eq.\ 3.9)$$

3.2.5.3 Light barrier properties and Opacity value

The barrier properties of the films against ultraviolet (UV) and visible light were determined by measuring their absorption spectra at wavelengths ranging from 230 to 800 nm with 10 nm increments using a microplate reader (Infinite M1000 Pro, Tecan, USA). Circular samples of 5 mm diameter were punched out from the films and placed in a 96-well transparent plate (Fisherbrand™, Thermo Scientific, USA). The absorption values for empty wells were considered as a reference. Opacity values of the samples were calculated by integrating the area under the absorption curve within the respective wavelength ranges (230 - 400 nm for UV and 400 – 800 nm for visible light) divided by the thickness of the film. The values were expressed as absorbance units per thickness unit (A/mm). All measurements were performed in triplicates to ensure reproducibility, and their average was reported.

3.2.5.4 Mechanical properties

The mechanical properties of the prepared films, i.e. tensile strength (TS), percentage elongation at break (%EAB) and elastic modulus (EM), were measured according to ASTM standard method D882-18 using a universal testing machine (EZ Test EZ-LX HS, Shimadzu, Japan) equipped with a 1 kN load cell (ASTM Internation, 2018). Briefly, films with known thickness were cut into rectangular strips (70 x 6 mm^2) and conditioned in $52 \pm 2\%$ RH at RT (21 $\pm$ 2 °C) for at least 48 h before testing to ensure equilibrium conditions. The stress-strain curves for the samples were produced at an initial grip separation and mechanical cross-head speed of 30 mm and 12.5 mm/min. Trapezium-X software (Shimadzu, Japan) was used to analyze the results and determine TS, %EAB and EM for the films. Average values from at least six replicates for each film were reported.

3.2.5.5 Water vapour barrier properties

The ASTM standard E96/96-16 water method with slight modifications was used to determine the water vapour permeability of the film samples (ASTM Internation, 2016). As depicted in Figure 3.1, each film sample without any pinholes and known thickness was sealed over the circular opening (0.00028 m^2) of a 5 mL glass vial containing 4 mL distilled water (100% RH). The vial lid was additionally sealed with Parafilm^{TM} M to ensure that it was air-tight. Subsequently, the sealed vial was placed into an air-tight container containing 10 grams of silica gel desiccant (0% RH) to maintain a constant relative humidity gradient across the film. Finally, the whole set-up was placed into an oven maintained at 25 °C. The silica gel present in the air-tight container absorbed the water vapours transferred through the film, and the reduction in weight of the vial was recorded with a precision of 0.1 mg at different time intervals over a week. Steady-state and uniform vapour pressure conditions were assumed considering the relatively small volume of the outside container with desiccant.

The change in mass of the vial was plotted against time, and the water vapour permeability (*WVP*) of the samples was calculated using the following expressions –

$$WVTR = \frac{\Delta m}{\Delta t \times Ar} \qquad\qquad\text{(Eq. 3.10)}$$

$$WVP = \frac{WVTR \times FT}{P_{Sat} \times (RH_O - RH_I)} \qquad\qquad\text{(Eq. 3.11)}$$

Here, *WVTR* is the water vapour transmission rate (g/hr.m^2), $\Delta m/\Delta t$ is the slope of the weight loss vs time graph (g/h), *Ar* is the exposed area of the film (m^2), P_{Sat} is the saturation vapour pressure at 25 °C (3.171 kPa), RH_O and RH_I are relative humidity outside and inside of the glass vial, respectively (expressed as a fraction), and *FT* is the average film thickness (mm).

Errors in the *WVP* measurements due to resistance in permeability caused by the stagnant air gap between the exposed film surface and water were corrected using the formulae described by the ASTM standard method (ASTM Internation, 2016). Measurements were done in triplicates for each film type to ensure reproducibility, and their average was reported.
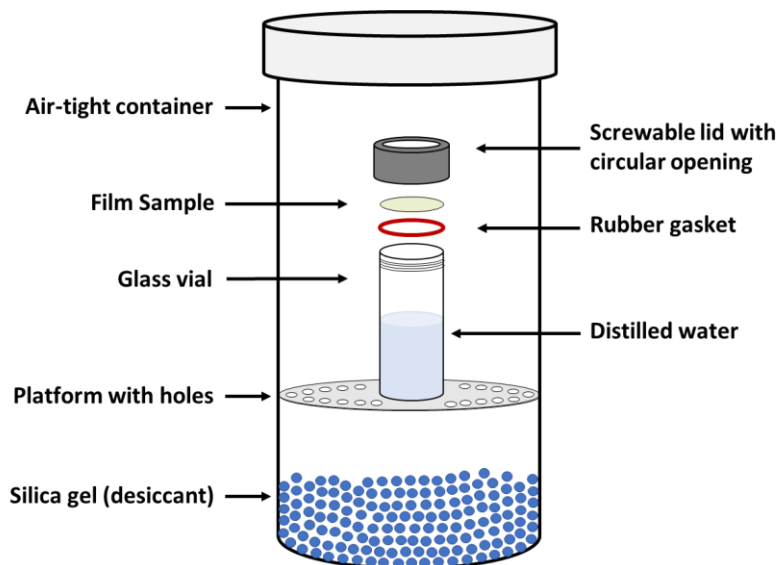
Figure 3.1: Set-up for evaluating the water vapour barrier properties of chitosan films.

3.2.5.6 Surface hydrophobicity

The hydrophobicity of the film surface was assessed by measuring the surface contact angle (CA) with the sessile drop method using ethylene glycol (polar liquid) according to the procedure described by (Pereda et al., 2012) with minor modifications. Prior to the analysis, rectangular strips of the film samples (50 x 10 mm^2) were cut and conditioned in $52 \pm 2\%$ RH at RT (21 ± 2 °C) for at least 48 h to ensure equilibrium conditions. The measurements were taken at RT using a drop shape analyzer instrument (DSA25B, Krüss GmbH, USA) with a drop volume of 20 µL. The shape of the drops was analyzed using Krüss Advance software within the first 20 seconds of the deposit to avoid variations due to the swelling of the films. All measurements were performed in triplicates for each film type, and their average was reported.

3.2.5.7 Statistical analysis

Data collected from each test were statistically analyzed using single-factor analysis of variance (ANOVA) in Minitab 19 Statistical Software. Comparison of the means was performed by employing posthoc Tukey's HSD (Honest significant difference) test, and a p-value of less than 0.05 was considered statistically significant. All results are reported as mean ± standard deviation.

3.3 RESULTS AND DISCUSSION

3.3.1 Characterization of Extracted Chitin and Chitosan

3.3.1.1 *Appearance, proximate composition and extraction yield*

Chitosan extracted from lobster shells had a light pink appearance, indicating the presence of carotenoids that did not get removed during the harsh deacetylation process (Figure 3.2). Crustacean shells are considered a rich source of high-value carotenoids, especially astaxanthin, which is one of the most potent antioxidants present in nature with approximately ten times the activity of other common carotenoids like β-carotene and lutein (Miki, 1991; Nguyen, Barber, Corbin, et al., 2017). Commercially available chitosan is generally depigmented using organic solvents or strong oxidizing agents to achieve the high purity required for its several applications (Chen et al., 2016; Yadav et al., 2019). However, this depigmentation step was skipped in the present study, as it could have numerous benefits in the context of edible films. For example, the high purity of chitosan is not essential for the development of films; hence the cost of its extraction can be significantly reduced while eliminating the need for organic solvents or oxidizing agents, making the process a bit cheaper and a little more sustainable. Moreover, the small amounts of carotenoids present in the chitosan could improve its overall antioxidant and antimicrobial activity, a highly desirable aspect of chitosan films.
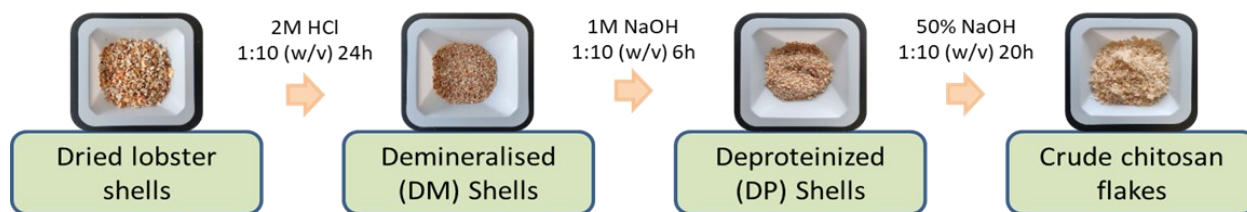
Figure 3.2: Intermediary and final extraction products obtained from lobster shell-waste.

The proximate composition of dried lobster shells, demineralized (DM) shells, lobster-shell derived chitin and chitosan (LCh) is shown in Table 3.1. Crustacean shells are generally rich in minerals (20-60% w/w db), proteins (20-40% w/w db) and chitin (15-40% w/w db); however, their

composition can significantly vary depending on the species, season and parts of the shell (Boßelmann et al., 2007; Hülsey, 2018). In the present study, the lobster shells were found to contain large amounts of minerals (≈58% w/w db) and relatively smaller amounts of organic material (proteins + chitin + lipids; ≈34% w/w db) which is in accordance with the previously reported findings of Boßelmann et al. (2007).

The extraction process followed in this study efficiently removed most minerals, proteins, and lipids from the shells (> 99% removal), providing a reasonably pure product with a high extraction yield of 21.3% and 18.4% (w/w dry lobster shells) for chitin and chitosan, respectively. In addition, the moisture content for both extracted chitin and chitosan was less than 5% which is well within the acceptable range for commercialization (Alishahi et al., 2011).

Table 3.1: Proximate composition of dried lobster shells, demineralized shells, lobster-shell chitin and lobster-shell chitosan.

% Dry matter basis (db)	Lobster shells	Demineralized shells	Lobster-shell chitin	Lobster-shell chitosan
Moisture content	7.16 ± 0.39	7.81 ± 0.14	4.41 ± 0.11	2.50 ± 0.09
Ash content	58.39 ± 0.89	0.74 ± 0.06	0.59 ± 0.08	NA
Lipid content	0.09 ± 0.01	NA	NA	NA
Protein content	12.92 ± 0.66	18.27 ± 1.27	NA	ND
Chitin content	21.45 ± 0.67	73.18 ± 1.27	7.16 ± 0.39	ND

NA: Not available; ND: Not determined

3.3.1.2 FT-IR and N-acetylation/deacetylation degree

The FT-IR spectra for lobster shells, lobster-shell chitin, lobster-shell chitosan (LCh), commercially available crab-shell chitosan (CCh), and analytical grade high MW chitosan (HCh) are shown in Figures 3.3 and 3.4. Additionally, representative IR-bands identified in the chitin and chitosan samples are shown in Table 3.2.
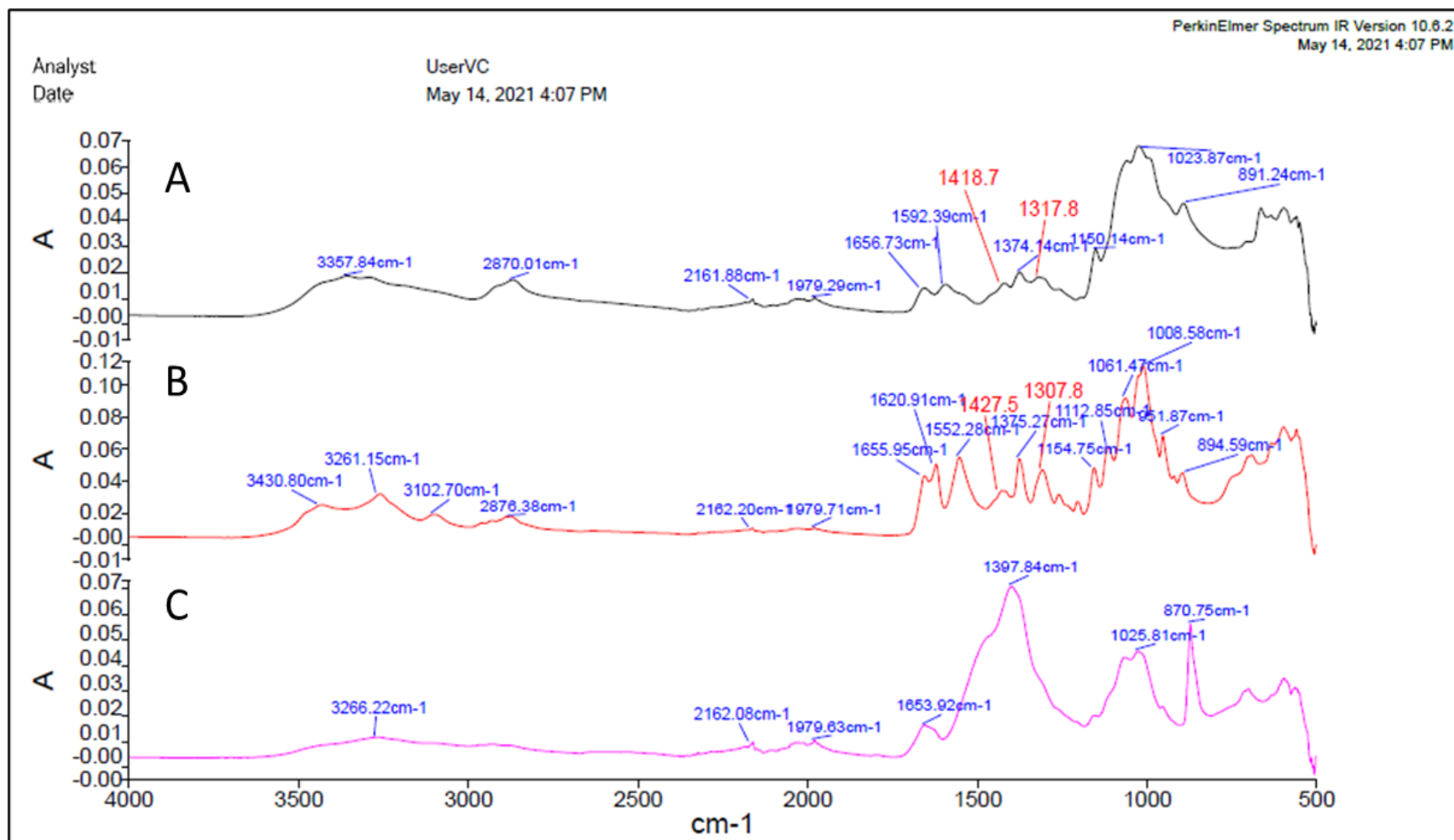
Figure 3.3: FTIR spectra for A) lobster-shell chitosan (LCh); B) lobster-shell chitin; and C) lobster shells.
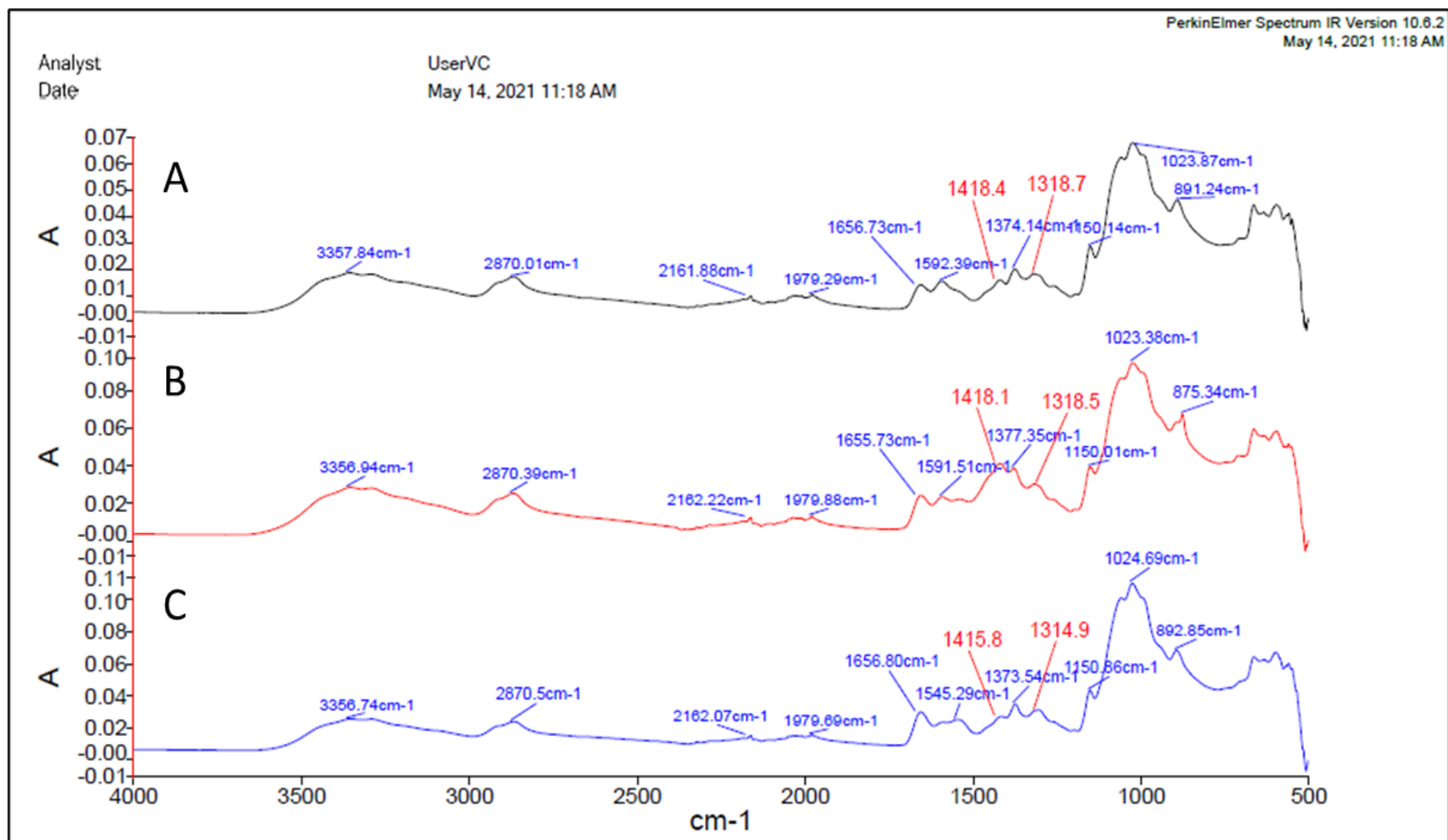
Figure 3.4: FTIR specta for A) lobster-shell chitosan (LCh); B) commercial crab-shell chitosan (CCh); and C) high MW analytical grade chitosan (HCh).

Table 3.2: Identified and assigned FT-IR peaks for lobster-shell chitin, lobster-shells chitosan (LCh), commercial crab-shell chitosan (CCh), and high MW analytical grade chitosan (HCh) (References - Ioelovich, 2017; Kaya et al., 2014; Lizardi-Mendoza et al., 2016).

Vibration assignments	Wavenumber (cm^{-1})					
	Characteristic IR-bands for chitin	Lobster-shell chitin	Characterstic IR-bands for chitosan	Lobster-shell chitosan (LCh)	Crab-shell chitosan (CCh)	High MW chitosan (HCh)
O-H stretching	3400-3450	3431	3400-3500	3358	3357	3357
N-H stretching	3250-3270	3261	3250-3300	-	-	-
CH_3 sym. and CH_2 asym. stretching	2930-2950	3103	-	-	-	-
CH stretching and CH_3 asym. stretching	2850-2900	2876	2850-2900	2870	2870	2871
C=O secondary amide stretching (amide I)	1640-1660	1656	1640-1660	1657	1656	1657
C=O secondary amide stretching (amide I)	1620-1630	1621	-	-	-	-
Amine groups bending	-	-	1580-1600	1592	1592	1590
N-H bending and CH stretching (amide II)	1550-1560	1552	1540-1560	-	-	1545
CH_2 bending and CH_3 deformation	1400-1420	1428	1420-1430	1418	1418	1416
CH bending and sym. CH_3 deformation	1370-1380	1375	1370-1380	1374	1377	1374
CH_2 wagging (amide III)	1300-1320	1308	1310-1330	1319	1318	1315
Asym. Bridge oxygen stretching	1150-1200	1155	-	-	-	-

Table 3.2: Continued.

Vibration assignments	Wavenumber (cm^{-1})					
	Characteristic IR-bands for chitin	Lobster-shell chitin	Characterstic IR-bands for chitosan	Lobster-shell chitosan (LCh)	Crab-shell chitosan (CCh)	High MW chitosan (HCh)
Asym. In-plane ring stretching	1100-1150	1113	1150-1160	1150	1150	1151
C-O-C asym. Stretching in phase ring	1000-1060	1061	1030-1070	1024	1023	1025
C-O asym. In phase ring	1000-1030	1009	-	-	-	-
CH$_3$ wagging	950-980	952	-	-	-	-
CH ring stretching	850-900	895	850-900	891	875	893

All identified absorption peaks for lobster-shell derived chitin and chitosan were consistent with the previously reported characteristic IR-bands for chitin samples (Ioelovich, 2017; Kaya et al., 2014; Lizardi-Mendoza et al., 2016). In nature, chitin predominantly occurs in two polymorphic crystalline forms, α or β-chitin, based on the spatial arrangement of their chains (Kumari & Kishor, 2020). The amide-I bands attributed to the stretching vibrations of C=O and C-N groups can be used to differentiate these two polymorphs of chitin from each other. For α-chitin, two distinct amide-I bands appear at 1660 cm^{-1} and 1630 cm^{-1}, whereas only one band appears at around 1660 cm^{-1} for β-chitin (Kumirska et al., 2010). Referring to Table 3.2 and Figure 3.3, it can be observed that extracted chitin showed two distinct amide-I bands at 1656 and 1621 cm^{-1}, indicative of the α polymorph. Another characteristic marker for differentiating α from β-chitin is the vibration band associated with the CH stretching and deformation, which shifts from 895 cm^{-1} in α-chitin to 890 cm^{-1} in β-chitin (Ioelovich, 2017; Kumirska et al., 2010). The vibration band observed at 895 cm^{-1} for the extracted chitin further confirmed its structural nature. The spectra of lobster shells looked significantly different from the spectra of chitin or chitosan because of the presence of large quantities of minerals and proteins (Figure 3.3); however, a peak at 1654 cm^{-1} associated with amide I (characteristic to chitin) indicated the presence of chitin in the shells. Vibrational bands at 1400-1450 and 870 cm^{-1} observable in the shell spectra can be assigned to the stretching and bending vibrations of calcite ($CaCO_3$) minerals present in the shell (Gbenebor et al., 2017).

Structural changes associated with the derivatization of chitin to chitosan can be easily identified from their FT-IR spectra. For example, with an increase in deacetylation of chitin and its conversion to chitosan, the intensity of amide I, II and III bands gradually decreases and a new peak at 1590 cm^{-1} emerges indicative of free amine (NH_2) groups. Moreover, the two distinct peaks associated with amide I in α-chitin merge into a single band observable at around 1650 cm^{-1} (Kumari & Kishor, 2020; Kumirska et al., 2010). The same characteristics can be observed for both LCh and CCh samples (Figure 3.4). However, the HCh sample showed a significant amide II peak (1545 cm^{-1}), while an observable peak at 1590 cm^{-1} could not be detected, indicating a low degree of deacetylation for the sample.

The degree of acetylation (DA) or deacetylation (DD) for chitin and chitosan samples were determined using the equations mentioned in Section 3.2 (materials and methods) and are

44

presented in Table 3.3. The ratio of absorption peaks at 1320 cm^{-1} and 1420 cm^{-1}, representing CH_2 wagging (amide III) and CH_2 bending, was chosen for the calculation of DA and DD%, as this ratio is not sensitive to the FT-IR measurement technique and the moisture content of the sample, and provides a high correlation (r = 0.99) between the actual and estimated values of DA/DD (Brugnerotto et al., 2001; W. Xu et al., 2020). The DD for the analyzed chitosan samples were significantly different (p < 0.05) from each other, with CCh showing the highest value followed by LCh and HCh.

Table 3.3: Degree of acetylation (DA) for extracted chitin and degree of deacetylation (DD) for chitosan samples.

	Lobster-shell chitin	Lobster-shell chitosan (LCh)	Commercial crab-shell chitosan (CCh)	High MW analytical grade chitosan (HCh)
DA (%)	97.6 ± 2.3	-	-	-
DD (%)	-	80.2 ±2.7[A]	96.1 ± 3.9[B]	73.0 ± 1.2[C]

The difference between the two mean values followed by the same letter in the same row is statistically insignificant (p > 0.05) as determined by Tukey's HSD test.

The DA/DD is one of the most critical parameters for chitin or chitosan and influences their various physicochemical properties and applications (Lizardi-Mendoza et al., 2016). A DA of 97.6% for extracted chitin is relatively high and suggests that the extraction procedure did not significantly affect the chemical composition of chitin present in the lobster shells. On the other hand, HCh showed a relatively low DD of only 73%, which is similar to the reported DD (>75%) by the production company (Sigma-Aldrich, USA). The variation in DA/DD mostly depends on the extraction procedure (time, temperature and alkali concentration); however, the initial substrate (source of chitin) can also impact the DA/DD of the final product. Our results for DA/DD of lobster shell chitin and chitosan (LCh) were similar to the results reported by W. Xu et al. (2020), who utilized the same substrate (lobster shells) and a similar extraction procedure.

Overall, the FT-IR spectra for all chitosan samples analyzed (LCh, CCh and HCh) were similar to each other, showing only a few minor differences in the intensities and positions of the

absorption peaks. Therefore, it can be concluded that the extracted lobster-shell-derived crude chitosan was structurally comparable to the commercially available products.

3.3.1.3 Molecular weight (MW) of chitosan

Molecular weights (peak, weight average and number average) for different chitosan samples determined by gel permeation chromatography (GPC) along with their polydispersity index (PDI = M_W/M_N) are shown in Table 3.4.

Table 3.4: Average molecular weights (MW) and polydispersity index for different chitosan samples.

	Peak MW (M_P)	Weight average MW (M_W)	Number average MW (M_N)	Viscosity average MW (M_V)	Polydispersity Index (PDI)
LCh	389 ± 22 kDa[A]	341 ± 47 kDa[A]	308 ± 25 kDa[A]	363 ± 23 kDa[A]	1.10 ± 0.06[A]
CCh	356 ± 18 kDa[A]	304 ±27 kDa[A]	267 ± 47 kDa[A]	327 ± 15 kDa[A]	1.14 ± 0.10[A]
HCh	408 ± 84 kDa[A]	360 ± 56 kDa[A]	204 ± 23 kDa[A]	415 ± 57 kDa[A]	1.76 ± 0.08[B]

LCh: lobster-shell chitosan; CCh: commercial crab-shell chitosan; HCh: high MW analytical grade chitosan. The difference between the two mean values followed by the same letter in the same column is statistically insignificant (p > 0.05) as determined by Tukey's HSD test.

Molecular weight (MW) is a critical characterization parameter for chitosan that significantly influences its physical, chemical and antimicrobial properties (Annu et al., 2017; Aranaz et al., 2014; S. Y. Park et al., 2002). Generally, chitosan is classified into three broad categories based on its MW, i.e., low MW chitosan (< 50 kDa), medium MW chitosan (50-250 kDa) and high MW chitosan (> 250 kDa) (Kumari & Kishor, 2020). In this study, all three chitosan samples analyzed (LCh, CCh and HCh) had an average MW (M_W) of more than 250 kDa and thus were identified as high MW chitosan. Although HCh had the highest M_W and M_V followed by LCh and CCh, the differences were statistically insignificant (p > 0.05). Moreover, the M_W of HCh was within the range reported by the production company (310 – 375 kDa; Sigma-Aldrich, USA), which demonstrates the efficacy of the procedure followed in this study for accurately determining the MW of chitosan.

The polydispersity index (PDI) of a polymer describes the broadness of its MW distribution and overall homogeneity (Danaei et al., 2018; Shrivastava, 2018). The observed PDI for LCh and CCh was around 1.1, which was significantly lower ($p < 0.05$) than that of HCh (PDI = 1.76), suggesting a narrower MW distribution and better homogeneity of LCh and CCh compared to HCh. Chitosan with a low PDI (0.85 – 1.15) is generally preferred for material synthesis applications as they exhibit higher uniformity in their properties and functionality (Annu et al., 2017; Hülsey, 2018). Therefore, due to their low PDI, LCh and CCh might be more suitable for producing edible films with consistent properties compared to HCh.

3.3.1.4 Thermogravimetric analysis (TGA) and differential scanning calorimetry (DSC)

The thermal behaviour and overall thermal stability of LCh were evaluated using thermogravimetric analysis (TGA) and differential scanning calorimetry (DSC). TGA and its derivative (DTGA) and DSC thermograms for LCh are presented in Figure 3.5. The thermograms provided a comprehensive overview of thermal degradation of LCh, and weight loss was observed in two distinct stages/zones.

The first degradation stage starting from 40 °C to 170 °C, represents an endothermic region with a weight loss of around 5% and is associated with the removal of absrobed and bound moisture from the chitosan sample (Rodrigues, de Mello et al., 2020). The second stage corresponding to the loss of organic material due to the dehydration of saccharide rings, and depolymerization and disintegration of chitosan molecules ($\approx$40% weight loss) occurred from 260 °C up till the final temperature of the analysis with the maximum decomposition rate ($T_{d,max}$) at 303 °C (Figure 3.5A - DTGA curve) (Kumari & Kishor, 2020). This degradation region was highlighted with a sharp exothermic peak at the maximum decomposition temperature evident in the DSC thermogram (Figure 3.5B). Several previous articles have reported similar results with the maximum decomposition temperatures for chitosan ranging between 280 - 340 °C depending on the measurement conditions, source of chitosan, and DD% (Corazzari et al., 2015; Kaya et al., 2014; Rodrigues de Mello et al., 2020; Siriprom et al., 2014). The residual mass remaining at the end of the analysis represents the thermal degradation products of chitosan, i.e. carbon and ash. No thermal events or peaks due to the glass transition of LCh could be identified from these thermograms.
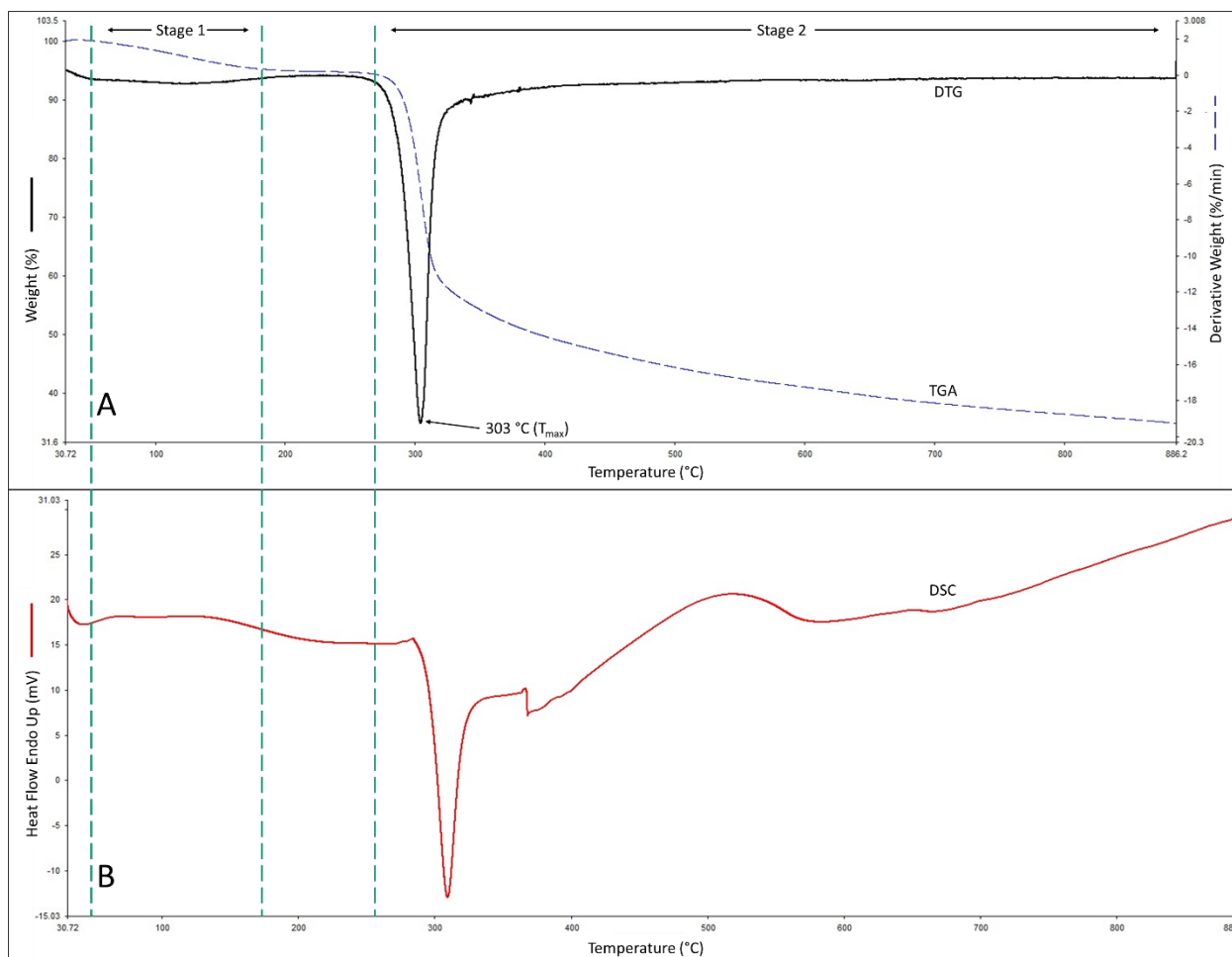
Figure 3.5: A) TGA and DTGA thermograms for lobster-shell chitosan; B) DSC thermogram for lobster-shell chitosan.

3.3.2 Development and Characterization of Solvent Cast Chitosan Films

All chitosan samples were fairly soluble in 1% (v/v) acetic acid (AA) and gave highly viscous, clear (free of undissolved particles) and transparent (HCh) to slightly yellowish (LCh and CCh) film-forming solutions (FFS - 2% w/v). The observable viscosity of the solutions was in the order of HCh > LCh > CCh, which followed the trend observed from their M_V values (Table 3.4). All three chitosan samples exhibited excellent film-forming ability, and the resultant solvent cast films were homogeneous, flexible and resembled clear plastic films (Figure 3.6B).
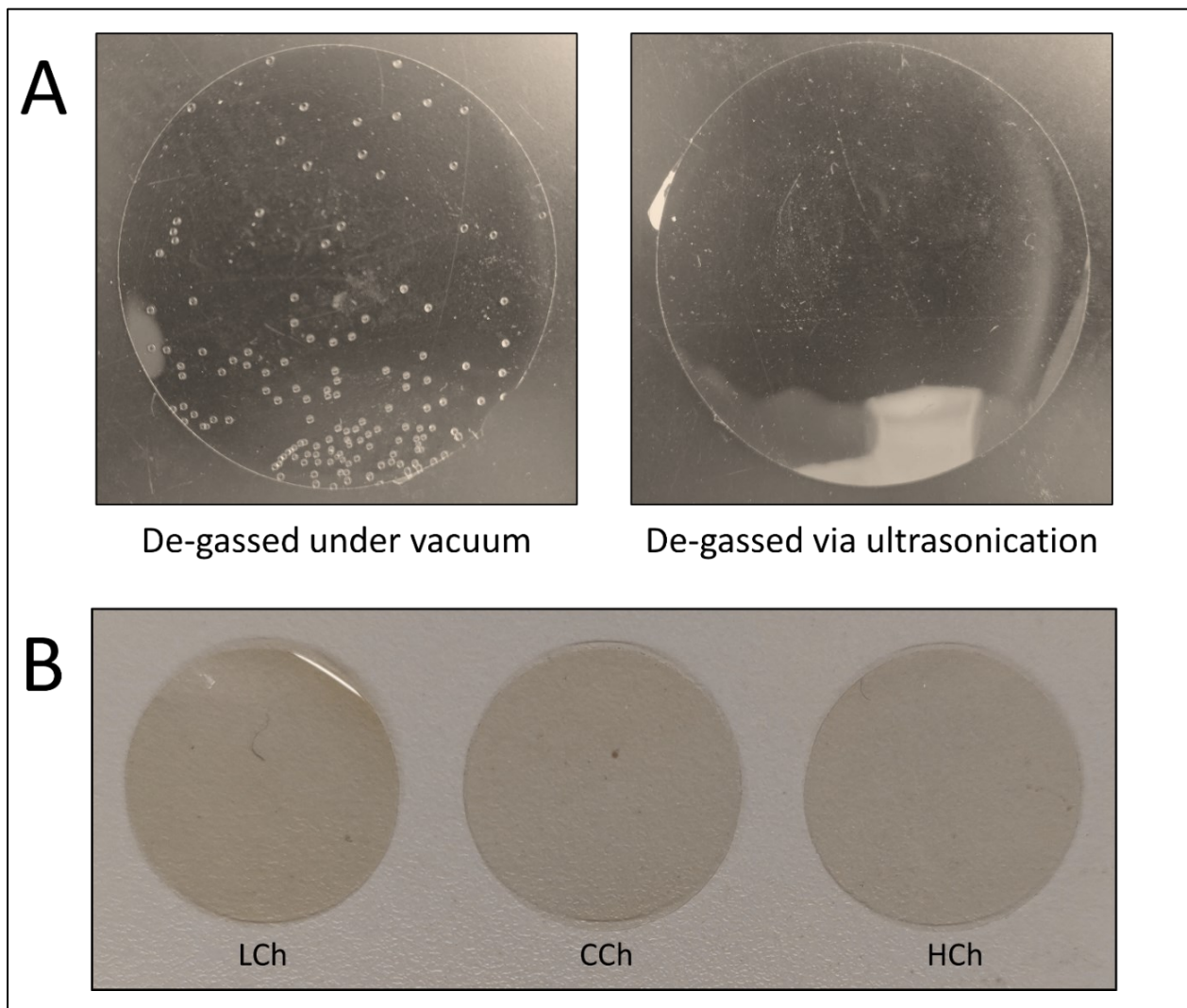
Figure 3.6: A) Solvent cast films obtained from chitosan solutions de-gassed either via application of vacuum or ultrasonication; B) Films prepared from 2% (w/w) solutions of lobster-shell chitosan (LCh), commercial crab-shell chitosan or high MW analytical grade chitosan (HCh).

De-gassing of chitosan solutions before casting is essential to remove solubilized air and prevent the formation of air bubbles in the films during the drying process. In this study, two methods for de-gassing, i.e. applied vacuum and ultrasonication, were evaluated. In contrast to previously reported studies, the application of vacuum over chitosan solutions was not sufficient to remove all solubilized air and resulted in a lot of tiny air bubbles present in the film matrix after drying (Figure 3.6A) (Srinivasa et al., 2004; Ziani et al., 2008). This may be attributed to the high

viscosity of our chitosan solutions that may have prevented the solubilized air from escaping under the vacuum. On the other hand, films obtained from the solutions treated with ultrasonication had no visible air bubbles present, indicating an adequate removal of solubilized air from the solutions (Figure 3.6A) (Baron et al., 2017). Moreover, these films were visually smoother and more homogeneous compared to the vacuum de-gassed films, and therefore only these films were pursued further for characterization. Among the three different chitosan films (LCh, CCh and HCh films), no apparent difference in their appearance could be identified apart from the slight variations in their colour (Figure 3.6B).

3.3.2.1 Thickness, equilibrated moisture content, degree of swelling and water solubility

Table 3.5 presents the values for thickness, equilibrated moisture content (EMC), degree of swelling (DS) and water solubility (WS) of films obtained from different chitosan samples (LCh, CCh and HCh). Film thickness is a critical parameter that influences several physicochemical properties of the films (mechanical, barrier and optical properties) and indicates the structural arrangement and overall packing of polymer chains in the film matrix. In the current study, the average thickness of the chitosan films ranged between $45 - 55$ µm. Films obtained from both LCh and HCh had a similar thickness and were significantly thicker than the CCh films ($p < 0.05$). As the amount of chitosan solution poured into each petri dish while casting was kept constant, and the moisture content of all three films was similar, this variation in thickness may be attributed to a difference in the DD% of chitosan samples. A significantly higher DD% (Table 3.3) of CCh compared to LCh and HCh may have contributed to a denser packing of CCh chains in the films due to a high degree of substitution of bulky acetyl groups ($-C=OCH_3$) with small free amino groups ($-NH_2$), resulting in increased intermolecular hydrogen bonding interactions (Nunthanid et al., 2001) and thus a thinner film.

Chitosan is a hydrophilic biopolymer that tends to have a high affinity towards water. As such, dried chitosan films absorb moisture from the surroundings until an equilibrium is reached, and this absorption depends on various factors, including the environmental temperature and RH, film processing conditions, additives and type of solvents (Homez-Jara et al., 2018; Nadarajah, 2005; Nunthanid et al., 2001; Ziani et al., 2008). The assessment of the equilibrated moisture content (EMC) of chitosan films is critical as the present moisture acts as a plasticizer and

significantly affects the mechanical and barrier properties of the films (Hamdi et al., 2019; Ziani et al., 2008). The three chitosan films analyzed here had comparable EMC lying between 16 to 19% (w/w db), and the differences in %DD of chitosan did not affect the moisture uptake of the films (Ziani et al., 2008). Similar values of EMC have been reported by Leceta, Guerrero, & de la Caba (2013) (15 – 19% w/w) and Ziani et al. (2008) (16 – 18% w/w) for 1% (w/w) neat chitosan films prepared under similar conditions in 1% acetic acid without the addition of plasticizer.

Table 3.5: Values for thickness, equilibrated moisture content, degree of swelling and water solubility values of the prepared chitosan films.

Films	Thickness (μm)	Equilibrated moisture content (%)	Degree of swelling (%)	Water solubility (%)
LCh	55.2 ± 6.6[A]	16.0 ± 0.8[A]	247 ± 10[A]	23.7 ± 0.5[A]
CCh	44.1 ± 7.9[B]	18.7 ± 0.6[B]	294 ± 6[B]	27.3 ± 0.6[B]
HCh	55.4 ± 4.4[A]	16.7 ± 0.5[A,B]	228 ± 8[A]	17.7 ± 1.1[C]

LCh: lobster-shell chitosan; CCh: commercial crab-shell chitosan; HCh: high MW analytical grade chitosan. The difference between the two mean values followed by the same letter in the same column is statistically insignificant (p > 0.05) as determined by Tukey's HSD test.

The degree of swelling (DS) is a measure of the ability of biopolymer-based films to absorb and hold water in their matrix and directly correlates with the presence of hydrophilic functional groups in their structure (Homez-Jara et al., 2018). All three investigated chitosan films showed excessive swelling in water (>200%) due to their high hydrophilicity, which is consistent with the literature (Cui et al., 2018; Homez-Jara et al., 2018; Mayachiew et al., 2010; Nunthanid et al., 2001). However, the DS of CCh films was significantly higher than LCh and HCh films, which could be justified by the presence of more hydrophilic groups in the CCh film matrix (due to higher %DD), enabling it to absorb and hold more water. Moreover, CCh also had comparatively lower MW (though not significantly lower), which may have also contributed to its higher DS (Nunthanid et al., 2001).

The integrity and stability of chitosan films during and after swelling can be crucial in dictating their applicability as a packaging material for liquid or high-moisture food products. In contrast to some of the previous studies where the neat/pure chitosan films either disintegrated or

showed extremely high DS and became highly fragile after swelling, films obtained in this study remained intact and showed relatively low DS due to the high MW of chitosan used, which provided improved structural integrity to the films (Krkić et al., 2012; Maria et al., 2016; Nadarajah, 2005; Nunthanid et al., 2001; Rodríguez-Núñez et al., 2014). Water solubility (WS) is another aspect of assessing the hydrophilicity of the chitosan films describing their resistance against water (Pereda et al., 2011). Once again, CCh with the highest DD% and comparatively lower MW among the three chitosan samples showed the highest WS ($p < 0.05$), which is in good agreement with the literature (Alves et al., 2019; García et al., 2015; Leceta, Guerrero, & de la Caba, 2013).

3.3.2.2 Light barrier properties and opacity value

Consideration of optical properties while designing edible food packaging is essential in terms of food preservation and customer acceptance. While packaging materials with high visual transparency are generally preferred to allow visual inspection of the contained products by the consumer, they should also be able to protect food products from photo-oxidation and degradation caused by high energy ultraviolet (UV) radiations. Therefore, an ideal edible packaging film should be opaque in the UV spectrum and transparent in the visible spectrum of light. As shown in Figure 3.7, all three chitosan films were found to be an effective barrier against UVB radiations (280-315 nm) as their transmittance was less than 35% in this region. On the other hand, films were relatively transparent in the visible region (transmittance > 70%), which is also apparent from the physical appearance of these films (Figure 3.6). These observations are in alignment with the literature (Hamdi et al., 2019; Hosseini et al., 2013; Leceta et al., 2013, 2015).

No significant correlation could be established between the DD% of chitosan and the appearance and transparency of their films. However, HCh films presented significantly lower opacity values ($p < 0.05$) compared to LCh and CCh in both UV (OP_{UV}) and visible (OP_{VIS}) spectrum of light (Table 3.6). This variation in the transparency of the films could be attributed to the HCh being analytical grade with a corresponding lack of impurities. An important point to note here is that LCh was not depigmented during the extraction process and had a light pink appearance (Figure 3.2) in contrast to the clear white colour of CCh and HCh. Nevertheless, the pigments did

not affect the appearance and transparency of the LCh films, thus justifying the omission of the depigmentation step.
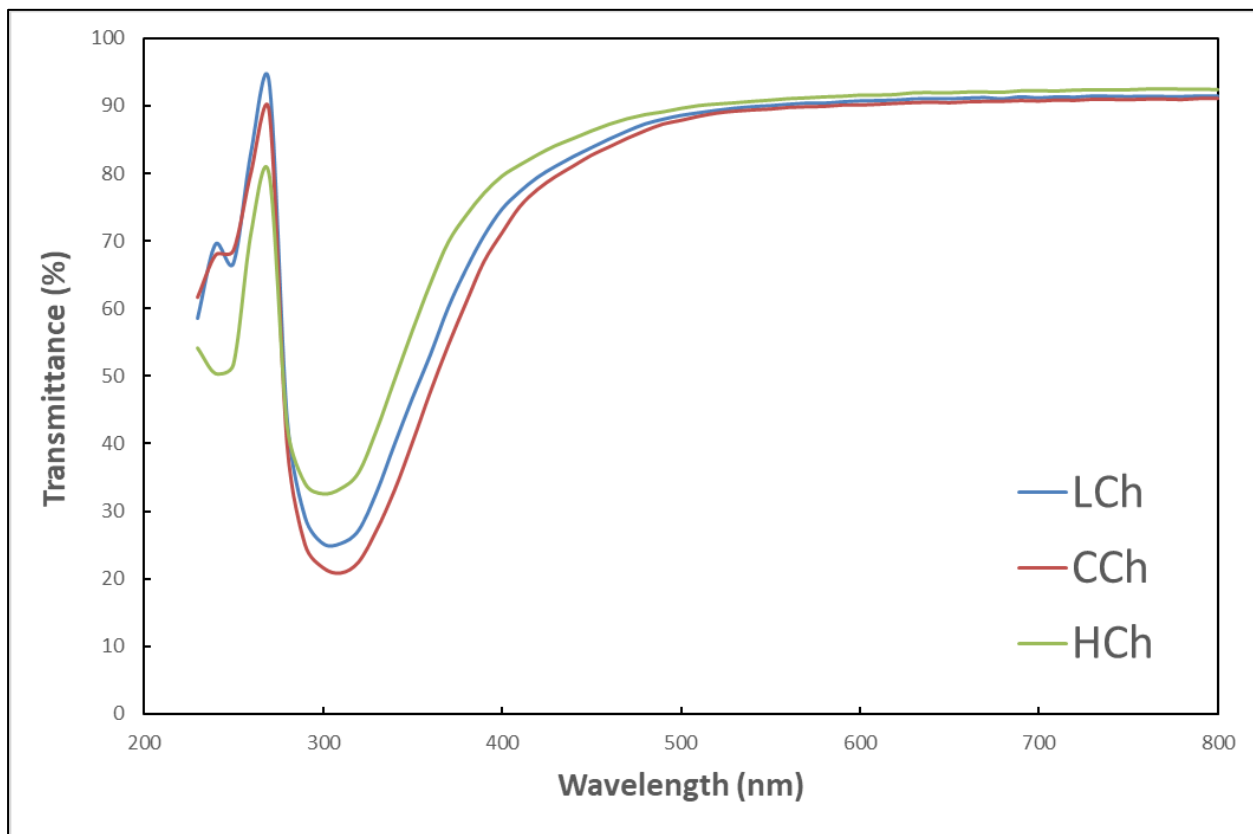
Figure 3.7: Light transmission (%) of films obtained from lobster-shell chitosan (LCh), commercial crab-shell chitosan (CCh) and high MW analytical grade chitosan (HCh).

Table 3.6: Values for film opacity observed in the UV (230-400 nm) and visible (400-800 nm) light spectrum for the prepared chitosan films.

Films	Opacity in the UV spectrum (OP_{UV}) (A.nm/mm)	Opacity in the visible spectrum (OP_{VIS}) (A.nm/mm)
LCh	807 ± 13[A]	395 ± 10[A]
CCh	834 ± 18[B]	419 ± 16[A]
HCh	742 ± 10[B]	344 ± 7[B]

LCh: lobster-shell chitosan; CCh: commercial crab-shell chitosan; HCh: high MW analytical grade chitosan. The difference between the two mean values followed by the same letter in the same column is statistically insignificant ($p > 0.05$) as determined by Tukey's HSD test.

3.3.2.3 Mechanical properties

In terms of food packaging, the applicability of edible films strongly depends on their mechanical properties. In general, edible films should possess adequate strength and flexibility in order to withstand different sorts of external stress and serve the containment function while maintaining their structural integrity. Figures 3.8, 3.9 and 3.10 show the average stress (σ) – strain (ε) curves obtained from the mechanical testing of all three chitosan films. It can be observed from these curves that all three chitosan films followed the typical deformation behaviour of ductile/plastic materials under an applied load. At a low value of strain (< 6%), chitosan films displayed Hookean behaviour (elastic region) where the stress increased rapidly with strain, and the slope of this region defined the elastic modulus of the films. Beyond this region (strain > 6%), the films showed plastic behaviour, and the stress increased more slowly with strain till the point of fracture. Similar observations of the stress-strain relationship for chitosan films were reported by Pereda et al. (2011) and Hosseini et al. (2013).
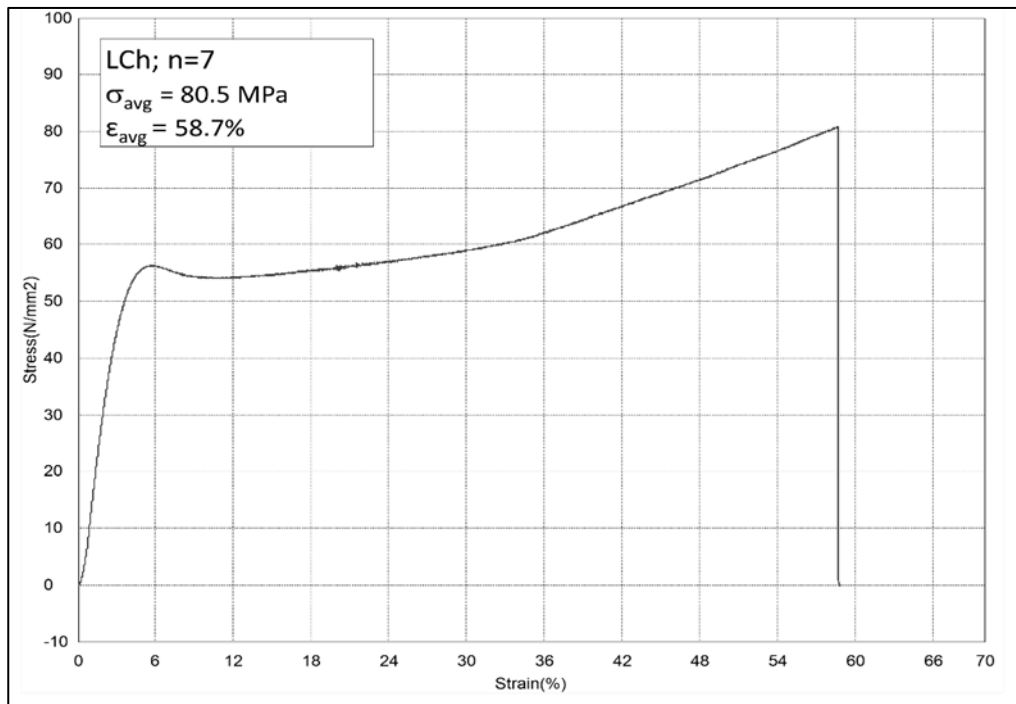
Figure 3.8: Average stress (σ_{avg}) – strain (ε_{avg}) curve for lobster-shell chitosan films (LCh). Here, n denotes the number of analyzed replicates.
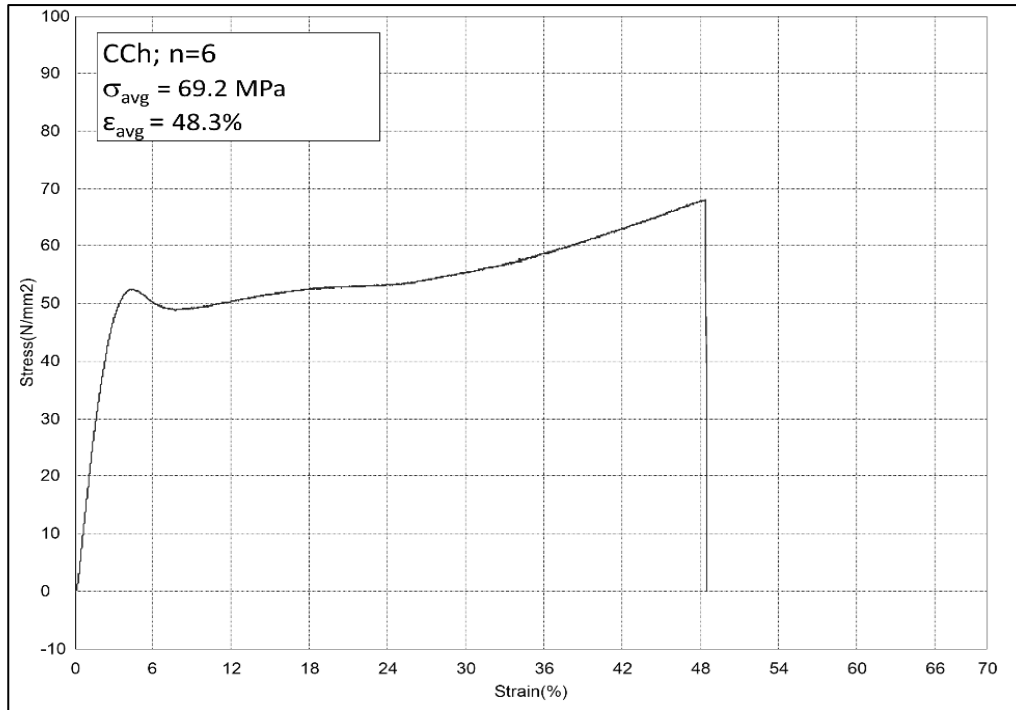
Figure 3.9: Average stress (σ_{avg}) – strain (ε_{avg}) curve for commercial crab-shell chitosan films (LCh). Here, n denotes the number of analyzed replicates.
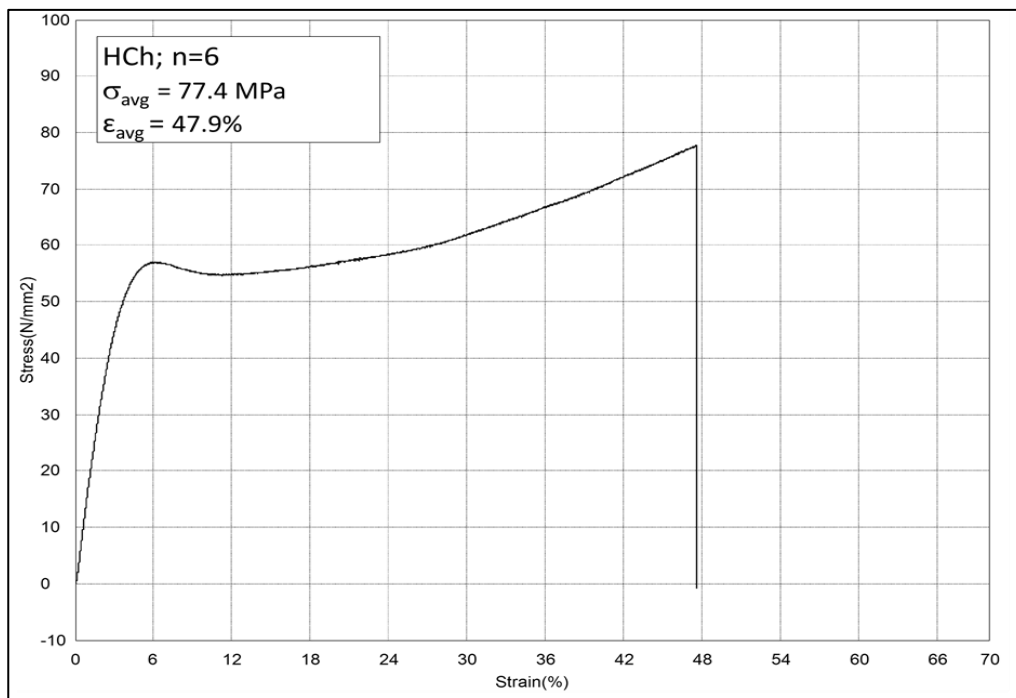
Figure 3.10: Average stress (σ_{avg}) – strain (ε_{avg}) curve for high MW analytical grade chitosan films (LCh). Here, n denotes the number of analyzed replicates.

Table 3.7 summarises the mechanical parameters, i.e., tensile strength (TS), elongation at break (%EAB) and elastic modulus (EM), of all three chitosan films obtained from their stress-strain curves. The films had high TS (70 - 80 MPa) and EM (1900 – 2100 MPa) and unexpectedly high EAB (48 – 58%), and despite the observable variations in the mean values, no significant differences were found among all mechanical parameters of the three films ($p > 0.05$). According to several previous reports, the TS of chitosan films increases with an increase in the molecular weight of chitosan (Nunthanid et al., 2001; Park et al., 2002; Rivero et al., 2009; Ziani et al., 2008). Nunthanid et al. (2001) suggest that this increase in TS occurs due to the formation of an entanglement network of high MW chitosan chains resulting in a higher resistance towards applied stress. In this instance, though CCh films had a lower TS value than LCh or HCh films, the difference in their molecular weight was not enough to provide a significant effect.

Table 3.7: Values for the mechanical properties of the prepared chitosan films.

Films	Tensile strength (MPa)	Elongation at break (%)	Elastic modulus (MPa)
LCh	80.5 ± 4.6[A]	58.7 ± 3.9[A]	1987 ± 217[A]
CCh	69.2 ± 5.9[A]	48.3 ± 12.1[A]	2053 ± 207[A]
HCh	77.4 ± 10.3[A]	47.9 ± 5.5[A]	2130 ± 76[A]

LCh: lobster-shell chitosan; CCh: commercial crab-shell chitosan; HCh: high MW analytical grade chitosan. The difference between the two mean values followed by the same letter in the same column is statistically insignificant ($p > 0.05$) as determined by Tukey's HSD test.

Data comparison with the literature for mechanical parameters of chitosan films is difficult as several factors, including properties of chitosan, type of solvent acid, drying and storage conditions, and additives like plasticizers, may heavily influence the tensile properties of the films (Homez-Jara et al., 2018; Nunthanid et al., 2001; Park et al., 2002; Rivero et al., 2009; Trung et al., 2006). Ziani et al. (2008) and Leceta, Guerrero, Ibarburu, et al. (2013) reported TS values of unplasticized 1% w/w chitosan films (prepared in 1% AA) in the range of 55 to 77 MPa, which were similar to the values observed in this study. However, the EAB values significantly differed among these two studies from 42 - 49% (Ziani et al., 2008) to 4 - 5% (Leceta, Guerrero, Ibarburu, et al., 2013). Comparing several other previous works, TS and EAB for unplasticized chitosan

films prepared in acetic acid have ranged between 39 to 150 MPa and 4 to 38%, respectively (Khouri, 2019; Kittur et al., 1998; Miranda et al., 2004; Nadarajah, 2005; Park et al., 2002). These significant variations in the mechanical properties of the chitosan films can be partially explained by the differences in the chitosan characteristics and the drying and storage conditions of the films.

The elastic modulus (EM) of a polymeric film is a measure of its ability to resist elastic deformation under applied stress and is equal to the slope of its stress-strain curve in the elastic region. The values of EM observed here (Table 3.7) indicated high film stiffness and are comparable to the previously reported values of unplasticized chitosan films prepared in acetic acid ranging between 1470 to 3300 MPa (Bégin et al., 1999; Khouri, 2019; Nadarajah, 2005). High standard deviations have been reported in the mechanical properties of the solvent cast chitosan films throughout the literature, including in the current study, and may suggest the high heterogeneity in the microstructure of the chitosan films.

3.3.2.4 *Water vapour barrier properties and surface hydrophobicity*

One of the primary functions of food packaging is to avoid, limit or control the transfer of moisture between a food product and its surroundings. Hence, the ability of an edible film to allow or resist permeation and transfer of water vapours through it, assessed by its water vapour transmission rate (WVTR) and water vapour permeability (WVP), is one of the most critical parameters that define its food packaging applications. The obtained values of WVTR, measured WVP (WVP$_{mea}$) and corrected WVP (WVP$_{cor}$) for all three chitosan films are shown in Table 3.8. Although the differences between the WVP/WVTR of LCh, CCh and HCh films were not significant ($p < 0.05$), an inverse correlation can be observed between these properties and the DD% of chitosan. Films obtained from CCh (highest DD%) showed the lowest WVTR/WVP values, followed by LCh and HCh (lowest DD%). This could be associated with the high packing density and low free volume in CCh films (refer to Section 3.3.2.1), which did not allow for a high degree of permeation of water vapours through the film matrix. Similar observations on the effect of %DD of chitosan on the WVP of chitosan-gelatin composite films have been previously observed by Liu et al. (2012). A wide range of values for WVP/WVTR of chitosan films have been reported in the literature due to differences in test conditions (RH gradient, temperature, air circulation) and film compositions (Homez-Jara et al., 2018; Hosseini et al., 2013; Yao et al., 2017;

Ziani et al., 2008). Alves et al. (2019) reported uncorrected WVP values measure at a 100% RH gradient for unplasticized chitosan films prepared in 1% acetic acid in the range of 0.46-0.57 g.mm/KPa.h.m^2, which are similar to the values observed in this study (Table 3.8).

Table 3.8: Values for the water vapour transmission rate (WVTR), measured WVP (WVP$_{mea}$), corrected WVP (WVP$_{cor}$) and surface contact angle (CA) for the prepared chitosan films.

Films	WVTR (g/h.m^2)	WVP$_{mea}$ (g.mm/kPa.h.m^2)	WVP$_{cor}$ (g.mm/kPa.h.m^2)	CA (°)
LCh	25.6 ± 1.1[A,B]	0.62 ± 0.06[A]	0.90 ± 0.09[A]	71.1 ± 0.6[A]
CCh	24.4 ± 0.9[B]	0.60 ± 0.04[A]	0.86 ± 0.08[A]	64.7 ± 1.4[B]
HCh	26.9 ± 0.5[A]	0.66 ± 0.03[A]	0.97 ± 0.04[A]	67.4 ± 0.4[A,B]

LCh: lobster-shell chitosan; CCh: commercial crab-shell chitosan; HCh: high MW analytical grade chitosan. The difference between the two mean values followed by the same letter in the same column is statistically insignificant (p > 0.05) as determined by Tukey's HSD test.

In general, edible films based on biopolymers, including chitosan films, are hydrophilic in nature and offer very high WVP (10 to 100 times) compared to hydrophobic olefin-based plastic films (Khouri, 2019; Nadarajah, 2005). Moreover, the WVP of a hydrophobic polymeric film is independent of its thickness and the driving force, i.e., the vapour pressure gradient across the film (Khouri, 2019; Miranda et al., 2004). However, the WVP of hydrophilic films generally shows a positive exponential correlation with the relative humidity (RH) gradient and linear correlation with the thickness of the films (Bertuzzi et al., 2007; McHugh et al., 1993). The equilibrium RH at the inner surface of the hydrophilic films (exposed to higher RH conditions) increases exponentially with their thickness due to the increased mass transfer resistance and complex non-linear nature of their sorption isotherms (McHugh et al., 1993). This results in an increased effective vapour pressure gradient across the two surfaces of the films, which in turn increases their WVP. Rivero et al. (2009) observed that the WVP of chitosan films remained independent of film thickness for thinner films (up to 60-70 μm) and then linearly increased with the thickness. Therefore, in this study, the thickness of the tested films was kept in the range of 40 – 60 μm to minimize errors in the WVP values arising from thickness variations.

The vapour barrier properties of hydrophilic films are also strongly influenced by the air gap between the film surface and water inside the test cup. This layer of stagnant air offers resistance to mass transfer developing a partial pressure gradient between the mounted film and water. This results in an underestimation of WVP (measured by the standard ASTM method) by up to 65% (McHugh et al., 1993). Thus, the measured WVP (WVP$_{mea}$) values were corrected (WVP$_{cor}$) to account for the effect of still air according to the correction method described by ASTM standard E96/96-16 (ASTM Internation, 2016). The values of WVP$_{cor}$ obtained in this study were significantly higher (≈40%, $p < 0.05$) than WVP$_{mea}$, demonstrating the implications of the stagnant air gap effect in the determination of water vapour barrier properties for chitosan films.

In terms of surface contact angle (CA), all three films presented relatively similar values (65 - 71°) with slight variations that can be explained by minor surface imperfections (Table 3.8). The contact angle created by water or any other polar solvent on the surface of polymeric films indicates their degree of superficial hydrophilicity or hydrophobicity (Leceta, Guerrero, & de la Caba, 2013). Moreover, the final state of the solvent droplet on the film provides information regarding their surface wettability which can be a critical parameter in designing edible films for packaging liquid or high-moisture food products (Aguirre-Joya et al., 2018; Leceta, Guerrero, & de la Caba, 2013). Generally, with an increase in the hydrophilic nature of the film surface, the interaction of polar solvents with the surface increases resulting in a decrease in CA (Aguirre-Joya et al., 2018). Although we hypothesized that a higher DD% would make the surface of chitosan films more hydrophilic due to the presence of more free -NH$_2$ groups, our observations indicated no correlation between %DD of chitosan and the surface hydrophobicity of their films.

In this study, ethylene glycol was used as the polar solvent instead of distilled water for measuring CA of chitosan films as the use of water droplets caused instantaneous swelling of films resulting in skewed CA measurements (Pereda et al., 2012). Typically, a water contact angle (WCA) of more than 65° represents a hydrophobic surface (Córdoba & Sobral, 2017). Previous studies have reported WCA for unplasticized chitosan films in the range of 116 to 72.5°, indicating the hydrophobic nature of their surface (Ghanem & Katalinich, 2005; Khouri, 2019; Leceta, Guerrero, & de la Caba, 2013; Leceta et al., 2015). Although ethylene glycol is less polar than water, the CA of ethylene glycol tends to be less for a given surface due to its low surface tension

and high spreadability (Katalinich, 2001). Hence, the obtained results of CA were comparable to the literature.

3.4 SUMMARY AND CONCLUDING REMARKS

The observations from this chapter established the applicability of crude chitosan extracted from the shells of Atlantic lobsters in the production of edible films for potential food packaging applications. The extracted crude chitosan showed structural, thermal and film-forming characteristics similar to commercially available or analytical grade chitosan. The crude chitosan also produced homogeneous, flexible and robust solvent cast films with physicochemical properties comparable to the reported literature.

While preparing chitosan film-forming solutions, ultrasonication was a more effective technique for de-gassing and homogenization in contrast to the widely reported vacuum application. The unplasticized chitosan-acetate films obtained in this study were highly transparent but acted as an effective UV barrier and presented exceptional strength and stretchability. In addition, the films offered a high degree of swelling and high vapour permeation but had low water solubility and a relatively hydrophobic surface. Small changes in the deacetylation degree of chitosan significantly influenced the overall hydrophilic nature of the films; however, no observable effect was found on their WVP and CA. The pigments that remained in the LCh after extraction did not affect any physicochemical characteristics of the films and thus eliminated the need for depigmentation/bleaching of chitosan for edible film applications. This study can be regarded as a proof of concept and paves the way for exploring other processing and compositional factors to modify or improve the functionality of LCh based edible films.

CHAPTER 4

EVALUATION OF PLASTICIZED LOBSTER-SHELL CHITOSAN AND COMPOSITE FILMS

4.1 INTRODUCTION

Single component biopolymeric films, commonly polysaccharide or protein-based, almost always offer some associated disadvantages that significantly limit their applications (Aguirre-Joya et al., 2018; Debeaufort & Voilley, 2009; Falguera et al., 2011; Pavlath & Orts, 2009). Stand-alone chitosan films are no exception, as observed from the results of Chapter 3. While chitosan films can offer excellent strength and integrity with high transparency and resistance towards UV radiations, their flexibility and stretchability are often inadequate (Wang et al., 2017, 2021). Moreover, the hydrophilic nature of chitosan renders these films highly permeable to moisture and sensitive to environmental humidity, which in turn significantly impacts their mechanical and physical properties (Cerqueira et al., 2012a; Pereda et al., 2012). Therefore, incorporating and blending other bio-components that can interact with chitosan at a molecular level and provide functional improvements without significantly altering any desirable properties or production costs could be necessary for the commercialization of chitosan-based edible films (Ansorena et al., 2018; Wang et al., 2017).

Fish-gelatin is a potential blending biopolymer for chitosan films due to its excellent compatibility with chitosan and its ability to improve the mechanical, physical and thermal properties of the films (Hosseini et al., 2013; Yao et al., 2017). In addition, its cheap availability can reduce the overall cost of film production. On the other hand, incorporating hydrophobic components in the chitosan film matrix, such as edible oils, can help reduce their hydrophilicity and improve resistance towards moisture sensitivity and permeation (Cerqueira et al., 2012a; Pereda et al., 2012). Therefore, in order to improve the functionality of lobster-shell-derived chitosan films, the present study aimed to incorporate fish-gelatin and sunflower oil into these films and evaluate their effect on the structural, thermal and physicochemical properties of the resultant films. Moreover, the study also aimed at evaluating the effect of drying temperature and

polymer concentration on the film properties. Although several authors have reported on chitosan-gelatin composite films in the past, limited literature is available utilizing fish-gelatin as a blending polymer with chitosan. Furthermore, no comprehensive reports are available on the effect of edible oil incorporation and drying temperature on chitosan-fish gelatin composite films, and none involving lobster-shell-derived chitosan, which motivated the present study.

4.2 MATERIALS AND METHODS

4.2.1 Materials and Reagents

The chitosan utilized in this study was derived from Atlantic lobster shell-waste (refer to Chapter 3, Section 3.2.2). Gelatin derived from cold-water fish skin was purchased from Sigma-Aldrich (ON, Canada), and glycerol (proteomics grade) was purchased from BDH® VWR Chemicals (USA). Sunflower oil (100%, Kernel brand) was procured from the local market. All reagents utilized in this study were of analytical grade and were purchased from either Sigma-Aldrich (ON, Canada), Fisher Scientific (ON, Canada) or BDH® VWR Chemicals (USA).

4.2.2 Development of Lobster-Shell Chitosan-based Edible Films

4.2.2.1 Experimental design

Chitosan or chitosan composite edible films obtained from five different formulations of film-forming solutions (FFS) and prepared at three different drying temperatures (37, 60 and 80 °C) were analyzed in this study (Table 4.1). The obtained films were evaluated for their structural, thermal and physicochemical properties depending on their formulations and drying temperatures.

Table 4.1: Investigated formulations of lobster-shell chitosan-based film-forming solutions.

Formulations	Lobster-shell chitosan (% w/v sol)	Fish gelatin (%w/v sol)	Sunflower oil (% w/w polymer)	Glycerol (% w/w polymer)
1%LCh	1	-	-	20
2%LCh	2	-	-	20
LCh-O	2	-	10	20
LCh-Ge	1	1	-	20
LCh-Ge-O	1	1	10	20

LCh: lobster-shell chitosan; Ge: fish gelatin; O: sunflower oil

4.2.2.2 *Preparation of films*

The procedure for preparing chitosan-based edible films (Figure 4.1) was adopted from Haghighi, Biard, et al. (2019) with various modifications. For preparing fish-gelatin (Ge) solution (2%, w/v), Ge powder along with plasticizer (glycerol at 20%, w/w polymer) was first allowed to swell in distilled water at 4 °C for 30 mins followed by continuous stirring (300 rpm) at 60 °C for an hour. Lobster-shell chitosan (LCh) FFS (2%, w/v or 20 mg/mL) were prepared by dissolving LCh powder and glycerol (20%, w/w polymer) in aqueous acetic acid (1%, v/v). The solution was continuously stirred (300 rpm) for three hours at 60 °C and filtered while still hot through a 25 μm wire mesh using vacuum filtration to remove impurities. The resultant 2%LCh FFS was mixed with aqueous acetic acid (1%, v/v) at a 1:1 ratio to get the 1%LCh FFS. LCh-Ge blend was obtained by mixing equal amounts of 2% solution of LCh and Ge. To prepare FFS with sunflower oil (10%, w/w polymer), a mixture of oil and Tween-20 (30%, w/w of oil) was added to the LCh or LCh-Ge blend solutions as required and stirred for 15 mins. All the above-prepared FFS were homogenized and degassed via ultrasonication using a probe sonicator (VCX 750, Vibra-CellTM, Sonics and Materials, USA) for 10 mins at 40% amplitude and 15-second pulse.

Approximately 0.25 g/cm^2 of each sonicated FFS was poured into polystyrene Petri dishes (100x15 mm, FisherbrandTM, USA) and dried at either 37 °C for three days in a water-jacketed incubator (Forma Scientific 3250, USA), 60 °C for 12 hours in a hot-air oven (Hermatherm, Thermo Scientific, USA) or 80 °C for 6 hours in the same oven. The dried films were carefully

peeled off from the dishes and were conditioned at RT (21 ± 2 °C) in a desiccator with a saturated magnesium nitrate solution (52 - 54% RH) for at least three days prior to any analysis.
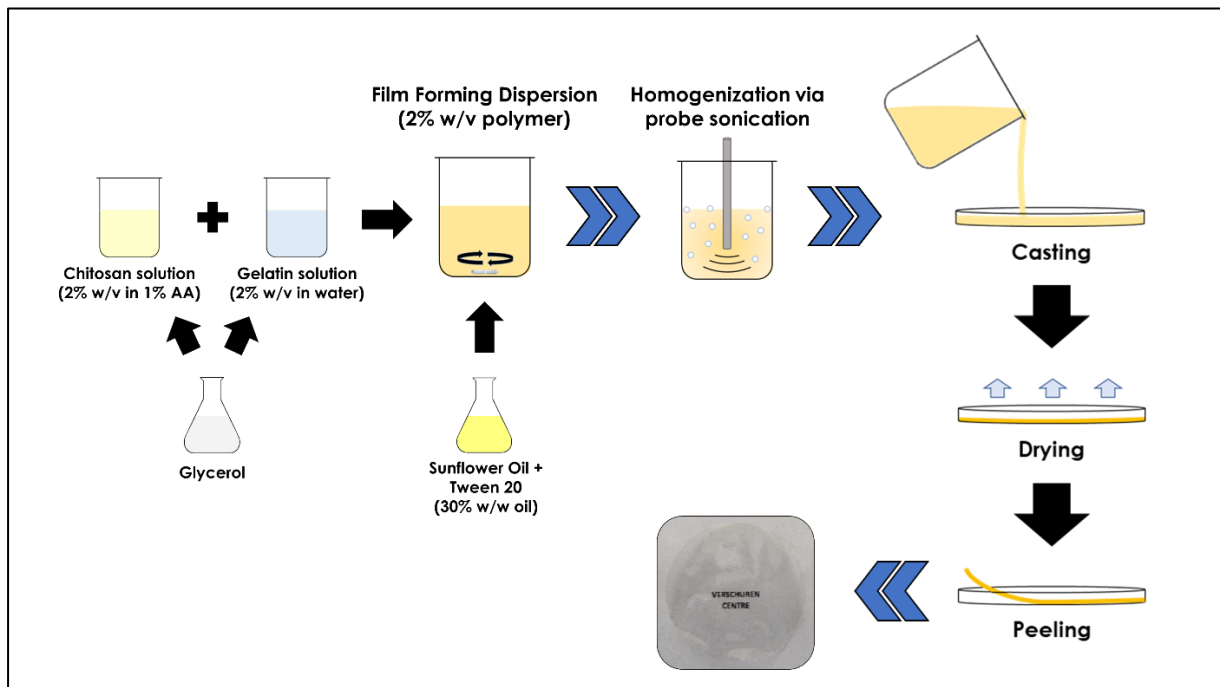
Figure 4.1: Pictorial representation of the procedure for developing chitosan composite films.

4.2.3 Structural and Thermal Characterization of the Films

4.2.3.1 FT-IR spectroscopy

Analysis of molecular interactions between different components of the plasticized chitosan and composite films prepared at different drying temperatures was performed by FT-IR spectroscopy (Spectrum Two, PerkinElmer, USA) using an attenuated total reflection (ATR) accessory (MIRacleTM Single Reflection ATR, PIKE Technologies, USA) with a diamond ATR crystal. The analysis was performed using a method described by (Leceta et al., 2015) with slight modifications. Prior to the analysis, the samples were conditioned at 52-54% RH for at least three days. Measurements were taken for the lower surface of the films (the surface that was in contact with the Petri dish) to avoid any variations in spectral intensities due to surface imperfections. The

final spectra for each sample was an aggregate of 32 scans recorded at a resolution of 4 cm^{-1} between 4000 cm^{-1} to 500 cm^{-1}. At least three replicates were run for each sample type.

4.2.3.2 X-ray diffraction spectroscopy

The arrangement of polymer chains and the occurrence of ordered structures in the chitosan-based films were analyzed using an X-ray diffractometer (D8 Advance, Bruker AXS Germany) equipped with a CuKα$_1$ radiation source (λ = 1.54 Å) operating at an applied voltage and current of 40 kV and 40 mA. The XRD patterns were recorded in ambient conditions between 5 and 40° (2θ) with a step size of 0.1° and a scanning rate of 5 seconds/step. The film samples were conditioned for at least three days prior to recording their diffractograms. The relative crystallinity of the samples was estimated from the diffractograms as per the following equation described by Khouri (2019).

$$Crystallinity\ index\ (CrI) = \frac{A_c}{A_c + A_a} \times 100\ \%$$
(Eq. 4.1)

Here, A_c and A_a represent the area under the crystalline and amorphous regions of the diffractograms, respectively.

4.2.3.3 Thermogravimetric analysis

The thermal stability and degradation behaviour of chitosan and composite films were determined by thermogravimetric analysis (TGA) using a simultaneous thermal analyzer (STA 8000, PerkinElmer, USA). The films were dried at 60 °C for 48 h prior to the analysis, and their thermograms were recorded from 30 to 500 °C (10 °C/min) under a constant nitrogen gas purge (20 mL/min). The weight of the samples taken for analysis ranged between 10 and 20 mg, and at least duplicate runs were performed from each film type.

4.2.4 Physicochemical Characterization of the Films

In order to evaluate the effect of FFS composition and drying temperature on their physicochemical parameters, all prepared films were characterized based on their physical (thickness, moisture content, water-solubility, surface hydrophobicity), optical (UV and visible opacity), mechanical (tensile strength, elongation at break and elastic modulus), and barrier (water vapour permeability) properties by following the methods and using the equipment previously described in Chapter 3 (refer to Section 3.2.5).

4.2.5 Statistical Analysis

Data collected from each physicochemical test were statistically analyzed using single-factor analysis of variance (ANOVA) in Minitab 19 Statistical Software. Comparison of the means was performed by employing posthoc Tukey's HSD test, and a p-value of less than 0.05 was considered statistically significant. All results are reported as mean ± standard deviation.

4.3 RESULTS AND DISCUSSION

4.3.1 Qualitative Observations

The prepared fish-gelatin solution (2% w/v) was highly transparent and significantly less viscous than the chitosan solution at the same concentration. Additionally, both solutions were fairly miscible in each other and provided clear homogeneous FFS by simple stirring. Oil incorporated FFS were bright white, homogeneous and opaque in appearance (post-sonication), suggesting a high degree of emulsification. These FFS emulsions remained stable without any indication of separation for more than six months (visual observations). Although chitosan in itself is considered an effective emulsifier due to its ability to bind lipids through hydrophobic interactions, an additional emulsifier (Tween-20) was utilized in this study as per previously reported procedures (Córdoba & Sobral, 2017; Gutiérrez, 2017; Valenzuela et al., 2013) to ensure high emulsion stability during evaporation and drying of the solvent (water).

Figure 4.2 presents the photograph of the chitosan and composite films prepared at different drying temperatures. The films obtained at low-temperature drying (37 °C) were visually more homogeneous and smooth in comparison to the films obtained at 60 or 80 °C, with a few air bubbles appearing in some films (1%LCh and LCh-Ge dried at 80 °C), which may be attributed to the rapid evaporation of the solvent. All films presented good structural integrity and were easy to handle and process during their characterization. However, 1%LCh and LCh-Ge films were significantly thinner (discussed later in Section 4.3.3.1) than the other films and were particularly hard to peel off from the Petri dishes. On the contrary, oil incorporated films (LCh-O and LCh-Ge-O) separated from the Petri dishes by themselves, indicating a slightly lubricated film surface.
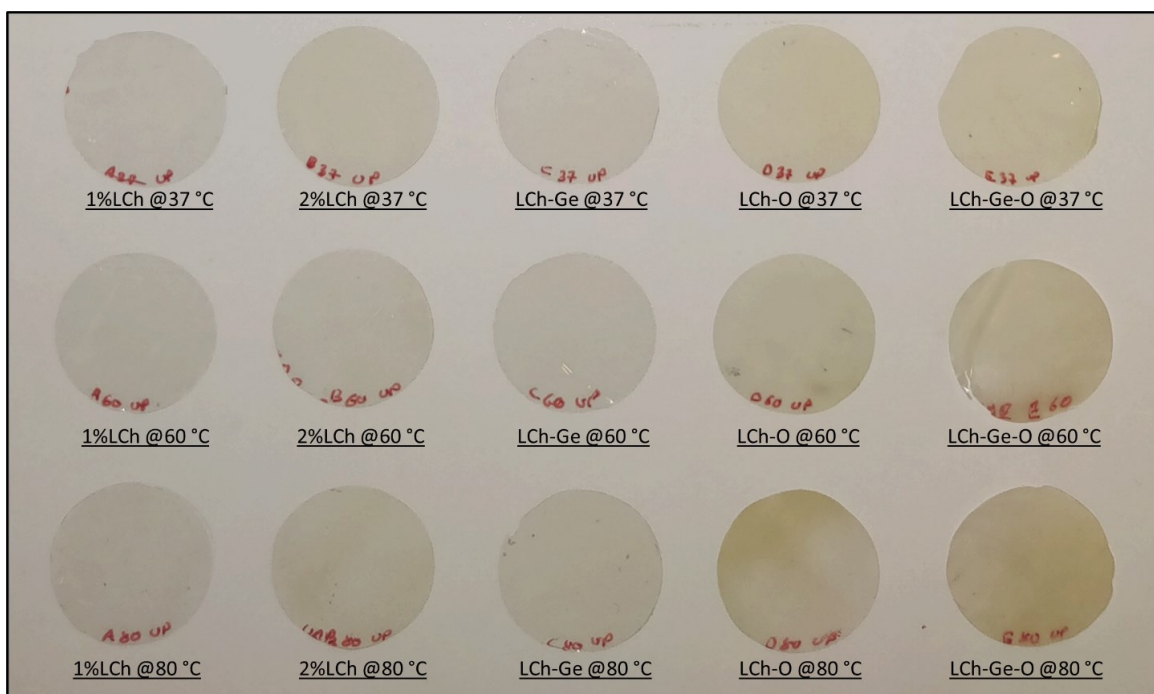
Figure 4.2: Chitosan and composite films prepared at low (37 °C) and high (60 and 80 °C) drying temperatures. LCh: lobster-shell chitosan; Ge: fish gelatin; O: sunflower oil.

4.3.2 Structural and Thermal Properties of Lobster-Shell Chitosan-based films

4.3.2.1 *FT-IR spectroscopy*

FT-IR spectroscopy was performed to characterize the intermolecular interactions between different components of the composite films and the effect of drying temperature on those interactions. Figure 4.3 presents the FT-IR spectra of all five tested film formulations prepared at 37 °C. As reported by previous authors, stand-alone plasticized chitosan films (1% and 2%LCh) showed characteristic absorption bands at approximately 1633 cm^{-1} (amide I band due to C=O stretching), 1548 cm^{-1} (amide II band superimposed with NH^{3+} absorption band), and 1335/1254 cm^{-1} (amide III band due to C=N stretching and N-H bending) (Fernandez-Saiz et al., 2009; Pereda et al., 2011; Talón et al., 2017). The broad absorption band between 3200 and 3500 cm^{-1} with a peak at 3259 cm^{-1} was attributed to the hydrogen-bonded N-H and O-H stretching vibrations (Cui et al., 2018; Haghighi, Biard, et al., 2019; Homez-Jara et al., 2018; Martínez-Camacho et al., 2010; Talón et al., 2017). Two small peaks at 2927/2874 cm^{-1} were assigned to asymmetric and

symmetric CH_2/CH_3 stretching vibrations (Córdoba & Sobral, 2017; Haghighi, Biard, et al., 2019; Mehdizadeh et al., 2020). The absorption peak at 1406 cm^{-1} was associated with the carboxylate groups (linked with the antimicrobial activity of chitosan films) (Fernandez-Saiz et al., 2009; Leceta, Guerrero, Ibarburu, et al., 2013). Furthermore, absorption peaks between 850 and 1200 cm^{-1}, i.e. 898, 926, 1024, 1061 and 1152 cm^{-1}, can be associated with the C–O, C–O–C, and C=C stretching vibrations form the saccharide structure of chitosan (Cui et al., 2018; Haghighi, Biard, et al., 2019; Homez-Jara et al., 2018; Liu et al., 2019; Pereda et al., 2011; Yao et al., 2017; Yin et al., 2005). Some of these peaks (926 and 1061 cm^{-1}) have also been attributed to the absorption bands of glycerol (plasticizer) (Leceta, Guerrero, Ibarburu, et al., 2013). Polymer concentration of the FFS did not significantly affect the position of the absorption bands (Homez-Jara et al., 2018); however, the intensity of the overall FT-IR absorption spectra was significantly lower for 1%LCh film, which could be due to the significantly lower thickness of these films (discussed later in Section 4.3.3.1) resulting in less pressure on the ATR crystal.

The obtained spectra of LCh-Ge composite films were very similar to that of LCh films but had distinct variations in the position and intensities of some of the absorption bands. LCh-Ge films showed a significant increase in the intensity of the amide I band (1639 cm^{-1}), which can be partially explained by the presence of β-sheet secondary structure of gelatin in the film matrix (Haghighi, De Leo, et al., 2019) but may also indicate electrostatic interactions between the carboxyl groups and amino groups of Ge and LCh forming polyelectrolytic complexes (PECs) as suggested by (Pereda et al., 2012). The shift of the amide I peak from 1633 cm^{-1} (LCh film) to 1639 cm^{-1} can be attributed to the conformational changes in the secondary structure of Ge, further demonstrating its interactions with LCh (Haghighi, De Leo, et al., 2019; J. Xu et al., 2020). The absorption peak attributed to the amide II vibrations also shifted in the composite films but to a lower wavenumber (from 1548 to 1537 cm^{-1}). Generally, a shift of IR bands to a lower wavenumber is indicative of increased interactions due to hydrogen bonding (Liu et al., 2012). Therefore the shift of the amide II band further suggests strong hydrophilic interactions between the two polymers. Other subtle changes in the spectra of LCh-Ge, such as increased intensity and shift of broad N-H and O-H stretching vibrational bands (between 3200 and 3500 cm^{-1}), and minor spectral differences in the wavelengths between 1110 and 750 cm^{-1}, can be attributed to the superimposed characteristic bands of Ge.
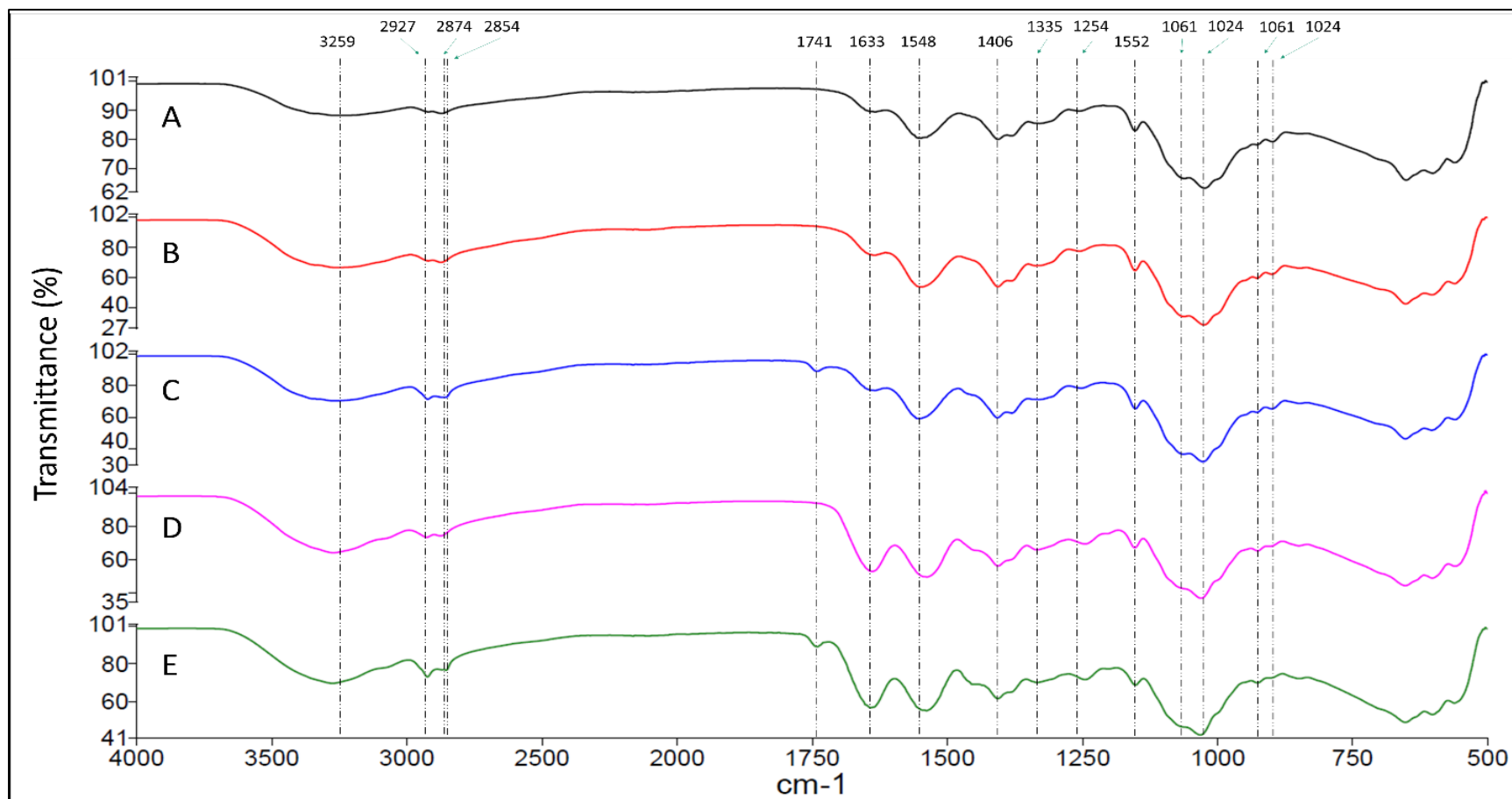
Figure 4.3: FT-IR spectra of A) 1%LCh; B) 2%LCh; C) LCh-O; D) LCh-Ge and E) LCh-Ge-O films prepared at 37 °C. LCh: lobster-shell chitosan; Ge: fish gelatin; O: sunflower oil.

The incorporation of sunflower oil in both LCh and LCh-Ge films resulted in the appearance of two new peaks at 2854 or 2857 cm^{-1} and 1741 cm^{-1} in the spectra of composite films (LCh-O and LCh-Ge-O). While the peak at 2854 cm^{-1} may be attributed to the asymmetric stretching of aliphatic groups (CH$_2$) contributed by sunflower oil, the peak at 1741 cm^{-1} represents C=O stretching vibrations from the carbonyl radicals of the ester group of triglycerides, confirming the presence of oil in the film matrix (Cerqueira et al., 2012a; Liang et al., 2013). Similar results have been reported by Valenzuela et al. (2013) for quinoa protein-chitosan composite films incorporated with sunflower oil. Furthermore, the broad absorption band of N-H and O-H stretching vibrations decreased in intensity and shifted to a higher frequency by a small degree for both composite films (from 3258 to 3269 cm^{-1} for LCh-O and 3275 to 3278 cm^{-1} for LCh-Ge-O). This may indicate a decrease in hydrogen bonding interactions and the presence of electrostatic and/or hydrophobic interactions of chitosan's amino groups with fatty acid carboxylates (electrostatic interactions) or chitosan's acetyl groups with the aliphatic chains of fatty acids (hydrophobic interactions) (Valenzuela et al., 2013). Simultaneous occurrence of both types of interactions between chitosan and oils have been previously reported in the literature (Dimzon et al., 2013; Lozano-Navarro et al., 2020; Wydro et al., 2007). A small but significant shift of amide II and amide III vibration bands from 1548 to 1552 cm^{-1} and 1254 to 1251 cm^{-1} and a reduction in their intensities in the spectra of LCh-O films may further imply the existence of such interactions. However, no such shifts in amide bands were observed for LCh-Ge-O films, which may be correlated with the lower concentration of chitosan in these films (50% of LCh-O films).

Figure 4.4 shows the comparative FT-IR spectra of chitosan and composite films prepared at 37, 60 or 80 °C (except for the spectra of 1%LCh films as they were similar to 2%LCh films). While comparing films prepared at different drying temperatures, no significant differences were observed in the spectra of LCh or LCh-O films except for some subtle peak shifts and intensity differences that may be associated with minor changes in the intermolecular interactions between film components and Maillard reaction between carbonyl and amine groups of chitosan during high-temperature drying (Leceta, Guerrero, Ibarburu, et al., 2013; Singh et al., 2015). This could also be the reason behind a noticeable increase (visual observation) in the yellowness of these films (Figure 4.2).
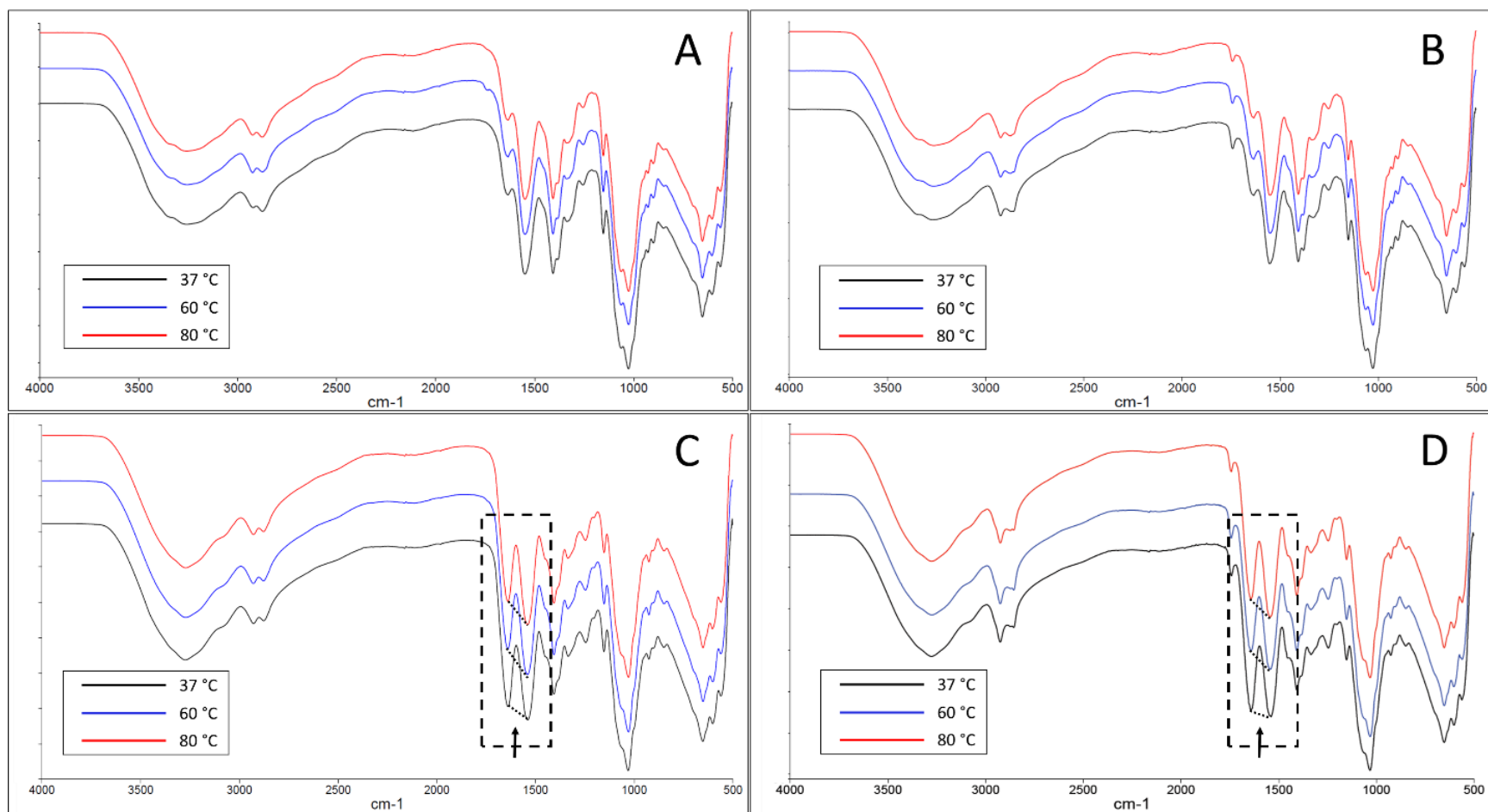
Figure 4.4: Comparative FT-IR spectra of A) 2%LCh; B) LCh-O; C) LCh-Ge and D) LCh-Ge-O films prepared at 37, 60 or 80 °C. Dotted lines in C) and D) show a change in relative intensities of amide I and II bands. LCh: lobster-shell chitosan; Ge: fish gelatin; O: sunflower oil.

On the other hand, along with these subtle shifts, LCh-Ge and LCh-Ge-O films showed a significant decrease in the relative intensities (ratio) of amide I and II bands (1639 and 1537 cm^{-1}) at high drying temperatures. Amide I band of proteins is particularly sensitive to the changes in their secondary structure (Jahit et al., 2016). Therefore, these variations in band intensities may suggest considerable changes in the hydrogen bonding and electrostatic interactions between gelatin, chitosan and glycerol when dried at higher temperatures. However, no literature references could be found to support this line of reasoning.

4.3.2.2 X-ray diffraction spectroscopy

The ordered arrangement or packing of polymer chains (chitosan/gelatin) in the microstructure of edible films is one of the primary factors affecting most of their physicochemical and thermal properties (Khouri, 2019; Nunthanid et al., 2001; Prateepchanachai et al., 2019). Therefore, X-ray diffraction spectroscopy was performed to determine the crystalline structures of chitosan films and understand the effect of different additives and drying temperatures on the overall crystallinity of the films. The diffractograms for chitosan and composite films are shown in Figure 4.5, and the crystallinity index (CrI) of the films indicating a relative change in their crystallinity with a change in film composition or drying temperature is presented in Table 4.2. All film samples showed a broad diffraction band between 15 and 25°, associated with the amorphous structure of the films suggesting the semicrystalline nature of chitosan-based films (Pereda et al., 2011).

For plasticized chitosan films (2% LCh @37 °C), three distinct crystalline diffraction peaks were observed at 8.7°, 11.6° and 18.8° along with a narrowing of the amorphous band at around 20.1°, which are characteristic of chitosonium-monocarboxylate salt crystals (Kumirska et al., 2010; Pereda et al., 2011). However, these crystalline peaks were not observed for 1%LCh films (reflected in their CrI), and the overall intensity of their diffractograms was approximately half, compared to 2%LCh films. Although the reason behind these observations is unclear, the low polymer concentration in the FFS (affecting the molecular arrangement during the evaporation) and significantly lower thickness of these films (affecting the XRD analysis itself) may have contributed to these changes. Two small XRD peaks at around 24 and 38.5° were also observed

for every tested film without exception; however, no literature reference could be found to identify these peaks.

LCh-Ge films showed similar diffraction peaks to that of LCh films but had changes in their relative intensities. While the crystalline peak of 2%LCh film (@37 °C) at 8.7° shifted to 8.5° for LCh-Ge and showed a significant increase in its intensity, peaks at 11.6° and 18.8° decreased in intensities. The former change can be explained by the superimposition of the characteristic crystalline peak of gelatin chains arranged in a triple helix collagen-like structure (Liu et al., 2012; Pereda et al., 2011; Qiao et al., 2017). On the other hand, the latter is a clear indication of interactions between chitosan and gelatin polymer chains which do not allow for a high degree of ordered packing, as suggested by Pereda et al. (2011) and Prateepchanachai et al. (2019). The electrostatic interactions between amino groups of LCh and carboxyl groups of Ge (PEC formation) led to the breakage of intermolecular hydrogen bonds between amino and hydroxyl groups of chitosan (Prateepchanachai et al., 2019). This results in a more amorphous film structure evident from the decrease in its CrI from 25.8% (2%LCh @37 °C) to 18.4% (LCh-Ge @37 °C).

Films with sunflower oil also had a reduced CrI compared to films without oil (Table 4.2). Both LCh-O and LCh-Ge-O films (@37 °C) showed an apparent decrease in the intensity of crystalline peak at 11.6° while no peaks could be observed at 8.7°and 18.8°. Valenzuela et al. (2013) and Sugumar et al. (2015) also reported a similar decrease in film crystallinity for chitosan films incorporated with sunflower oil and eucalyptus oil, respectively. These results may again indicate the interactions between chitosan and sunflower oil which led to the limited movement of polymer chains, preventing them from arranging in an ordered structure. Alternatively, this could also be an indication of the presence of triglycerides between polymer chains acting as a plasticizer by increasing the intermolecular spacing and reducing the ordered arrangement of the polymer (Yao et al., 2017).
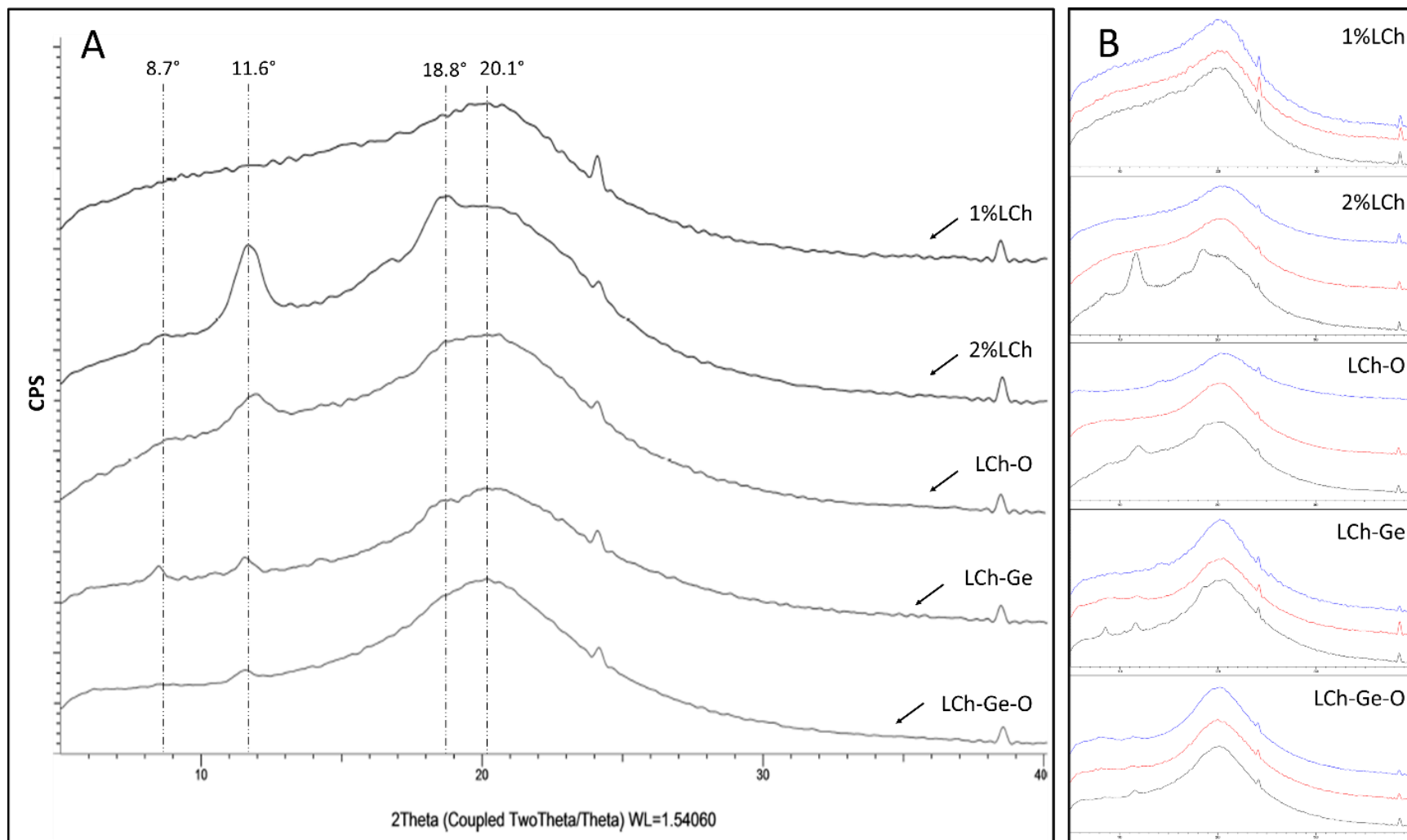
Figure 4.5: XRD diffractograms for A) all films prepared at 37 °C and B) all films prepared at 37 (**black lines**), 60 (*red lines*) or 80 °C (*blue lines*). LCh: lobster-shell chitosan; Ge: fish gelatin; O: sunflower oil.

Table 4.2: Values for the crystallinity index (CrI) of the prepared chitosan and composite films.

Films type	Drying temperature	Crystallinity index (%)
1% LCh	*37 °C*	9.3
	60 °C	9.2
	80 °C	9.5
2% LCh	*37 °C*	25.8
	60 °C	22.3
	80 °C	21.8
LCh-O	*37 °C*	21.5
	60 °C	19.8
	80 °C	18.1
LCh-Ge	*37 °C*	18.4
	60 °C	17.6
	80 °C	17.1
LCh-Ge-O	*37 °C*	15.2
	60 °C	14.8
	80 °C	14.9

LCh: lobster-shell chitosan; Ge: fish gelatin; O: sunflower oil.

The drying temperature had a significant effect on the crystallinity of the films. As shown in Figure 4.5B, the crystalline peaks disappeared for films dried at 60 or 80 °C, causing a reduction in their CrI. However, LCh-Ge-O films did not show much change as they were already highly amorphous at 37 °C. This decrease in the crystallinity of the films is more associated with drying time rather than drying temperature (Mu, 2016). The solvent (water) evaporates rapidly during high-temperature drying, giving less time for polymer chains to arrange in an ordered packing before gelation occurs, leading to a low degree of crystallization in the matrix (Homez-Jara et al., 2018; Mu, 2016). Leceta, Guerrero, & de la Caba (2013) and Mayachiew & Devahastin (2008) have also reported similar findings while evaluating films dried at different drying temperatures. As evident from their diffractograms and CrI, films dried at 80 °C did not show much change from the films dried at 60 °C, which is a recurring theme across all structural, thermal and physicochemical assays. This is due to the relatively short drying times at both 60 and 80 °C, i.e. 12 and 6 hours, with a small difference compared to the three days of drying needed at 37 °C.

4.3.2.3 Thermogravimetric analysis (TGA)

TGA was performed to analyze the thermal stability of the films as affected by film composition and drying temperature. Figure 4.6 shows the TGA and its first derivative curves (DTGA) for all five films prepared at three different drying temperatures. Depending on the film type, these thermograms can be characterized by three or four distinct thermal stages of mass loss. The peak degradation temperatures (T_d) and % loss in weight (Δw) for the films during each thermal stage are presented in Table 4.3. The first observed weight loss event from the initial run temperature to around 120 °C is generally associated with the evaporation of the residual solvent (water and acetic acid) (Maria et al., 2016; Shen & Kamdem, 2015). Although prior to the analysis, all films were dried at 60 °C for 48 hours to avoid this peak as it interferes with the other thermal events that can be detected in this region, a significant loss in weight was still observed ($\Delta w_1 = 1.7$ - 5.8%), indicating the reabsorption of moisture by the films from the surroundings during the pre-analysis steps. This is supported by the fact that the peak degradation temperature ($T_{d,1}$) for all films with $\Delta w_1 > 3\%$ was below 100 °C (except for 2% LCh, LCh-O and LCh-Ge-O films dried at 37 °C, as they did not show a clear DTGA peak and thus had no T_d in this region), which suggests that the observed weight loss was primarily due to the evaporation of free moisture that should have been removed during prolonged drying of the films at 60 °C.

Another key point to note is the positive correlation of Δw_1 with the drying temperature indicating a higher moisture content for the films dried at 60 or 80 °C. These observations contradict the equilibrated moisture contents (EMC) of these films (negative correlation of EMC with drying temperature – Section 4.3.3.1). Therefore, it can be inferred that the films dried at higher temperatures are perhaps more sensitive to the environmental humidity, i.e. they rapidly gain or lose moisture depending on the surrounding RH. This phenomenon was also confirmed in a different preliminary experiment (data not shown), where high-temperature dried films took less time to attain EMC at a constant RH. Moreover, the observation from that experiment also showed high sensitivity to environmental humidity for films prepared from FFS with low polymer concentrations (due to lower film thickness), which was evident from these TGA results as well.
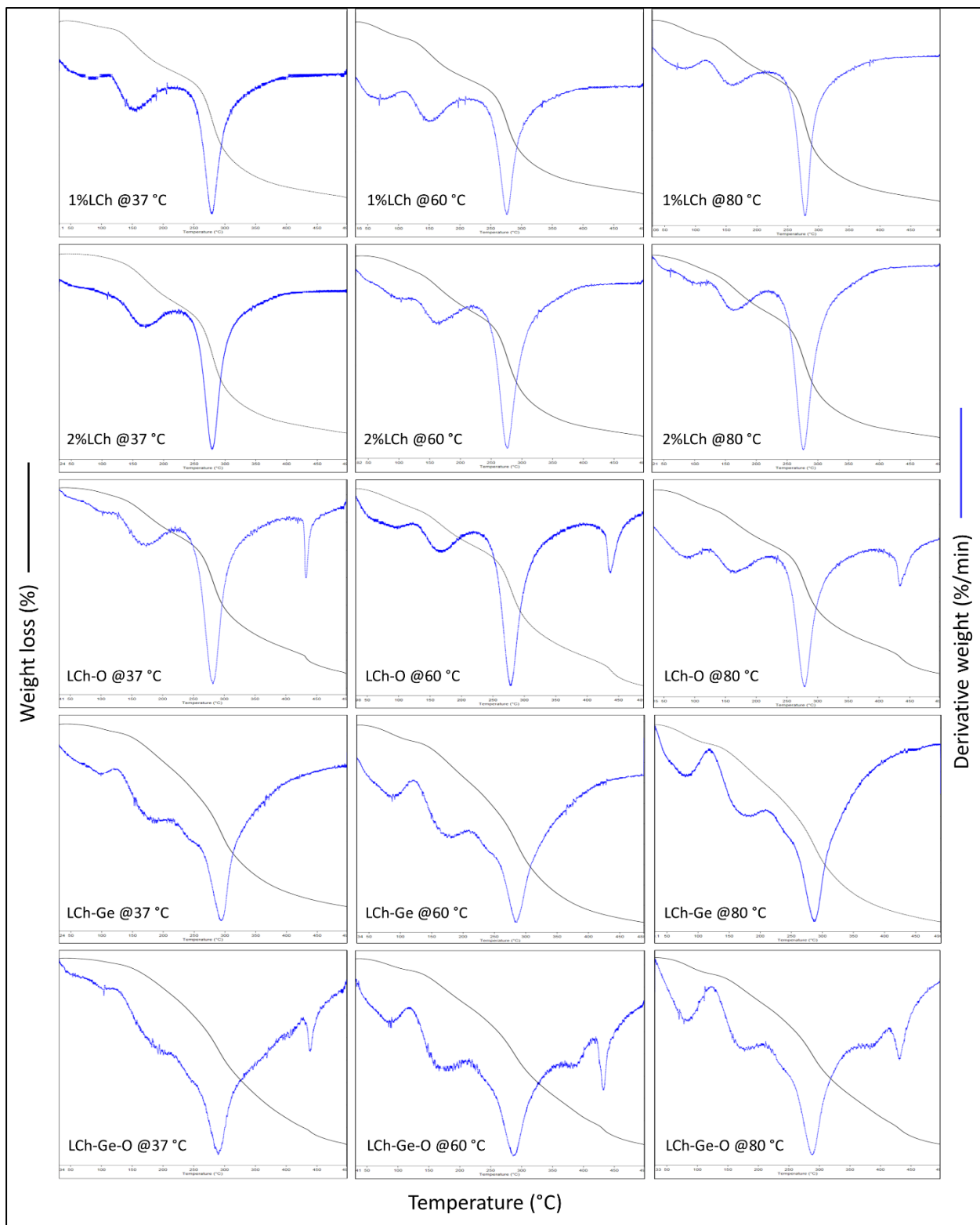
Figure 4.6: TGA and DTG thermograms of all tested chitosan and composite films. LCh: Lobster-shell chitosan; Ge: Fish gelatin; O: Sunflower oil.

Table 4.3: Thermal degradation data for all tested chitosan and composite films.

Film type	Drying temperature	Thermal degradation region 1			Thermal degradation region 2			Thermal degradation region 3			Thermal degradation region 4		
		Temperature range (°C)	T_d (°C)	Δw (%)	Temperature range (°C)	T_d (°C)	Δw (%)	Temperature range (°C)	T_d (°C)	Δw (%)	Temperature range (°C)	T_d (°C)	Δw (%)
1%LCh	*37 °C*	30.8-120	79	2.77	120-230	157	16.14	230-500	279	48.33	NA	NA	-
	60 °C	30.8-120	70	5.42	120-230	158	15.09	230-500	276	49.83	NA	NA	-
	80 °C	30.8-120	76	5.56	120-230	158	14.73	230-500	278	50.77	NA	NA	-
2%LCh	*37 °C*	30.8-120	NA	2.01	120-230	166	16.04	230-500	279	48.28	NA	NA	-
	60 °C	30.8-120	102	3.9	120-230	161	16.53	230-500	276	49.03	NA	NA	-
	80 °C	30.8-120	96	4.24	120-230	158	16.64	230-500	276	48.88	NA	NA	-
LCh-O	*37 °C*	30.8-120	NA	1.81	120-230	173	15.11	230-420	281	43.05	420-500	433	24.58
	60 °C	30.8-120	88	4.97	120-230	162	15.26	230-420	278	44.92	420-500	433	24.99
	80 °C	30.8-120	90	5.19	120-230	164	15.27	230-420	278	45.07	420-500	434	24.11
LCh-Ge	*37 °C*	30.8-120	102	2.48	120-230	NA	15.9	230-500	294	48.6	NA	NA	-
	60 °C	30.8-120	83	4.43	120-230	181	15.89	230-500	286	49.45	NA	NA	-
	80 °C	30.8-120	79	5.32	120-230	179	15.94	230-500	288	49.1	NA	NA	-
LCh-Ge-O	*37 °C*	30.8-120	NA	1.59	120-230	NA	15.11	230-420	289	44.85	420-500	438	23.25
	60 °C	30.8-120	90	3.83	120-230	175	15.73	230-420	286	47.31	420-500	433	24.59
	80 °C	30.8-120	84	4.59	120-230	177	15.74	230-420	288	46.14	420-500	428	24.35

LCh: lobster-shell chitosan; Ge: fish gelatin; O: sunflower oil; T_d: peak degradation temperature; Δw: weight loss; NA: Not available (No DTGA peaks identified in the thermal degradation region)

The second thermal event (Δw_2 = 13.1 - 16.6%) marked by a distinct weight loss peak (T_{d2}) corresponding to the removal of bound water and degradation of low molecular weight film components such as glycerol, acetic acid derivatives and side groups of polymers was observed till about 230 °C (Khouri, 2019; Pereda et al., 2008). Thermal degradation of pure glycerol occurs between 140 and 260 °C with the maximum degradation temperature ($T_{d,max}$) at around 250 °C, yet we witnessed $T_{d,2}$ for the films between 154 and 188 °C (Almazrouei et al., 2019). Various other authors have reported similar trends of thermal degradation for plasticized chitosan films (Boy et al., 2016; Homez-Jara et al., 2018; Pereda et al., 2008; Zhang et al., 2019). Lima et al. (2017) attributed this trend to the dehydroxylation of glycerol and biopolymers occurring in this temperature range. They suggested that the removal of bound water from the film matrix promotes the approximation of organic compounds, which may induce a dehydroxylation process at low temperatures leading to the observed DTGA peaks. Gelatin incorporated films (LCh-Ge and LCh-Ge-O) showed a broadening of this peak and an increase in $T_{d,2}$, whereas no distinct peaks were observed for these films prepared at 37 °C, indicating the superior ability of gelatin to bind glycerol through hydrophilic interactions compared to chitosan due to the presence of more hydrophilic functional groups in its structure. Similar observations were reported by Radovic et al. (2019) while comparing TGA thermograms of chitosan, gelatin and chitosan-gelatin (50:50) composite films.

Furthermore, 2%LCh and LCh-O films dried at higher temperatures showed a slight shift of $T_{d,2}$ towards lower temperatures, while a clear peak and distinction event between the second and third thermal stages for LCh-Ge and LCh-Ge-O films were discernable only for films dried at 60 or 80 °C. These observations may indicate decreased hydrogen bonding interactions between glycerol and biopolymers (LCh and Ge) with increasing drying temperatures. As suggested by the XRD observations, a decrease in film crystallinity with decreasing drying times may have contributed to this shift since a film with higher crystallinity would have a higher thermal resistance in this region (Homez-Jara et al., 2018). The correlation between peak shift and drying temperature for 1%LCh films was not observed and could be due to the low signal-to-noise ratio and high variability between replicate TGA/DTGA thermograms. The absence of change in CrI for these films at different drying temperatures may also explain a lack of peak shift trend.

The third thermal event (primary degradation stage, Δw_3 = 43.1 - 49.5%) associated with the depolymerization and degradation of chitosan and gelatin started at around 230 °C and continued until the end of the run (Shen & Kamdem, 2015). When comparing this stage of thermal degradation for chitosan-based films with LCh powder (refer to Chapter 3, Section 3.3.1.4), there was a significant reduction in $T_{d,max}$ from 303 °C to 278-295 °C, which may confirm the dehydroxylation process occurring in the films (Homez-Jara et al., 2018). Gelatin incorporated films (LCh-Ge and LCh-Ge-O) presented significantly higher $T_{d,max}$ values than the chitosan films (1%,2%LCh and LCh-O). This can be explained by the strong interactions between LCh and Ge (PEC formation), producing composites with increased thermal stability. The present observations agreed with the literature and were supported by the FT-IR and XRD analysis findings (Radovic et al., 2019; Wang et al., 2021). Qiao et al. (2017) reported a similar increase in the $T_{d,max}$ for chitosan-gelatin composite films. However, they also observed a shoulder in the mass loss thermograms of the composite films with higher proportions of gelatin during the maximum degradation stage, indicating two different biopolymer components in the films. In the present study, no shoulders or double DTGA peaks were observed in this region, which would imply an optimum blend of LCh and Ge with a high degree of intermolecular interactions. The highest $T_{d,max}$ (294 °C) was reported for LCh-Ge films prepared at 37 °C and the values significantly reduced with increasing drying temperatures or the incorporation of oil, suggesting a drastic reduction in chitosan gelatin complexion with both factors. However, such variations were not significant for other film types.

Lastly, a fourth thermal event between 420 and 500 °C was witnessed only for oil incorporated films with a weight loss (Δw_4) of around 24% associated with the degradation of high thermal stability components of the films, i.e. sunflower oil and tween-20, along with the gradual advanced degradation of chitosan and gelatin (Balau et al., 2004; Cerqueira et al., 2012a; Shen & Kamdem, 2015). No observable trends in the $T_{d,4}$ were found between the two composite films (LCh-O and LCh-Ge-O) prepared at different drying temperatures. However, a small peak at around 405 °C was observed for LCh-Ge-O films prepared at high temperatures. Although the reason behind these observations is unclear, it could be linked with the degradation of some thermally stable complexes between gelatin and Tween-20 that could have formed during high-temperature drying as Tween-20 offers a lower degradation peak temperature (around 350-400 °C)

compared to sunflower oil (Kishore et al., 2011). However, no such interactions were observed through the FT-IR spectra of these films. The observed phenomenon could also be associated with the degradation of free unbound Tween-20 that came out of complexion with chitosan/gelatin/oil during high-temperature drying. This argument would be supported by the slight broadening of the DTGA peak observed in this region for LCh-O film prepared at 60 or 80 °C.

4.3.3 Physicochemical Properties of Chitosan-based films

4.3.3.1 Film thickness, moisture content, degree of swelling and water solubility

Table 4.4 lists values for films thickness (FT), equilibrated moisture content (EMC), degree of swelling (DS) and water solubility (WS) of chitosan and composite films prepared at different drying temperatures. Film thickness ranged from 33 to 102 µm and was affected by all variables, i.e. chitosan concentration, incorporation of gelatin, incorporation of oil and drying temperatures. As expected, 1%LCh films presented significantly lower thickness ($p < 0.05$) compared to other films due to the low polymer concentration (50% less) in their FFS. The incorporation of oil in the films significantly increased their thickness ($p < 0.05$), whereas the presence of gelatin had a slight but inverse effect. The former trend can be explained by the non-volatile nature of sunflower oil and Tween-20, essentially increasing the overall dry matter in the films by around 13%. Moreover, this increase in thickness also suggests a reduction in film compactness and increased free volume in the films due to intermolecular interactions between oil and biopolymers (Haghighi, Biard, et al., 2019; Valenzuela et al., 2013). Similar reports have been made by Yao et al. (2017) and Haghighi, Biard, et al. (2019) while testing chitosan-gelatin composite films incorporated with different essential oils.

Table 4.4: The values of film thickness (FT), equilibrated moisture content (EMC), degree of swelling (DS), water solubility (WS) and film opacity in the UV (OP_{UV}) and visible (OP_{VIS}) spectrum obtained for all tested chitosan and composite films.

Film type	Drying temperature	FT (µm)	EMC (%)	DS (%)	WS (%)	OP_{UV} (A.nm/mm)	OP_{VIS} (A.nm/mm)
1%LCh	37 °C	35.4 ± 1.5[A]	24.15 ± 0.47[A]	26.6 ± 2.2[A]	35.8 ± 0.7[E,F]	944 ± 34[A,B,C]	366 ± 8[A,B,C]
	60 °C	33.8 ± 2.5[A]	20.76 ± 0.31[B,C]	33.4 ± 2.2[B]	28.7 ± 0.9[B]	965 ± 10[C]	410 ± 44[B,C,D]
	80 °C	33.4 ± 2.7[A]	19.84 ± 0.34[C,D]	33.5 ± 2.4[B]	26.5 ± 1.0[A]	963 ± 45[B,C]	390 ± 17[B,C,D]
2%LCh	37 °C	87.0 ± 1.6[D,E]	24.66 ± 0.46[A]	42.9 ± 1.2[C]	34.5 ± 0.4[D,E]	842 ± 36[A,B,C]	286 ± 25[A]
	60 °C	84.4 ± 4.7[C,D]	21.2 ± 0.30[B,C]	65.9 ± 1.3[E]	31.8 ± 0.7[C]	764 ± 16[A,B]	336 ± 27[A,B]
	80 °C	82.6 ± 6.1[C,D]	21.83 ± 0.47[B]	65.1 ± 1.2[E]	32.5 ± 0.5[C,D]	820 ± 10[A,B,C]	369 ± 33[A,B,C]
LCh-O	37 °C	102.8 ± 2.6[G]	22.19 ± 0.52[B]	37.6 ± 1.4[B,C]	31.2 ± 0.6[C]	2052 ± 79[F]	432 ± 5[D]
	60 °C	97.2 ± 6.0[F,G]	19.81 ± 0.26[C,D]	53.6 ± 2.7[D]	29.0 ± 0.9[B]	1316 ± 110[D]	681 ± 11[E]
	80 °C	94.4 ± 5.4[E,F,G]	18.68 ± 0.50[D,E,F]	56.6 ± 2.5[D]	28.7 ± 0.7[B]	1504 ± 113[D,E]	725 ± 23[E]
LCh-Ge	37 °C	82.2 ± 1.6[C,D]	19.11 ± 0.76[D,E]	58.6 ± 2.6[D]	35.5 ± 0.4[E,F]	825 ± 6[A,B,C]	322 ± 22[A,B]
	60 °C	77.2 ± 4.4[B,C]	17.13 ± 0.65[F,G,H]	72.7 ± 1.3[F]	37.2 ± 0.4[F]	808 ± 25[A,B,C]	372 ± 26[A,B,C]
	80 °C	72.2 ± 4.8[B]	16.64 ± 0.93[G,H,I]	75.1 ± 1.9[F]	40.3 ± 0.5[G]	751 ± 34[A]	382 ± 22[A,B,C]
LCh-Ge-O	37 °C	97.6 ± 2.1[F,G]	17.71 ± 0.63[E,F,G]	54.9 ± 0.2[D]	28.9 ± 0.8[B]	2020 ± 56[F]	418 ± 44[C,D]
	60 °C	91.2 ± 4.2[D,E,F]	15.69 ± 0.42[H,I]	75.3 ± 1.7[F]	31.9 ± 0.1[C]	1572 ± 68[E]	1290 ± 14[G]
	80 °C	90.8 ± 6.5[D,E,F]	15.13 ± 0.46[I]	72.5 ± 2.5[F]	32.7 ± 0.5[C,D]	1441 ± 143[D,E]	1185 ± 79[F]

The difference between the two mean values followed by the same letter in the same column is statistically insignificant ($p > 0.05$) as determined by Tukey's HSD test.

The effect of gelatin on film thickness could be associated with the low molecular weight of Ge compared to LCh, therefore providing a much denser film matrix with the same dry matter. Jridi et al. (2014) reported an opposite effect of cuttlefish gelatin on the thickness of chitosan composite films; however, they mixed a 4% w/v gelatin solution with 2% w/v chitosan solution to obtain composite films, increasing their total dry matter and hence causing an increase in their thickness. A slight decrease in film thickness was also witnessed for films dried at higher temperatures (60 or 80 °C), while the observed effect was significant ($p < 0.05$) for LCh-O and LCh-Ge-O films. This could be attributed to the collapse of the gel-net structure of chitosan films when dried rapidly at high temperatures (Fernández-Pan et al., 2010; Homez-Jara et al., 2018; Singh et al., 2015). Another important observation made was the high variability (standard deviation) in thickness measurements for high-temperature dried films because of increased surface imperfections and heterogeneity of these films, as previously discussed (refer to Section 4.3.1).

Neat LCh films prepared at 37 °C had the highest equilibrated moisture content (EMC) among different film types (≈ 24%), and the incorporation of gelatin and oil both showed a statistically significant negative effect on the film's EMC. Although gelatin is considered more hydrophilic than chitosan (Hosseini et al., 2013), the electrostatic interactions between the two polymers may have reduced the amount of free hydrophilic functional groups that can bind water, causing a reduction in the film's moisture content. Moreover, increased film density and low free volume in these films may have contributed to a lower EMC (Pereda et al., 2011). Such an effect of gelatin incorporation in chitosan films has been previously reported by Pereda et al. (2011) and Patel et al. (2018). On the other hand, the effect of oil incorporation on the EMC of films is directly associated with their increased hydrophobicity, which prevents films from absorbing more moisture, as suggested by Valenzuela et al. (2013). A significant decrease ($p < 0.05$) in EMC was also observed with increasing drying temperatures, which can again be attributed to the increased compactness (reduced thickness) of these films and was in accordance with the observations made by Homez-Jara et al. (2018).

The evaluation of the degree of swelling (DS) for chitosan and composite films indicated a significant increase in their water uptake when dried at higher temperatures. Likewise, the presence of gelatin in the films also caused a significant increase in the DS. These observations

could be linked with the decreased crystallinity (CrI) of these films as hydrophilic functional groups present in amorphous regions of the films are more accessible to the water, which leads to increased water-binding (Trung et al., 2006). Similar observations regarding the effect of drying temperature on the DS of chitosan films were made by Homez-Jara et al. (2018). However, in another article by Mayachiew et al. (2010), an opposite trend in the film DS with drying temperature was observed, which may be associated with their use of significantly higher MW chitosan (900 kDa) with high %DD (90.2%). The presence of oil in the film matrix significantly reduced their swelling ability even with reduced crystallinity, confirming the increased hydrophobic nature of these films (Valenzuela et al., 2013).

Polymer concentration also had a significant effect ($p < 0.05$) on the DS of the films as 1% LCh showed a lower water uptake compared to any other film. Although the reason is unclear, it is perhaps associated with the increased interactions between glycerol and chitosan in these films as the low concentration of chitosan leads to significantly lower viscosity of the initial FFS, which would have allowed higher chain mobility and thus more intermolecular interactions. This argument could be supported by the fact that the presence of glycerol in all prepared films in this study showed a significantly lower DS compared to the unplasticized LCh films, which showed a DS of around 250% (refer to Chapter 3, Section 3.3.2.1). While these observations may seem counterintuitive at first due to the hydrophilic nature of glycerol, which should increase the ability of the films to bind water, similar negative effects of its presence on the swelling ability of chitosan films have been reported by Rodríguez-Núñez et al. (2014) in the past.

The water solubility (WS) of chitosan-based films decreased with the presence of oil as expected (increased hydrophobicity). Similar findings were reported by Cerqueira et al. (2012a), Valenzuela et al. (2013) and Yao et al. (2017) while evaluating chitosan-based films incorporated with oils. A decrease in WS of the chitosan films was also seen with high-temperature drying in accordance with some previous reports (Fernandez-Saiz et al., 2009; Homez-Jara et al., 2018; Leceta, Guerrero, Ibarburu, et al., 2013). However, this trend was reversed for chitosan-gelatin composites. While the former can be associated with the intermolecular crosslinking and formation of insoluble compounds at high temperatures, such as Maillard reaction products (Leceta, Guerrero, Ibarburu, et al., 2013), the latter may indicate decreased electrostatic interactions between chitosan and gelatin when prepared at higher temperatures, therefore allowing a greater

extent of gelatin in the films to solubilize in water. An unexpected decrease in the relative intensities of amide bands seen in the FT-IR spectra of these films dried at 60 or 80 °C may support this argument. In general, a higher solubility has been reported in the literature for chitosan-gelatin composite films compared to pure chitosan films (Haghighi, De Leo, et al., 2019; Pereda et al., 2011; Rui et al., 2017). However, some authors have also reported decreased solubility at certain proportions of chitosan to gelatin, suggesting that optimum interactions between these two polymers can significantly reduce the WS of the films (Hosseini et al., 2013; Jridi et al., 2014). In this study as well, a significant change in WS of LCh-Ge films dried at 37 °C was not observed, indicating good interactions between the two polymers and complementing the TGA and FT-IR results.

4.3.3.2 Light barrier properties and opacity value

All films without oil were fairly transparent (Figure 4.4) and presented no significant changes in their opacity in the visible spectra (OP_{VIS}: 400-800 nm) due to different polymer concentrations or the inclusion of gelatin (Table 4.3). Pereda et al. (2011) observed a significant decrease in the opacity for chitosan-gelatin composite films compared to the stand-alone chitosan film, which contrasts the results of this study. However, a higher concentration of glycerol (28% w/w polymer) and a different type of chitosan (no MW mentioned) and gelatin (bovine) utilized in this study may explain these contradictions. For LCh and LCh-Ge films dried at 60 or 80 °C, a slight but statistically insignificant ($p > 0.05$) increase in OP_{VIS} was observed, which, as mentioned earlier, could be due to the formation of coloured Maillard reaction products at these temperatures (Fernandez-Saiz et al., 2009; Leceta, Guerrero, Ibarburu, et al., 2013).

On the other hand, oil incorporated films showed a slight but statistically significant ($p < 0.05$) increase in their OP_{VIS} associated with the homogeneous dispersion of oil in the film matrix, causing increased light scattering because of their different refractive index (Haghighi, Biard, et al., 2019; Pereda et al., 2012). Moreover, in this case, the effect of temperature on increased OP was highly significant ($p < 0.05$), suggesting degradation of oil emulsion and hydrophobic interactions between chitosan and oil, causing aggregation of oil droplets at high-temperature drying. For LCh-Ge-O films, this effect was much more pronounced, with almost a four times increase in OP_{VIS} values and a very noticeable increase in the translucency of these films (Figure

4.4). This is supported by a double peak observed in the fourth thermal degradation region of the DTGA curves for these films (Figure 4.6), which was attributed to the availability of free unbound Tween-20.

Similarly, the polymer concentration and presence of gelatin did not significantly change the barrier properties of the prepared films against UV light (OP_{UV}: 230-400 nm), while the incorporation of oil showed a significant increase in OP_{UV}. However, unlike the increase in OP_{VIS} of oil incorporated films with drying temperature, a significant reduction in OP_{UV} ($p < 0.05$) was observed for LCh-O and LCh-Ge-O films dried at 60 or 80 °C. This may perhaps indicate a reduction in UV-sensitive interactions and functional groups of oil in the high-temperature dried films, although no literature reference could be found to support this argument.

4.3.3.3 Mechanical properties

The mechanical or tensile properties of chitosan and composite films are summarized in Table 4.5. The highest tensile strength (TS: 67 MPa) and elastic modulus (EM: 1956 MPa) were recorded for neat 1%LCh films prepared at 37 °C, while the highest elongation at break (EAB) was obtained for LCh-Ge-O films prepared at 80 °C. In general, the EAB and EM of the films showed a good negative correlation which was expected as both parameters represent opposite film properties (ability to deform and stretch vs resistance towards deformation); however, such a correlation could not be established with their TS. A decrease in polymer concentration of the FFS (comparing 1%LCh with 2%LCh films) significantly reduced the EAB and increased EM of the films ($p < 0.05$) but had no significant effect on their TS, suggesting an increased rigidity of these films. Although several factors could have affected the flexibility of 1% LCh films, the high moisture sensitivity of these films is believed to be the primary reason behind these observations. Due to the low thickness of 1% LCh films, moisture absorption and desorption in these films occur at a significantly higher rate than in other films. As there was a time lag between removal of films from the conditioning chamber and testing them for their tensile properties (sample preparation), the films could have lost a significant amount of moisture in the low RH testing environment (around 25-30% RH). Because moisture in the films acts as a plasticizer (Ziani et al., 2008), a loss of moisture likely made 1% LCh films more rigid, which was reflected in their EM and EAB.

Table 4.5: The values of the tensile strength (TS), elongation at break (EAB), elastic modulus (EM), water vapour permeability (WVP) and surface contact angle (CA) obtained for all tested chitosan and composite films.

Film type	Drying temperature	TS (MPa)	EAB (%)	EM (MPa)	WVP ($g.mm/kPa.h.m^2$)	CA (°)
1%LCh	*37 °C*	66.9 ± 7.3[A]	23.8 ± 5.3[A]	1956 ± 155[A]	1.66 ± 0.06[B]	60.1 ± 1.6[A]
	60 °C	51.8 ± 4.4[C,D]	34.5 ± 7.6[A]	1768 ± 101[A,B]	1.45 ± 0.09[E,F,G]	58.5 ± 3.2[A]
	80 °C	47.7 ± 5.8[C,D,E]	32.6 ± 9.7[A]	1680 ± 128[B,C]	1.48 ± 0.05[D,E,F,G]	63.3 ± 1.9[A]
2%LCh	*37 °C*	62.1 ± 6.5[A,B]	64.8 ± 8.1[B]	1665 ± 107[B,C,D]	1.82 ± 0.03[A]	61.2 ± 1.4[A]
	60 °C	38.9 ± 6.3[E,F,G]	56.8 ± 10.1[B]	1475 ± 37[D,E]	1.6 ± 0.06[B,C,D]	63.6 ± 1.1[A]
	80 °C	41.6 ± 3.7[D,E,F]	59.3 ± 10.7[B]	1495 ± 74[C,D,E]	1.5 ± 0.03[D,E,F]	62.8 ± 1.9[A]
LCh-O	*37 °C*	55.1 ± 2.4[B,C]	70.3 ± 7.7[B,C]	1437 ± 50[E]	1.52 ± 0.02[C,D,E,F]	74.2 ± 0.7[B]
	60 °C	34.8 ± 4.8[F,G,H]	57.8 ± 7.9[B]	1179 ± 58[F]	1.41 ± 0.03[E,F,G]	75.7 ± 1.8[B]
	80 °C	33.7 ± 3.4[F,G,H]	59.1 ± 10.9[B]	944 ± 64[G,H]	1.39 ± 0.03[F,G]	75.9 ± 1.6[B]
LCh-Ge	*37 °C*	37.3 ± 2.3[F,G]	61.6 ± 2.9[B]	1212 ± 125[F]	1.64 ± 0.06[B,C]	59.9 ± 1.7[A]
	60 °C	29.8 ± 2.5[G,H]	78.3 ± 12.6[B,C]	862 ± 53[G,H]	1.53 ± 0.03[C,D,E]	61.2 ± 2.1[A]
	80 °C	32.7 ± 3.5[F,G,H]	76.7 ± 9.8[B,C]	929 ± 66[G,H]	1.51 ± 0.03[C,D,E]	63.1 ± 2.6[A]
LCh-Ge-O	*37 °C*	34.8 ± 1.5[F,G,H]	68.3 ± 5.0[B,C]	1039 ± 68[F,G]	1.46 ± 0.01[E,F,G]	73.2 ± 1.6[B]
	60 °C	26.6 ± 3.0[H]	87.2 ± 11.4[C,D]	829 ± 60[H]	1.35 ± 0.02[G]	72.2 ± 1.5[B]
	80 °C	27.0 ± 3.3[H]	100.4 ± 16.3[D]	601 ± 39[I]	1.2 ± 0.04[H]	71.1 ± 3.5[B]

The difference between the two mean values followed by the same letter in the same column is statistically insignificant ($p > 0.05$) as determined by Tukey's HSD test.

Chitosan-gelatin composite films showed a significant reduction in the TS of the films compared to stand-alone LCh films. This behaviour was expected and is in accordance with the previous studies as generally neat chitosan films offer very high TS compared to protein-based films (Jridi et al., 2014; Li et al., 2017; Valenzuela et al., 2013). However, a simultaneous increase in EAB along with a decrease in the TS of the chitosan films with the incorporation of fish gelatin was not observed in this study, which contrasts the observations made by Hosseini et al. (2013). The use of high MW chitosan (LCh) along with an additional ultrasonication treatment may have caused increased interactions between chitosan and gelatin in this study and could explain the contradicting results. Moreover, the maximum TS and EAB for chitosan-gelatin composite films (40:60) reported by Hosseini et al. (2013) were 16.6 MPa and 25.3% which are significantly lower than the values reported in this study and may support this premise. A significant decrease in TS with no effect on EAB with the incorporation of gelatin in chitosan-gallic acid composite films was previously reported by Rui et al. (2017).

For films prepared at low temperature, the addition of oil significantly reduced the EM of the films ($p < 0.05$) and a slight but insignificant increase in EAB and decrease in TS was also observed. These observations indicate a plasticizing effect of oil on the films as triglyceride chains can penetrate into the chitosan or composite film matrix and increase the free volume and thus chain mobility in the films, which also caused an increased thickness of these films as explained earlier (Yao et al., 2017). However, the results of this study did not follow the observations made by Cerqueira et al. (2012a), who observed a significant decrease in TS as well as EAB of the films with the incorporation of corn oil in chitosan films. The authors attributed these observations to the incompatibility and inability of the chitosan matrix to hold oil. On the other hand, the present study has demonstrated good interactions between oil and chitosan/gelatin, which could have been linked with the use of an emulsifier (Tween-20) compared to the previous report.

Lastly, the drying temperature played a significant role in defining the mechanical properties of the films. LCh and LCh-O films experienced a significant drop in TS ($p < 0.05$) and EM ($p < 0.05$ only in the case of LCh-O films) when prepared at high temperatures. Moreover, a drop in EAB was also observed but was not significant. This could be explained by the loss of crystallinity in the films dried at 60 or 80 °C, which led to a decrease in hydrogen bonding and intermolecular interactions resulting in a weaker and less stretchable film (Fernández-Pan et al.,

2010). Similar observations regarding the effect of drying temperature on mechanical properties of chitosan films have been previously reported by Fernandez-Pan et al. (2010) and Liu et al. (2019).

However, LCh-Ge and LCh-Ge-O films behaved differently with increased drying temperature. Although a decrease in TS was observed for these films dried at high temperatures, the effect was not significant ($p > 0.05$). In addition, a significant decrease in EM was still observed ($p < 0.05$) but in conjugation with a significant increase in EAB ($p < 0.05$), suggesting increased flexibility and stretchability of these films. This behaviour of composite films could be associated with the reduced PEC formation between chitosan and gelatin when dried at higher temperatures, allowing enhanced chain mobility reflected in a higher EAB for these films. A similar increase in EAB of chitosan-gelatin composite films prepared at 60 °C compared to the films prepared at 25 °C was previously reported by Arvanitoyannis et al. (1998). In the case of LCh-Ge-O films, this effect was more pronounced, suggesting a more intense plasticizing effect of oil, perhaps due to the inability of chitosan to form hydrophobic bonds with oil in the presence of gelatin at higher temperature drying.

4.3.3.4 Water vapour barrier properties and surface hydrophobicity

The water vapour permeability (WVP) (corrected for stagnant air gap effect, refer to Chapter 3, Section 3.3.2.4) of the tested films (Table 4.5) was found to be directly associated with their moisture content (EMC) and hydrophobicity (Table 4.4), as previously reported by several authors (Cerqueira et al., 2012a; Homez-Jara et al., 2018; Pereda et al., 2012; Valenzuela et al., 2013; Yao et al., 2017). While an increased EMC of the films allows for better diffusion of water vapours through the film matrix due to increased intermolecular spacing and chain mobility, the presence of oil in the films can form a hydrophobic lipid network preventing adsorption of water molecules, thus lowering the vapour permeation (Cerqueira et al., 2012b; Hamdi et al., 2019; Homez-Jara et al., 2018; Valenzuela et al., 2013). However, incorporating and increasing the content of lipids in the films does not guarantee a reduced WVP as vapour permeation is also highly dependent on dispersion and particle size of emulsion droplets in the film matrix along with the continuous microstructure integrity of the films (Cheng et al., 2008; McHugh & Krochta, 1994; Wong et al., 1992).

2%LCh films prepared at 37 °C showed the highest EMC (24.6%) and also presented the highest WVP (1.8 g.mm/kPa.h.m^2) among all tested films. At the same time, LCh-Ge-O films prepared at 80 °C (lowest EMC: 15.13%) presented the lowest WVP (1.2 g.mm/kPa.h.m^2). However, despite showing no significant differences in their EMC, 1%LCh films showed a lower WVP ($p < 0.05$) than 2%LCh films. This inconsistency may be explained by the significantly lower thickness of 1%LCh films (Table 4.4), which is associated with the 'thickness effect' of the hydrophilic films on their vapour permeation, as discussed in Chapter 3 (refer to Section 3.3.2.4). A similar effect of chitosan concentration in the FFS on the WVP of the resultant films was observed by García et al. (2015) and was attributed to the differences in the film thickness.

As previously described, the high degree of intermolecular interactions between gelatin and chitosan in the LCh-Ge or LCh-Ge-O films decreased the availability of free -OH and -NH$_2$ groups that can interact with water molecules preventing a high vapour permeability through their matrix (Cheng et al., 2008). Moreover, a significantly low WVP obtained for oil incorporated films ($p < 0.05$) indicates a highly homogeneous oil dispersion and a small emulsion particle size (Cheng et al., 2008; McHugh & Krochta, 1994; Wong et al., 1992). These results also suggest that ultrasonication was an efficient way to produce chitosan-oil emulsions. A significant drop in WVP observed for the films prepared at 60 or 80 °C was associated with the collapse of their gel-net structure at high-temperature drying, which led to a low intermolecular spacing in these films and prevented efficient migration of water vapours through the film matrix (Fernández-Pan et al., 2010). These observations followed the previous reports made by Fernandez-Pan et al. (2010) and Homez-Jara et al. (2018).

The surface hydrophobicity of the chitosan and composite films, as measured through the contact angle (CA) formed by ethylene glycol on their surface, was between 58.5 and 75.9° (Table 4.5). No significant effects on CA were observed with a change in polymer concentration, presence of gelatin or the drying temperature. Leceta, Guerrero, Ibarburu, et al. (2013) also reported no significant changes in water contact angle of chitosan films dried at room temperature or at 105 °C. Generally, neat gelatin films are more hydrophilic and show a smaller CA compared to neat chitosan films (Córdoba & Sobral, 2017; Rodrigues, Bertolo et al., 2020). However, in the present study, the complexion between gelatin and chitosan may have prevented the hydrophilic groups of gelatin from contributing towards a more hydrophilic surface, explaining these observations. On

the other hand, a significant increase ($p < 0.05$) in CA by around 24% was observed for oil incorporated films, indicating an increased surface hydrophobicity. These observations are similar to the ones reported by Pereda et al. (2012) (incorporation of olive oil in chitosan films) and Yao et al. (2017) (incorporation of D-limonene in chitosan-fish gelatin composite films).

4.4 SUMMARY AND CONCLUDING REMARKS

The observations from the present study demonstrated excellent compatibility of lobster-shell-derived chitosan with fish gelatin and sunflower oil in the production of composite edible films. The FT-IR, XRD and TGA analysis confirmed the high degree of intermolecular interactions between the film components, which ultimately resulted in the improved functionality of the composite films. The films obtained from low polymer concentration FFS showed high variability in their properties, primarily due to their low thickness and high sensitivity to environmental humidity. The presence of fish gelatin reduced the rigidity and increased film flexibility and stretchability (after high-temperature drying) without significantly impacting the hydrophilic nature of LCh films. On the other hand, the incorporation of sunflower oil enhanced the hydrophobicity and resistance towards water solubility and swelling of the films without deteriorating their mechanical properties. When dried at 37 °C, oil incorporated films also did not significantly impact the transparency of the films while providing very high UV resistance. Moreover, both fish gelatin and sunflower oil significantly reduced the water vapour permeation through the composite films.

In order to commercialize chitosan-based edible films, a fast production process is paramount, and this calls for rapid evaporation of solvent by either using high-temperature or low RH conditions during the drying process. The present study demonstrates that drying time or temperature can significantly affect most physicochemical properties of chitosan and composite films by influencing the molecular arrangement and interactions between polymer chains in the film matrix. LCh-Ge-O composite films dried at 60 or 80 °C showed poor surface homogeneity and transparency and an increase in their swelling capacity. However, a significant improvement in their stretchability and water vapour permeability without a drastic effect on their tensile

strength and water solubility is highly desirable, making them a prospective candidate for future commercial applications with some further improvements.

Overall, this study has shown the potential of LCh composite films in providing improved applicability as an edible food packaging system. However, a comprehensive study on the effect of different proportions of film components can help further expand the ability to tailor chitosan film properties according to their needed applications, which is explored in the next chapter.

CHAPTER 5

OPTIMIZATION OF FORMULATIONS FOR LOBSTER-SHELL CHITOSAN – FISH GELATIN COMPOSITE FILMS INCORPORATED WITH SUNFLOWER OIL AND GLYCEROL

5.1 INTRODUCTION

As observed from the results of Chapter 4, most of the physicochemical properties of lobster-shell-derived chitosan films can be significantly influenced and enhanced by incorporating/ blending fish gelatin, sunflower oil and plasticizers (glycerol) with chitosan. While gelatin and glycerol can provide significant structural and mechanical enhancements to chitosan films, oil can increase hydrophobicity and influence film properties such as solubility in water and water vapour permeability (Pereda et al., 2011, 2012; Rodríguez-Núñez et al., 2014). The desired properties of edible films are primarily dictated by their intended applications, functionality, and the nature of the product to be packaged (Erkmen & Barazi, 2018; Pavlath & Orts, 2009). For instance, some food packaging applications may call for hydrophobic edible films with high resistance towards water vapour permeability to prevent or minimize moisture gain or loss by the product, while others may require films that can instantly solubilize in water and release their contents (Blanco-Pascual & Gómez-Estaca, 2017). Further, the antimicrobial activity that is exhibited by many chitosan-based films is a highly attractive property for food packaging materials (Nadarajah, 2005).

In order to tailor the properties of edible films towards their end-use, optimization studies and the development of prediction models based on various significant independent factors are important. These studies can provide a more detailed understanding regarding the individual and interaction effects of those factors on the properties of films, which may further help devise new strategies to improve and expand the functionality of the films. Thus, the main objective of the study presented in this chapter was to develop optimization models to formulate plasticized lobster-shell chitosan – fish gelatin – sunflower oil composite films based on their desired properties and functionality using response surface methodology (RSM). In addition, the

dependency of film properties on the molecular weight of chitosan was explored by replacing lobster-shell chitosan in optimized composite film formulations with its enzymatically hydrolyzed product. Moreover, the antimicrobial potential of lobster-shell chitosan and composite (optimized) films was also evaluated.

5.2 MATERIALS AND METHODS

5.2.1 Materials and Reagents

Viscozyme® L was purchased from Sigma-Aldrich (ON, Canada). Tryptic soy broth (BD Bacto™) and bacteriological grade agar were purchased from Fisher Scientific (ON, Canada). Luria-Bertini broth was purchased from BDH® VWR Chemicals (USA), and Escherichia coli (ATCC 8739) was provided by Verschuren centre (NS, Canada). The origin of all other materials and reagents utilized in this study is described in Chapter 4 (refer to section 4.2.1).

5.2.2 Development of Optimization Models for Lobster Chitosan Composite FIlms

5.2.2.1 Experimental design

In order to develop an optimization model for the physicochemical properties of lobster-shell chitosan (LCh) – fish gelatin (Ge) – sunflower oil (O) composite films, various formulations of film-forming solutions (FFS) were analyzed using response surface methodology (RSM) with a three-factor three-level Box-Behnken design. The three chosen factors for optimization were the proportions of LCh to Ge, the content of sunflower oil (O) and the content of plasticizer, i.e. glycerol (Gly) in the FFS. For evaluating different proportions of LCh to Ge, the amount of both polymers in the FFS were changed to maintain a constant polymer concentration (LCh + Ge) of 2% w/w FFS. However, only the content of Ge was considered a factor in the model (independent variable) as the LCh content is dependent on Ge, i.e. with increasing content of Ge in the FFS, LCh content should decrease to provide a final concentration of 2% polymer in the FFS. The

concentration levels of the tested factors are presented in Table 5.1 and were determined based on the observations from the previous experiments (Chapter 4) and literature review.

Table 5.1: Factors and levels used in the optimization experiment.

	Lobster-shell chitosan* (% w/w polymer)	Fish gelatin (% w/w polymer)	Sunflower oil (% w/w polymer)	Glycerol (% w/w polymer)
		X_1	X_2	X_3
	75	25 (-1)	0 (-1)	0 (-1)
Levels	50	50 (0)	10 (0)	20 (0)
	25	75 (+1)	20 (+1)	40 (+1)

*Not an independent variable; (-1): low-level concentrations; (0): mid-level concetrations; (+1) high-level concentrations.

In total, 17 FFS formulations were prepared according to the Box-Behnken design (Table 5.2), including five replicates at the centre point (run 13 to 17), which were used to determine the deviation and reproducibility of data. The sequence of experimental runs and their analysis for physicochemical properties were randomized to minimize the effects of uncontrolled factors on the optimization model. The obtained data from all response parameters (physicochemical properties) were analyzed using multiple linear regression and were fitted into a second-order polynomial equation (Eq. 5.1) as a function of the independent variables (Tomadoni et al., 2019).

$$Y_n = \beta_o + \sum_{i=1}^{3} \beta_i X_i + \sum_{i=1}^{2} \sum_{j=2, j>i}^{3} \beta_{ij} X_i X_j + \sum_{i=1}^{3} \beta_{ii} X_i^2 + \varepsilon_n \qquad \text{(Eq. 5.1)}$$

Here Y_n represents predicted response, β_o is the regression constant, β_i represents linear coefficients, β_{ij} represents coefficients for the interaction effect, β_{ii} represents quadratic coefficients, X_i represents the independent variables, and ε_n is the associated error with the predicted response.

Table 5.2: Box-Behnken experimental design matrix.

Experimental runs	Fish gelatin (% w/w polymer)	Sunflower oil (% w/w polymer)	Glycerol (% w/w polymer)
	X_1	X_2	X_3
1	25	0	20
2	75	0	20
3	25	20	20
4	75	20	20
5	25	10	0
6	75	10	0
7	25	10	40
8	75	10	40
9	50	0	0
10	50	20	0
11	50	0	40
12	50	20	40
13	50	10	20
14	50	10	20
15	50	10	20
16	50	10	20
17	50	10	20

5.2.2.2 Preparation of films

The required LCh-Ge/LCh-Ge-O FFS were prepared using the method previously described in Chapter 4 (refer to Section 4.2.2.2), with changes in the content of the film components (LCh, Ge, O and Gly) as per the optimization design matrix (Table 5.2). The obtained FFS were poured into polystyrene Petri dishes (0.25 g/cm^2) and dried at 37 °C for three days in a water-jacketed incubator (Forma Scientific 3250, USA). The dried composite films were carefully peeled off from the dishes and conditioned at RT (21 ± 2 °C) in a desiccator with a saturated magnesium nitrate solution (52 - 54% RH) for at least three days prior to any analysis.

5.2.2.3 Physicochemical characterization of films

All prepared composite films were characterized based on their physical (thickness, moisture content, water-solubility, surface hydrophobicity), optical (UV and visible opacity), mechanical (tensile strength, elongation at break and elastic modulus), and barrier (water vapour permeability) properties to obtain the response data for optimization by following the methods and using the equipment previously described in Chapter 3 (refer to Section 3.2.5).

5.2.2.4 Simultaneous optimization of physicochemical properties

Simultaneous optimization of predicted responses (evaluated physicochemical properties) based on their provided target ranges was carried out via Minitab 19 Statistical Software using the desirability function approach described by Derringer & Suich (1980). Each response parameter (Y_n) was first converted into a desirability function (d_n) with values ranging from 0 to 1, where d_n = 0 represents an unacceptable value for the parameter while d_n = 1 represents a highly desirable value. During the simultaneous optimization of FFS for the required parameters, their individual desirability functions were combined into an overall desirability function (D), also ranging from 0 to 1, by taking their geometric average. The contents of Ge, O and Gly that maximized D were then selected as the optimized formulations (Srinivasa et al., 2007; Tomadoni et al., 2019).

5.2.2.5 Development of optimized films and regression model validation

Three optimized LCh-Ge/LCh-Ge-O composite films were prepared (using the same procedure as before, Section 5.2.2.2), targeting different food packaging applications. The formulations for these composite films were obtained from the simultaneous optimization of their desired physicochemical properties. The experimental data for the response parameters observed for these films and the predicted values obtained from the regression equations were then compared to determine the validity and reliability of the developed regression models.

5.2.3 Development of Low MW Lobster-Shell Chitosan Composite Films

5.2.3.1 Preparation of low MW lobster chitosan

Enzymatic hydrolysis of LCh was performed to obtain low MW lobster chitosan (LLCh) using Viscozyme® L (Sigma-Aldrich, US), a non-specific cellulolytic enzyme. LCh was dissolved in 0.1 M sodium acetate buffer (pH 4.4) at a concentration of 10 mg/mL by continuous stirring (300 rpm) at 60 °C for three hours. The obtained chitosan solution was cooled down to room temperature followed by ultrasonication for 30 mins using a probe sonicator (VCX 750, Vibra-Cell™, Sonics and Materials, USA) at 40% amplitude and 5-second pulse. Viscozyme® with an activity of 100 Fungal Beta-Glucanase Units (FBGU) per mL was added into chitosan solution at an enzyme to substrate ratio of 1:100 (w/w) and incubated for 24 hours at 40 °C with continuous stirring (280 rpm). Post incubation, the chitosan hydrolysate was boiled for 10 mins to inactivate the enzyme, cooled down to room temperature using an ice bath and then filtered using vacuum filtration with Whatman filter paper (grade 1). The filtrate was neutralized by a solution of 1N NaOH to a final pH of 6.4 - 6.8 to precipitate high molecular weight chains, followed by centrifugation at 16,000 g for 20 mins. The supernatant was collected and purified using a dialysis tube (MWCO: 100-500 Da, Spectra/Por® Cellulose Ester Dialysis Membrane, Spectrum Laboratories, USA) to remove salts. Finally, LLCh powder was obtained using lyophilization (FreeZone 6, Labconco, USA), and the % yield was calculated using the following equation:

$$Low\ MW\ chitosan\ yield\ (\%) = \frac{Weight\ of\ the\ obtained\ LLCh\ powder}{Weight\ of\ the\ treated\ LCh\ powder} \times 100 \qquad \text{(Eq. 5.2)}$$

5.2.3.2 Characterization of low MW lobster chitosan

The prepared LLCh powder was characterized based on its proximate composition (only moisture content and ash content were determined) and molecular weight as per the procedures described in Chapter 3 (refer to Section 3.2.3).

5.2.3.3 Preparation of LLCh-based films

The LLCh composite films were prepared by replacing LCh in the optimized composite film formulations obtained from the regression models while using the same procedure (refer to Section 5.2.2.2). In addition, neat LLCh and LCh films without plasticizers were also prepared for comparison. All obtained films were conditioned at 21 ± 2 °C in a desiccator with a saturated magnesium nitrate solution (52 - 54% RH) for at least three days prior to any analysis.

5.2.3.4 Physicochemical characterization of LLCh films

In order to evaluate the effect of chitosan molecular weight on the physicochemical properties of neat and composite films, LLCh films were also characterized based on their physical, optical, mechanical and barrier properties by following the methods and using the equipment previously described in Chapter 3 (refer to Section 3.2.5).

5.2.4 Antimicrobial Testing of Chitosan and Composite Films

The antimicrobial activity of previously obtained neat and optimized LCh and LLCh films was evaluated against *E. coli* ATCC 8739 using a combination of methods described by Fernandez-Saiz et al. (2009) and Park et al. (2004) with several modifications. The tests were conducted by adding about 50 mg of UV sterilized film samples into T-flasks (25 cm^2, CORNING®, USA) containing 10 mL of TSB media (Tryptic Soy Broth, BD Bacto^{TM}, USA). Three control samples were also run for comparison, i.e. a negative control (low-density polyethylene film), a positive control (Ampicillin 10µg, Sensi-Disc^{TM} Susceptibility Test Disc, BD BBL^{TM}, USA) and an acetic acid control (10 µL/10 mL of TSB). Each sample and control flask was inoculated with a mid-log phase culture of *E. coli* at an initial inoculation size of approximately 10^6 colony-forming units (CFU)/mL and incubated in a shaker incubator (150 rpm) at 37 °C for 24 h. The bacterial growth in the TSB suspensions was evaluated by checking their optical density (OD @600 nm) at 0, 6, 12 and 24th h of incubation. In addition, to check the inhibition effect of films on CFUs, 20 µL of these TSB suspensions taken at 0 and 24 h of incubation were diluted in saline (0.85% w/w) and sub-cultivated on LB (Luria-Bertini broth, VWR Chemicals, USA) agar plates. Finally, the colonies were counted on the sub-cultivated plates

after 24 h of incubation at 37 °C, and the OD results were presented as percentage inhibition of *E. coli* with negative control as a reference. All tests were performed in duplicates to ensure the reproducibility of data.

5.2.5 Statistical Analysis

Minitab 19 Statistical Software was used for all data analysis, experimental design, model fitting, simultaneous optimization of responses and graphical representation of models using contour and main effect plots. Analysis of variance (ANOVA) was performed to determine the effects and regression coefficients of linear, interaction and quadratic terms. Statistical significance of models and individual terms were evaluated at a significance level of 1 or 5%. The fit quality and robustness of the prediction models were expressed by R^2 (coefficient of determination), adj-R^2 and pred-R^2 values. While comparing means using ANOVA, a p-value of less than 0.05 was considered statistically significant.

5.3 RESULTS AND DISCUSSION

5.3.1 Optimization of Chitosan (Lobster-Shell) – Gelatin – Oil Composite Films

5.3.1.1 *Fitting of response surface models*

Response surface methodology (RSM) is a powerful statistical tool that helps in evaluating the effects of several factors and their interactions on the response parameters while significantly reducing the required number of experimental runs (Tomadoni et al., 2019). In the present study, the effect of fish-gelatin (X_1), sunflower oil (X_2) and glycerol (X_3) concentrations in the FFS on the physical, mechanical, optical and barrier properties of the resultant chitosan films were evaluated using RSM. Moreover, prediction models for these properties based on FFS composition were built by employing multiple linear regression. Table 5.3 summarizes the experimental response data (physicochemical properties) obtained for all tested combinations.

Table 5.3: Experimental data for each response parameter.

Experimental runs	FT (μm)	EMC (%)	DS (%)	WS (%)	OP$_{UV}$ (A.nm/mm)	OP$_{VIS}$ (A.nm/mm)	TS (MPa)	EAB (%)	EM (MPa)	WVP (g.mm/kPa.h.m^2)	CA (°)
1	64.0	18.2	71.7	17.0	350.1	962.7	44.2	65.0	1031.1	1.28	49.27
2	46.4	15.8	97.9	23.6	364.4	548.9	27.5	40.0	644.3	0.90	38.27
3	89.2	13.6	52.6	16.3	427.2	2876.0	41.5	63.8	659.8	1.06	54.70
4	79.4	11.3	83.9	16.0	813.2	2361.4	13.5	38.0	303.9	0.86	37.22
5	66.3	10.9	145.0	18.1	400.3	2499.9	79.3	20.6	2097.7	0.84	69.89
6	58.4	5.7	187.7	25.8	600.9	1919.1	30.9	6.0	1676.9	0.61	63.00
7	77.7	31.4	63.3	14.1	393.3	2677.4	29.3	78.5	241.0	2.44	61.23
8	57.1	27.6	81.9	16.1	567.0	1940.1	15.1	99.7	11.2	2.25	40.87
9	51.8	9.7	230.0	32.1	361.7	557.5	79.1	7.4	1888.5	0.73	55.94
10	82.6	4.0	101.5	23.8	440.2	2620.3	62.9	10.9	1631.5	0.61	58.35
11	65.5	25.2	75.5	21.8	291.7	1084.6	34.5	96.3	20.4	2.27	43.02
12	84.3	23.3	64.0	21.1	453.1	2568.4	26.0	83.0	28.4	1.67	55.26
13	67.8	15.1	59.1	22.0	422.8	1967.0	33.8	57.5	633.7	1.45	61.70
14	67.4	13.8	70.3	22.3	394.4	2234.6	31.2	48.6	797.7	1.19	59.66
15	64.2	12.0	50.9	23.3	446.3	2327.1	34.1	55.4	711.5	1.41	64.73
16	65.0	12.2	76.0	22.1	430.2	2464.5	38.9	45.2	919.3	1.29	60.88
17	69.9	12.9	64.8	24.2	513.6	2291.1	36.7	48.1	830.0	1.22	66.55

FT: film thickness; EMC: equilibrated moisture content; DS: degree of swelling; WS: water solubility; OP$_{VIS}$ and OP$_{UV}$: film opacity in the visible and UV spectrum; TS: tensile strength; EAB: elongation at break; EM: elastic modulus; WVP: water vapour permeability; CA: surface contact angle.

Data from each investigated response parameter were fitted into a full second-order polynomial equation (Eq. 5.1) using regression analysis, and ANOVA was performed to identify the significance of the models and individual terms (linear, square and interaction terms). The F-statistics for each regression model and its associated terms are shown in Table 5.4, which shows that all quadratic models were significant at either 99 or 95% confidence/significance levels with a non-significant lack of fit ($p > 0.05$). In order to obtain the final fitted models and reduced regression equations, all insignificant terms ($p > 0.05$) were eliminated from the models (Table 5.4), and the adequacy of the reduced models was determined by their coefficient of determination (R^2), adjusted-R^2 (R^2_{adj}) and predicted-R^2 (R^2_{pred}) values. While R^2 tells about the overall fit of a model with a value closer to 1 (or 100) being an indication of a good fit, it can often be misleading as it increases with just an increase in the number of terms or predictors in a model, which can lead to overfitting of the model (Jim, 2013). Therefore, considering R^2_{adj} (R^2 values adjusted for the number of predictors in the model) and R^2_{pred} (indication of model's ability to predict responses for a new set of observations) values along with R^2 values is a much better way to evaluate the adequacy and robustness of regression models (Jim, 2013; Ratner, 2009; Robert Wall, 2020).

The following equations (Eq. 5.3-5.13) provide the fitted and reduced prediction models and their associated R^2-statistics for the physicochemical properties of the films, i.e., film thickness (FT), equilibrated moisture content (EMC), degree of swelling (DS), water solubility (WS), opacity in the visible and UV spectrum (OP$_{VIS}$ and OP$_{UV}$), tensile strength (TS), elongation at break (EAB), elastic modulus (EM), water vapour permeability (WVP) and surface contact angle (CA).

$$Y_{FT} = 58.37 - 0.153\,X_1 + 0.763\,X_2 + 0.627\,X_3 + 0.044\,X_2^2 - 0.006\,X_1X_3 \\ - 0.015\,X_2X_3$$

(Eq. 5.3)

$$R^2 = 97.14; \quad R^2_{adj} = 95.43; \quad R^2_{pred} = 91.19$$

$$Y_{EMC} = 21.52 - 0.452\,X_1 - 0.209\,X_2 + 0.159\,X_3 + 0.004\,X_1^2 + 0.008\,X_3^2$$

(Eq. 5.4)

$$R^2 = 97.31; \quad R^2_{adj} = 96.09; \quad R^2_{pred} = 93.04$$

103

Table 5.4: Significance of regression models and individual terms (F values) for each response parameter.

Source	DF[#]	FT	EMC	DS	WS	OP$_{UV}$	OP$_{VIS}$	TS	EAB	EM	WVP	CA
Full model	9	48.26**	41.19**	16.11*	48.94**	9.15*	40.79**	37.91**	18.65**	68.88**	29.75**	16.61*
Linear	3	132.04**	112.43**	30.23**	73.06**	19.09*	102.41**	89.61**	54.22**	197.59**	78.90**	22.55*
	1	80.51**	10.01*	6.79*	43.47**	28.74*	26.56*	88.63**	3.19	22.22*	6.56*	37.14**
	1	298.81**	14.77*	14.45*	52.40**	28.08*	278.28**	13.24*	0.27	10.56*	6.30*	6.33*
	1	16.81*	312.49**	69.44**	123.32**	0.46	2.39	166.96**	159.18**	559.99**	223.82**	26.19**
Square	3	6.49*	10.58*	13.49*	57.65**	3.69	18.67*	17.18*	0.05	8.23*	9.20*	24.74**
	1	2.33	10.54*	0.8	166.97**	9.20*	0.01	15.06*	0.09	0.01	0.29	15.07*
	1	17.75*	1.46	0.45	3.7	1.28	55.68**	4.9	0.02	5.24	13.93*	55.34**
	1	0.1	19.00*	37.84**	7.36*	1.14	0.02	33.31*	0.06	20.46*	14.83*	1.88
2-way interaction	3	6.26*	0.56	4.60*	16.09*	4.66*	1.3	6.95*	1.69	0.82	1.16	2.55
	1	3.12	0.02	0.02	16.48*	13.24*	0.11	2.01	0.01	0.02	0.43	1.01
	1	8.31*	0.2	0.56	11.38*	0.07	0.26	17.94*	4.16	0.84	0.02	4.34
	1	7.35*	1.49	13.21*	20.42*	0.66	3.53	0.91	0.92	1.61	3.02	2.31
Lack of fit	3	0.83	1.93	5.04	0.68	1.74	0.32	3.04	5.23	0.78	2.05	1.67

[#]degrees of freedom; *statistically significant at p < 0.05; **statistically significant at p < 0.001; FT: film thickness; EMC: equilibrated moisture content; DS: degree of swelling; WS: water solubility; OP$_{VIS}$ and OP$_{UV}$: film opacity in the visible and UV spectrum; TS: tensile strength; EAB: elongation at break; EM: elastic modulus; WVP: water vapour permeability; CA: surface contact angle.

$$Y_{DS} = 187.3 + 0.593\,X_1 - 5.090\,X_2 - 8.729\,X_3 + 0.122\,X_3^2 + 0.146\,X_2X_3 \tag{Eq. 5.5}$$

$$R^2 = 94.14; \quad R^2_{adj} = 91.48; \quad R^2_{pred} = 78.68$$

$$Y_{WS} = 0.20 + 1.0551\,X_1 - 0.065\,X_2 - 0.236\,X_3 - 0.008\,X_1^2 + 0.003\,X_3^2$$
$$- 0.007\,X_1X_2 - 0.003\,X_1X_3 + 0.010\,X_2X_3 \tag{Eq. 5.6}$$

$$R^2 = 97.61; \quad R^2_{adj} = 95.22; \quad R^2_{pred} = 86.46$$

$$Y_{OPVIS} = 603 - 11.44\,X_1 - 9.02\,X_2 + 0.116\,X_1^2 + 0.372\,X_1X_2 \tag{Eq. 5.7}$$

$$R^2 = 87.97; \quad R^2_{adj} = 83.95; \quad R^2_{pred} = 70.01$$

$$Y_{OPUV} = 1350 - 11.23\,X_1 + 203.0\,X_2 - 5.604\,X_2^2 \tag{Eq. 5.8}$$

$$R^2 = 96.44; \quad R^2_{adj} = 95.62; \quad R^2_{pred} = 94.33$$

$$Y_{TS} = 86.2 + 0.305\,X_1 - 0.518\,X_2 - 2.929\,X_3 - 0.012\,X_1^2 + 0.029\,X_3^2 + 0.017\,X_1X_3 \tag{Eq. 5.9}$$

$$R^2 = 95.75; \quad R^2_{adj} = 93.21; \quad R^2_{pred} = 81.42$$

$$Y_{EAB} = 11.77 + 1.953\,X_3 \tag{Eq. 5.10}$$

$$R^2 = 91.02; \quad R^2_{adj} = 90.42; \quad R^2_{pred} = 88.63$$

$$Y_{EM} = 2292 - 6.97\,X_1 - 12.01\,X_2 - 66.08\,X_3 + 0.559\,X_3^2 \tag{Eq. 5.11}$$

$$R^2 = 97.65; \quad R^2_{adj} = 96.87; \quad R^2_{pred} = 95.21$$

$$Y_{WVP} \times 10^{-3} = 944 - 5.0\,X_1 + 38.3\,X_2 + 10.79\,X_3 - 2.529\,X_2^2 + 0.643\,X_3^2 \tag{Eq. 5.12}$$

$$R^2 = 96.08; \quad R^2_{adj} = 94.31; \quad R^2_{pred} = 89.53$$

$$Y_{CA} = 45.4 + 0.682\,X_1 + 2.560\,X_2 - 0.293\,X_3 - 0.010\,X_1^2 - 0.116\,X_2^2 \qquad \text{(Eq. 5.13)}$$

$$R^2 = 89.44; \quad R_{adj}^2 = 84.64; \quad R_{pred}^2 = 70.84$$

All reduced regression models showed a high R^2 ranging from 87.97 to 97.61, indicating that only 3 to 12% of the total variations in the response data was not explained by the present models, which could be due to experimental variations or some other independent factors that were not included in this study (such as storage duration and ageing). Moreover, high R_{adj}^2 (83.95 – 96.87) and R_{pred}^2 (70.01 – 95.21) values also suggest a high significance and adequacy of the present models along with their ability to efficiently predict physicochemical properties of the LCh-Ge/LCh-Ge-O composite films based on the composition of their FFS (Azarifar et al., 2019; Singh et al., 2015).

5.3.1.2 Effect of independent variables on FT, EMC, DS and WS of the composite films

Film thickness (FT) was found to have a linear relationship with the content of gelatin and glycerol and a quadratic relationship with the content of oil in the films (Table 5.4, Eq. 5.3). Figure 5.1 shows the contour plots (the effect of two variables on the response when the third is set to the mid-level) and the main effect plot (consolidated effect of the individual variables) for film thickness. It is evident from these plots that film thickness was positively correlated with the oil and glycerol content of the films, while an increase in gelatin proportions of the films reduced their thickness. As explained earlier in Chapter 4 (refer to Section 4.3.3.1), the increase in film thickness with increasing contents of oil and glycerol is partially associated with the increase in the overall dry matter of the films. In addition, the presence of oil and glycerol molecules increases the intermolecular spacing between chitosan chains, which reduces the compactness and density of the film matrix resulting in thicker films (Maria et al., 2016; Valenzuela et al., 2013). On the other hand, the low molecular weight of gelatin compared to chitosan allows it to arrange in a much denser packing, which results in reduced film thickness with increasing proportions of gelatin in the films.
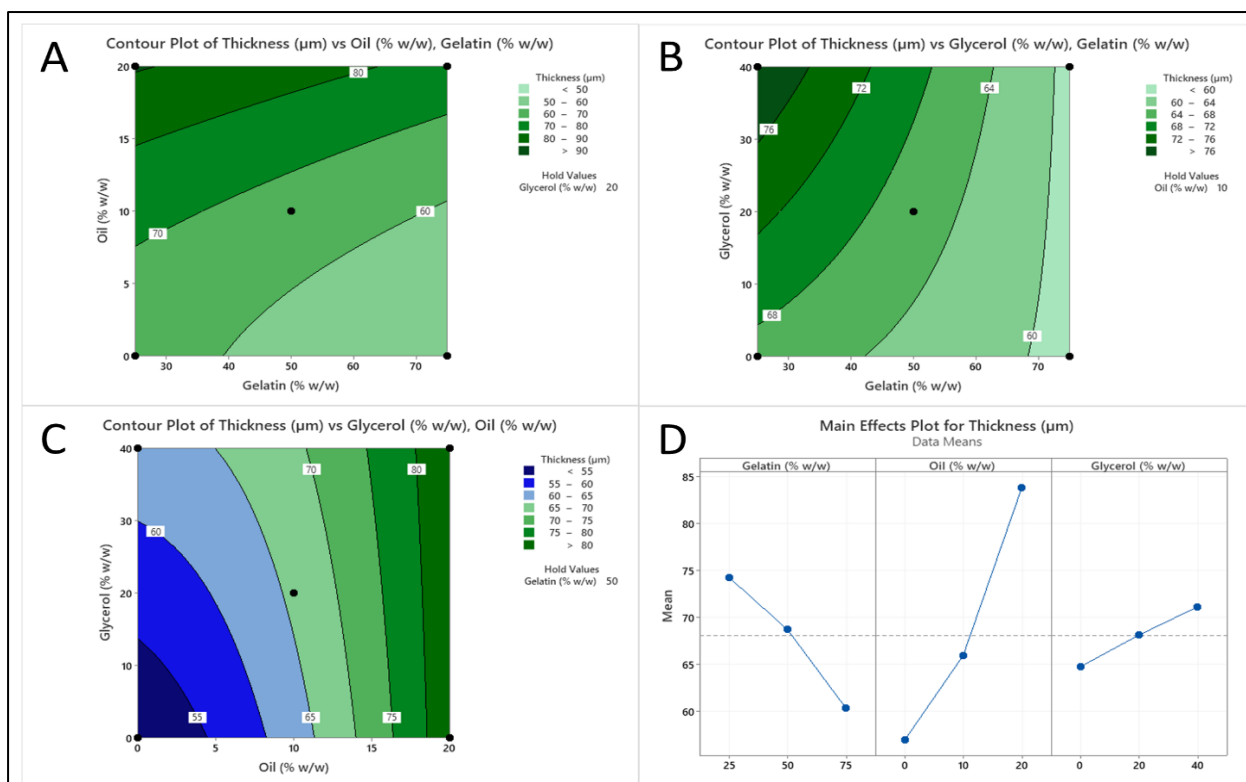
Figure 5.1: Contour plots for A) the effect of gelatin and oil levels on FT; B) the effect of gelatin and glycerol levels on FT; and C) the effect of oil and glycerol levels on FT. D) Main effect plot for FT.

As can be observed from Figures 5.1 B and C, the effect of glycerol on film thickness became less intense at higher levels of oil and gelatin in the films, which was also reflected in the regression model (Eq. 5.3) as interaction parameters of glycerol with gelatin or oil (X_1X_3, X_2X_3). The interaction effect of gelatin and glycerol (X_1X_3) may indicate a low degree of intermolecular interactions and migration of glycerol molecules between chitosan chains with high proportions of gelatin in the films. At the same time, the interaction effect of oil and glycerol (X_2X_3) could be explained by the small size of glycerol molecules that do not affect the intermolecular spacing when large triglyceride molecules are already present in between the chitosan chains. This difference in molecular size may also explain the higher significance of oil ($p < 0.001$) on film thickness than glycerol ($p < 0.05$).

The equilibrated moisture content (EMC) of the films presented a quadratic relationship with gelatin and glycerol content and a linear relationship with oil content (Eq. 5.4); however, no significant effect ($p > 0.05$) on the EMC was observed due to interaction parameters (Table 5.4).

The contour and main effect plots for EMC (Figure 5.2) along with the F-statistics (Table 5.4) show that glycerol was the most significant factor ($p < 0.001$) influencing the moisture content of the composite films. Due to the hydrophilic nature of glycerol, its increasing content significantly increases the ability of the film matrix to bind water, resulting in a high EMC for these films (Maria et al., 2016; Ziani et al., 2008). Similar results were reported by Thakur et al. (2017) while studying the effect of glycerol on pea starch-chitosan composite films. Conversely, the observed negative effect of oil content on EMC is directly associated with the increased hydrophobicity of the film matrix (Valenzuela et al., 2013).
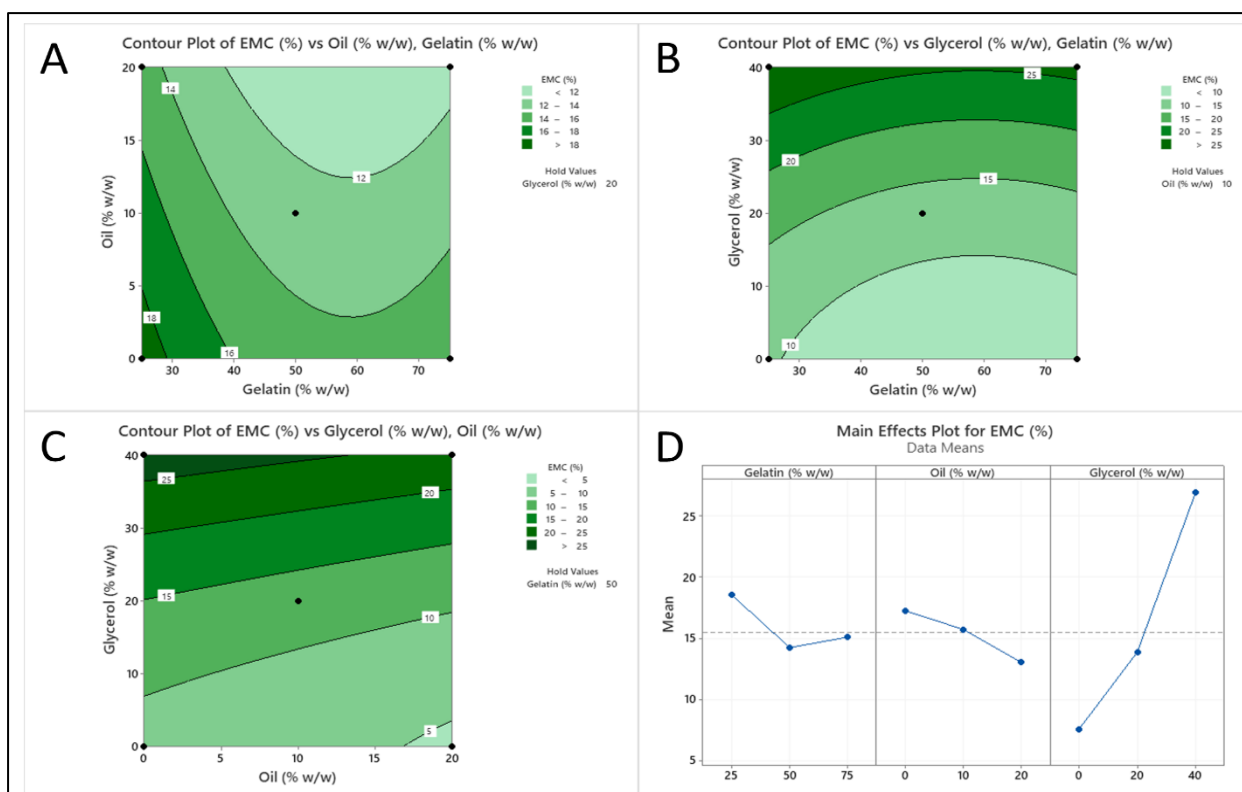
Figure 5.2: Contour plots for A) the effect of gelatin and oil levels on EMC; B) the effect of gelatin and glycerol levels on EMC; and C) the effect of oil and glycerol levels on EMC. D) Main effect plot for EMC.

The increasing proportions of gelatin in the films first caused a significant reduction in their EMC, followed by a slight increase at its maximum level (Figure 5.2A, B). This behaviour of composite films could be associated with the interactions between chitosan and gelatin and the availability of free -OH and -NH$_2$ functional groups in the film matrix contributed by these polymers. At a 1:1 ratio of Ge to LCh in the FFS, the interactions and polyelectrolyte complex

(PEC) formation between the two polymers were optimum, which reduced the number of available free hydrophilic groups that can bind water. However, at a lower or higher proportion of Ge to LCh, either one of these polymers seemed to be in excess compared to the other, which may have resulted in the availability of those hydrophilic groups to bind excess water and increase the EMC of the films.

The effects of linear terms of gelatin (X_1), oil (X_2) and glycerol (X_3) on the degree of swelling (DS) for composite films (Eq. 5.5) were as expected and followed the observations made in Chapter 4 (refer to Section 4.3.3.1). As shown in Figure 5.3, the increasing content of gelatin increased the swelling ability of the films due to a reduction in their crystallinity and increased hydrophilicity (Pereda et al., 2011; Trung et al., 2006). In contrast, increasing oil content had the opposite effect, which was associated with the ability of the oil to impart hydrophobicity to the films (Azarifar et al., 2019). The significant reduction in the DS of the plasticized films, i.e. films incorporated with glycerol, is associated with the strong hydrophilic interactions and hydrogen bonding between glycerol molecules and chitosan or gelatin chains. These interactions favour the dimensional stability of the film matrix and do not allow it to expand and swell extensively when submerged in water (Maria et al., 2016). Similar reports on the reduction in the swelling ability of plasticized films have been previously made by Maria et al. (2016) and Rodríguez-Núñez et al. (2014). Moreover, in accordance with the observations made by Maria et al. (2016), a slight increase in the DS was also observed with doubling the glycerol content of the films (Figure 5.3B, C), which is associated with the hydrophilic nature of glycerol and indicates its excess (presence of free and unbound glycerol molecules) in the film matrix. A significant positive effect ($p < 0.05$) on the DS of the films due to the interaction terms of oil and glycerol (X_2X_3) can also be observed from Eq. 5.4 and Figure 5.3C. This effect is perhaps associated with the hydrophilic nature of glycerol counteracting the hydrophobicity and resistance towards water absorption provided by oil incorporation in the films.
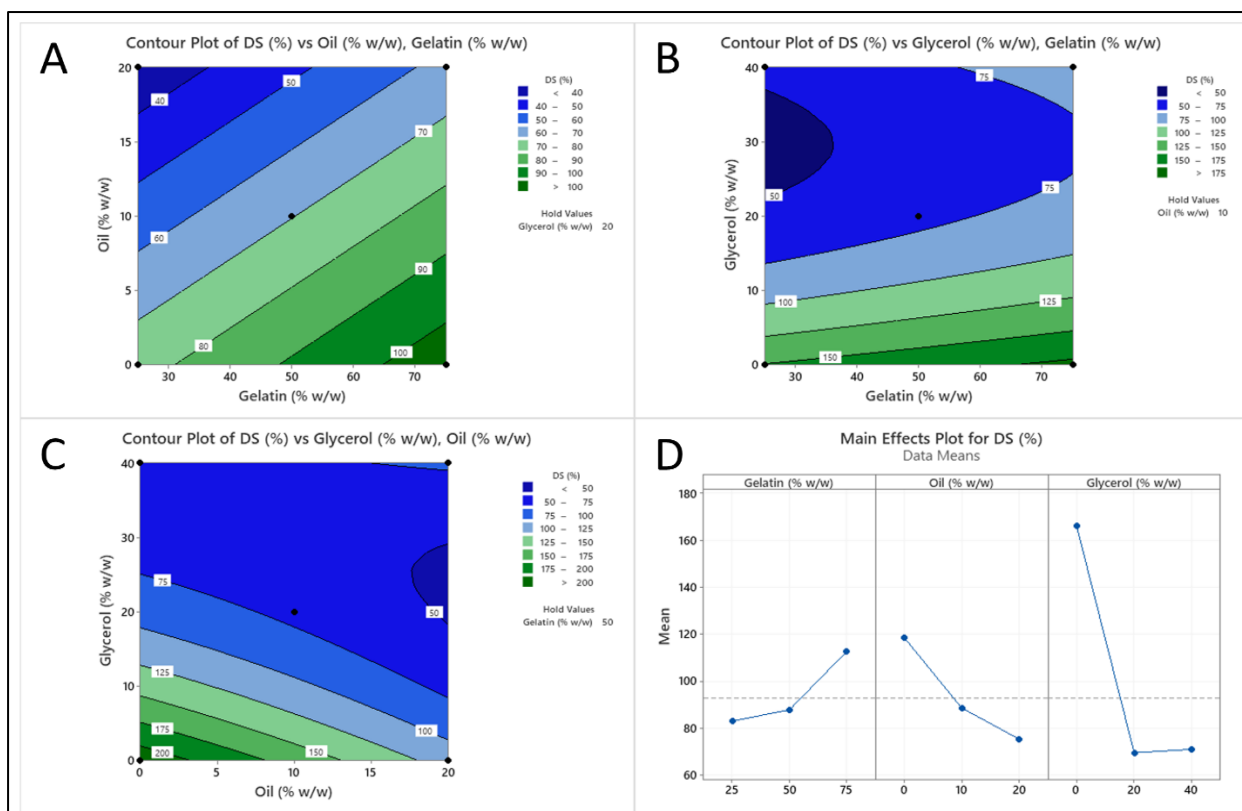
Figure 5.3: Contour plots for A) the effect of gelatin and oil levels on DS; B) the effect of gelatin and glycerol levels on DS; and C) the effect of oil and glycerol levels on DS. D) Main effect plot for DS.

Finally, the water solubility (WS) of the composite films was found to be significantly dependent ($p < 0.05$) on all linear, square and interaction terms of the independent variables (Eq. 5.6, Table 5.4) except for the square term of oil (X_2*X_2). The reduction in the WS of the films with the increasing content of oil and glycerol (Figure 5.4) can be again attributed to the increased hydrophobicity of the films and strong hydrogen bonding between glycerol and polymers, respectively (Cerqueira et al., 2012a; Rodríguez-Núñez et al., 2014; Tomadoni et al., 2019; Yao et al., 2017). Moreover, as observed for the DS of the films, the interaction term between oil and glycerol (X_2X_3) positively affected their WS, confirming the counteraction of glycerol's hydrophilicity against the hydrophobic nature imparted by the oil.

On the other hand, the WS of the films first increased and then slightly decreased with the increasing proportions of gelatin in the films (Figure 5.4A, B). While the initial increase in the WS can be explained by the high solubility of gelatin in water compared to chitosan (Pereda et al., 2011), the latter decrease could perhaps be associated with the high degree of intermolecular

interactions between gelatin molecules, which allowed for a denser packing (also reflected in film thickness) and therefore made films a bit more resistant to solubilize. In addition, the interaction terms of gelatin and oil (X_1X_2) and gelatin and glycerol (X_1X_3) both had a negative effect on the film's solubility, suggesting that the presence of oil or glycerol reduced the water solubility of gelatin.
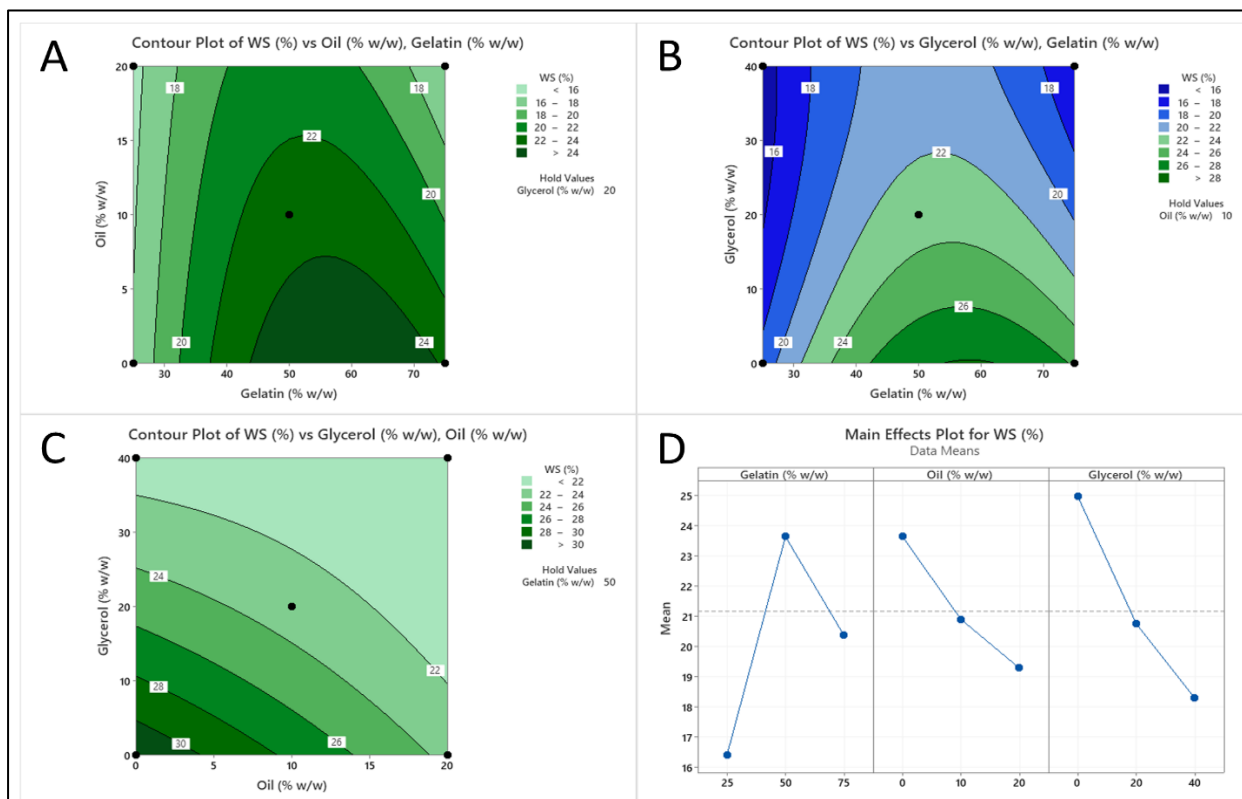
Figure 5.4: Contour plots for A) the effect of gelatin and oil levels on WS; B) the effect of gelatin and glycerol levels on WS; and C) the effect of oil and glycerol levels on WS. D) Main effect plot for WS.

5.3.1.3 Effect of independent variables on optical properties of the composite films

The opacity of the composite films in both visible (OP_{VIS}) and UV spectrum (OP_{UV}) was independent of their glycerol content, as shown in Eq. 5.7 and 5.8. Similar observations regarding the effect of glycerol on the opacity of the films in the visible spectrum were made by Tomadoni et al. (2019). The contour and main effect plots for OP_{VIS} and OP_{UV} are presented in Figure 5.5. At a low proportion of gelatin in the films (25% w/w), the incorporation of oil and its increasing content in the composite films did not show much impact on their OP_{VIS} (Figure 5.5A). However,

at higher proportions of gelatin (≥ 50% w/w), a significant and almost linear increase in film opacity was observed with increasing oil content. This behaviour of the composite films could have resulted from a reduction in the hydrophobic interactions between oil and chitosan due to the reduced chitosan content in the films with higher proportions of gelatin, which may have caused a partial breaking of emulsion and aggregation of oil droplets resulting in an increased opacity with increasing content of oil in the films.
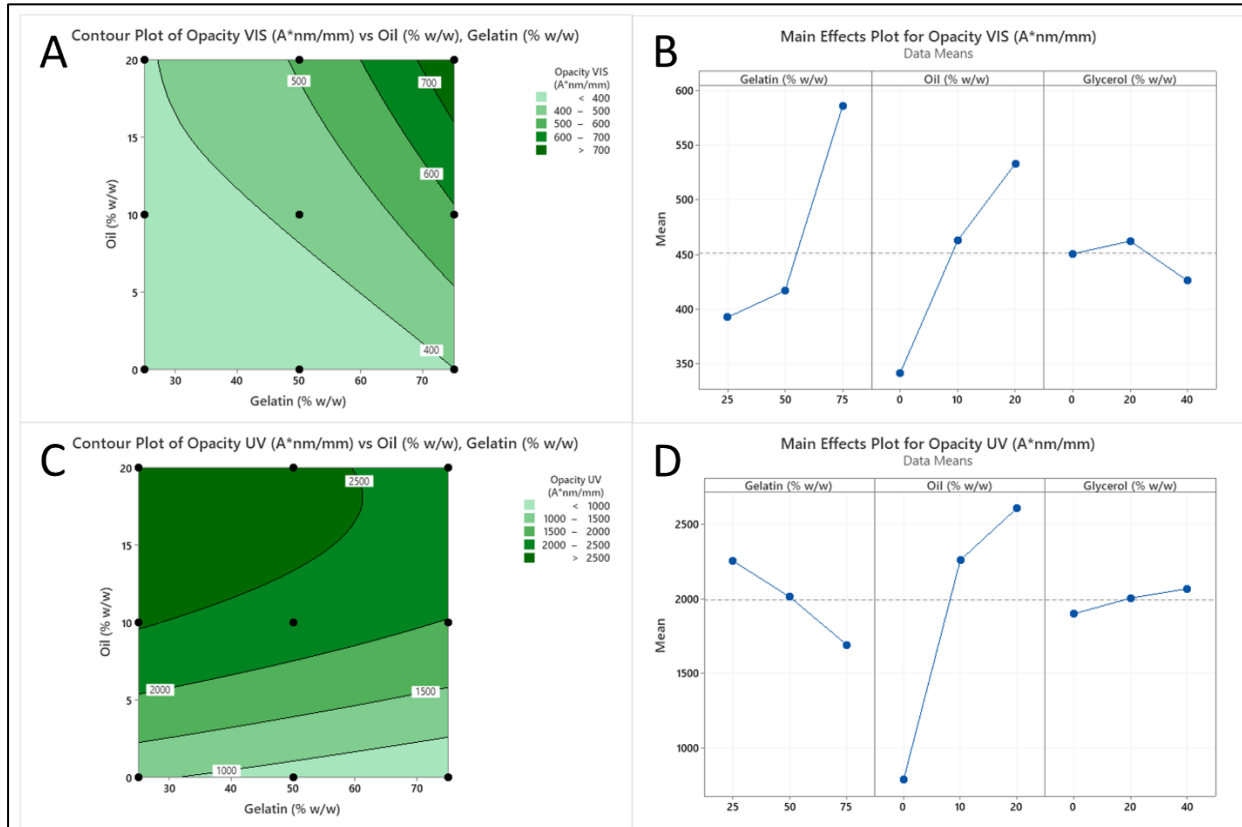
Figure 5.5: A) Contour and B) main effect plots for OP$_{VIS}$ as affected by glycerol and oil levels. C) Contour and D) main effect plots for OP$_{UV}$ as affected by glycerol and oil levels.

OP$_{UV}$ of the composite films had a negative linear correlation with the proportions of gelatin in the FFS (Eq. 5.8), which was in accordance with the reports made by Hosseini et al. (2013). On the other hand, a quadratic relationship was observed between OP$_{UV}$ and the oil content of the films. As shown in Figure 5.5C, films presented a significant increase in their OP$_{UV}$ with the incorporation of oil (10% w/w, mid-level). However, doubling the oil concentration in the films (20% w/w, high-level) did not show a further significant improvement in their UV resistance.

These observations suggest that the film's barrier properties against UV light became independent of their oil content after reaching a maximum value. Moreover, these effects of oil were independent of gelatin proportions in the films (no significant interaction effect).

5.3.1.4 *Effect of independent variables on mechanical properties of the composite films*

Tensile strength (TS) of the composite films decreased with an increase in the content of all three independent variables (Figure 5.6D, Eq. 5.9). Previous reports by Hosseini et al. (2013), Yao et al. (2017) and Ziani et al. (2008) have also made similar observations regarding the effect of gelatin, oil and glycerol on the TS of chitosan composite films, respectively. The detrimental effect of increasing oil content on the TS of the films was less intense ($p < 0.05$) and can be attributed to its interactions with the chitosan which led to an increase in intermolecular spacing between the chitosan chains (also reflected in increased film thickness) and a decrease in their intermolecular hydrogen bonding, resulting in a decreased TS (Haghighi, Biard, et al., 2019; Yao et al., 2017). This argument is supported by the fact that the effect of oil content on TS became more intense with higher gelatin content in the films (Figure 5.6A), which could be due to the increased proportions of oil to LCh in the films.

The influence of gelatin and glycerol content on the TS of the films was highly significant ($p < 0.001$), as also evident from their main effect plot (Figure 5.6D). Moreover, they also showed a complex positive interaction effect (X_1X_3) on film strength (Eq. 5.9). The effect of gelatin is associated with the inherently low TS and rigidity offered by its neat films, whereas glycerol's effect can be attributed to its plasticizing action (Hosseini et al., 2013; Pereda et al., 2011). At low proportions of gelatin, the hydrophilic interactions between LCh and Ge are more substantial, and therefore the detrimental effect of gelatin on the TS of the films is small (Figure 5.6A, B). However, at higher proportions, the LCh content decreases, and so do the interactions between the two polymers leading to a rapid decline in the film TS.

On the other hand, increasing glycerol content first showed a steep decline in the TS of the films at the mid-level concentration (20% w/w), following which the effect became less intense (Figure 5.6 B, C). This behaviour can be explained by the previously discussed dimensional stability and excessive hydrogen bonding provided by glycerol in the films, in addition to their

plasticizing effect. At high glycerol concentrations, the hydrogen bonding and cross-linking of polymer chains through glycerol could be much stronger, which may have provided additional strength to the film matrix, countering the detrimental effect of glycerol on film TS. The observed positive interaction effect of glycerol and gelatin can probably support this argument, as the presence of glycerol may have induced a high degree of cross-linking between LCh and Ge, lowering the negative effect of gelatin on film TS.
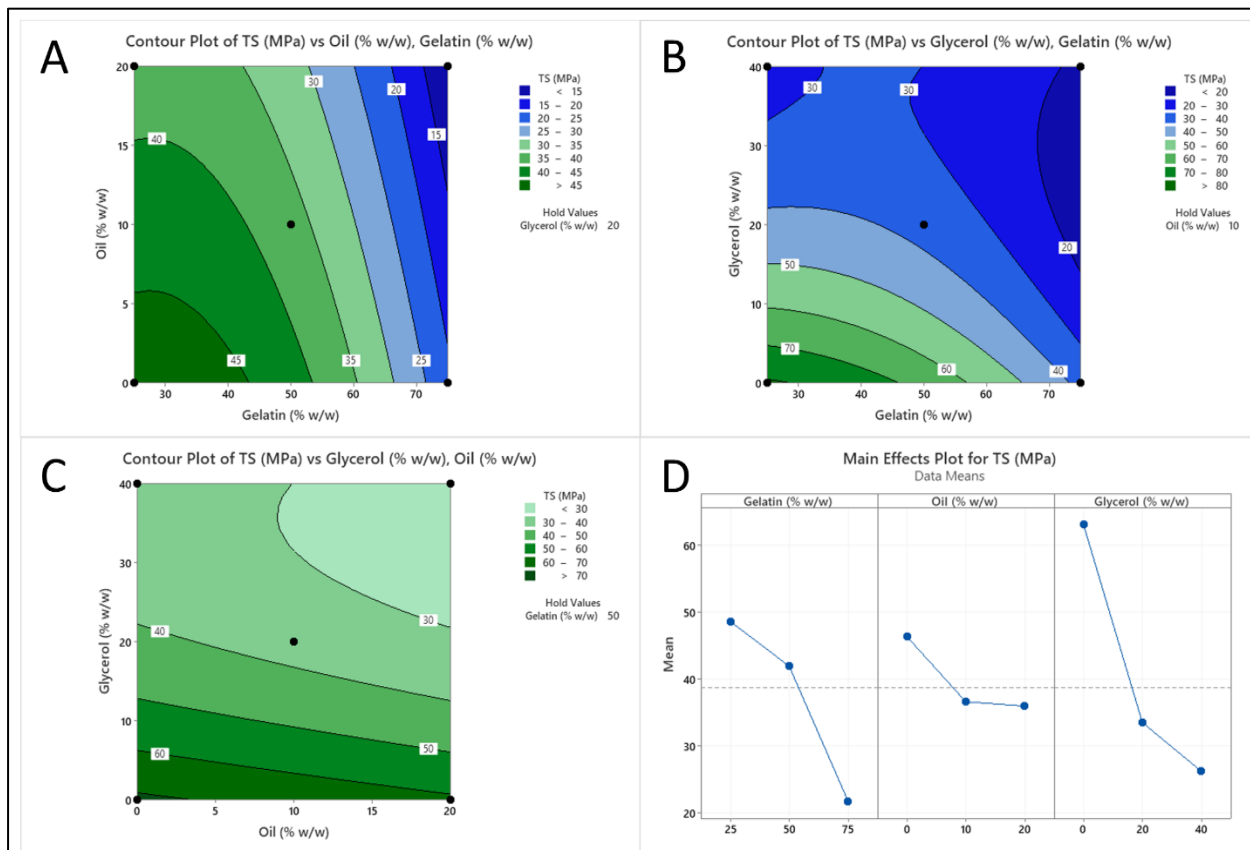
Figure 5.6: Contour plots for A) the effect of gelatin and oil levels on TS; B) the effect of gelatin and glycerol levels on TS; and C) the effect of oil and glycerol levels on TS. D) Main effect plot for TS.

The % elongation of the composite films (EAB) was found to be significantly dependent ($p < 0.001$) on only their glycerol content with a linear correlation (Table 5.4, Eq. 5.10) and therefore, no contour or main effect plots were obtained for EAB. The gelatin or oil proportions in the films did not show any significant effect ($p > 0.05$) on the EAB of the films, which was in accordance with the previous observations made in Chapter 4 (refer to Section 4.3.3.3). The linear relationship between the stretchability of the film and its glycerol content is directly associated

with the plasticizing effect of the glycerol, resulting in reduced intermolecular interactions between polymer chains and increased chain mobility (Rodríguez-Núñez et al., 2014).

Similar to the TS, the elastic modulus (EM) of the composite films also decreased with the increasing content of all three variables; however, gelatin and oil had a less significant effect ($p < 0.05$) and a linear relationship with the EM compared to the quadratic and highly significant effect ($p < 0.001$) of glycerol (Table 5.4, Eq. 5.11). As previously described, the effect of gelatin was associated with the inherently low TS and rigidity of fish gelatin films (Hosseini et al., 2013), while the effect of oil and glycerol was due to their plasticizing action (Arvanitoyannis et al., 1998; Yao et al., 2017). Moreover, as observed for film TS, the effect of glycerol on the EM of the films was less intense at higher concentrations which could be due to the excessive hydrogen bonding and cross-linking caused by glycerol.
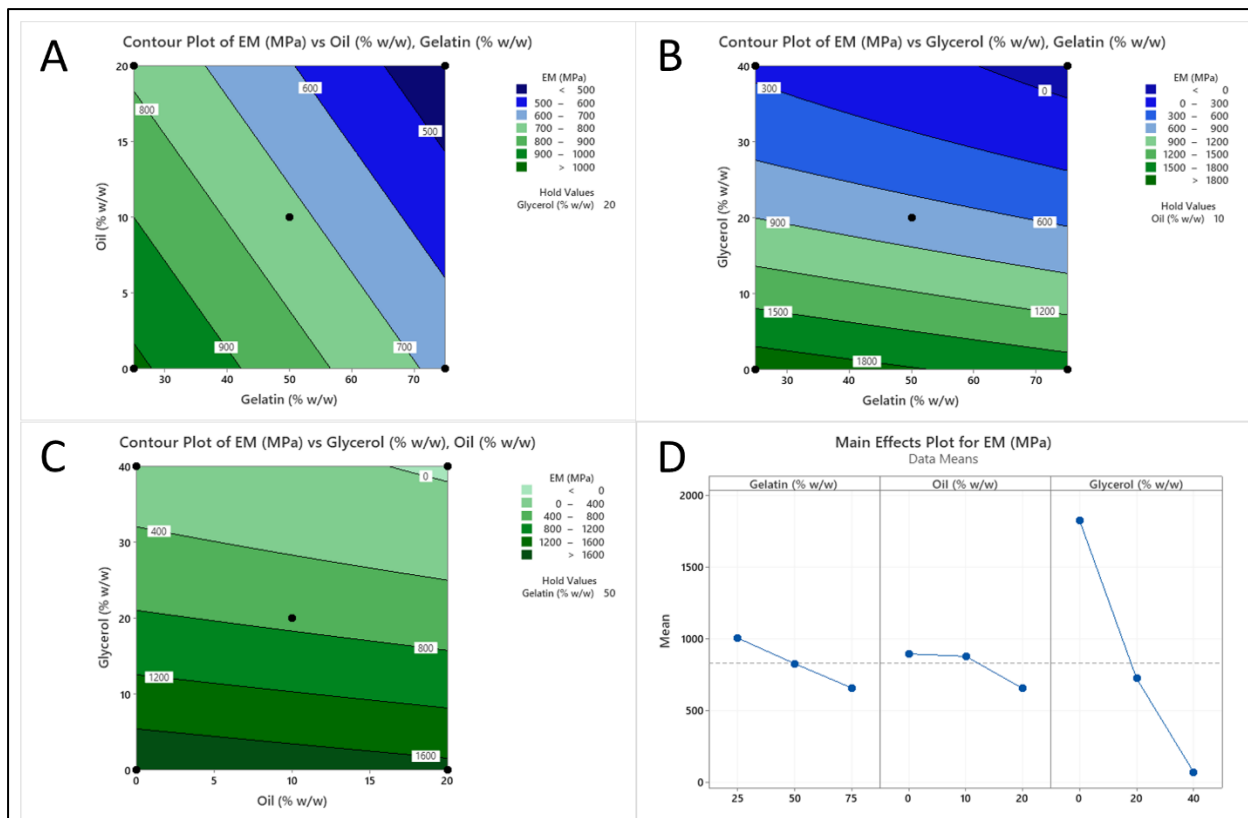
Figure 5.7: Contour plots for A) the effect of gelatin and oil levels on EM; B) the effect of gelatin and glycerol levels on EM; and C) the effect of oil and glycerol levels on EM. D) Main effect plot for EM.

5.3.1.5 Effect of independent variables on vapour permeability and surface hydrophobicity

The water vapour permeability (WVP) of chitosan-gelatin composite films showed a linear relationship with gelatin and a quadratic relationship with oil and glycerol without any interaction parameters (Table. 5.4, Eq. 5.12). Glycerol was the most significant factor ($p < 0.001$) affecting and enhancing the WVP of the films (Figure 5.8). As previously reported by other authors, the addition of glycerol in chitosan films increases their hydrophilicity, moisture content and intermolecular spacing, which leads to an improvement in water vapour diffusion and permeation through the film matrix (Cerqueira et al., 2012a; Maria et al., 2016; Rodríguez-Núñez et al., 2014). Similarly, the addition of oil reduces the hydrophilicity of the films, thus decreasing their WVP (Pereda et al., 2012). However, oil incorporation also increases the intermolecular spacing between the polymer chains that could counteract the lowering effect of oil on the WVP and may explain the observed slight increase in the permeation at lower oil concentrations in the composite films (Figure 5.8A, C). The decrease in WVP with increasing gelatin content of the films can again be associated with the higher density and low free volume of these films, which did not allow for a high degree of water vapour diffusion through the film matrix.

Similar to the WVP, the surface contact angle (CA) of the composite films also did not show any significant effect ($p > 0.05$) due to the interaction terms but had a linear relationship with glycerol and a quadratic relationship with gelatin and oil (Table. 5.4, Eq. 5.13). As per Figure 5.9, the decrease in CA with increasing glycerol concentrations in the films indicates the ability of glycerol to enhance their surface hydrophilicity, which is consistent with the WVP and EMC results. However, the effect of gelatin and oil proportions on the CA of the films was a bit more complex. With increasing gelatin proportions, the CA of the films remained unaffected up till the mid-level (50% w/w polymer). However, at its high-level concentration (75% w/w polymer), a significant reduction in the CA was observed (Figure 5.9A, B). Gelatin being more hydrophilic than chitosan can explain the low CA of composite films with high gelatin content (Córdoba & Sobral, 2017; Rodrigues, Bertolo et al., 2020; J. Xu et al., 2020). On the other hand, as discussed earlier in Chapter 4 (refer to Section 4.3.3.4), the interactions between chitosan and gelatin and the unavailability of free hydrophilic functional groups at similar proportions of both polymers could be the reason that no changes in the CA of the films were observed at low gelatin concentrations.
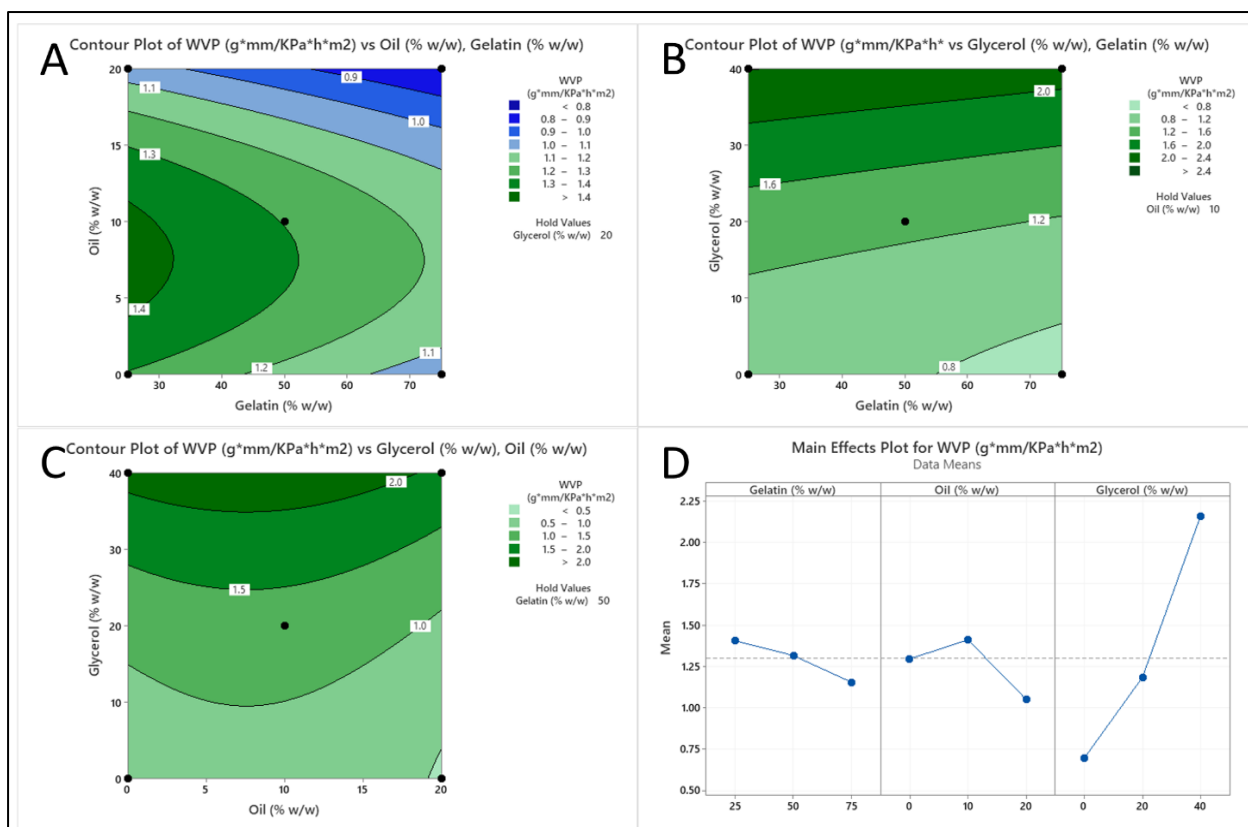
Figure 5.8: Contour plots for A) the effect of gelatin and oil levels on WVP; B) the effect of gelatin and glycerol levels on WVP; and C) the effect of oil and glycerol levels on WVP. D) Main effect plot for WVP.

Incorporation of oil in the films at 10% (w/w polymer) concentration significantly increased their CA, which can be explained by the relative substitution of hydrophilic groups of gelatin and glycerol with the hydrophobic groups of oil on the film surface (Azarifar et al., 2019; Yao et al., 2017). However, an increase in the oil content showed a negative effect on the surface hydrophobicity of the films. Although an apparent reason behind this reduction in CA is unclear, it could be linked with the high concentration of Tween-20 in films with high oil content (20 % w/w polymer) that might have contributed to the increased hydrophilicity of the film surface.
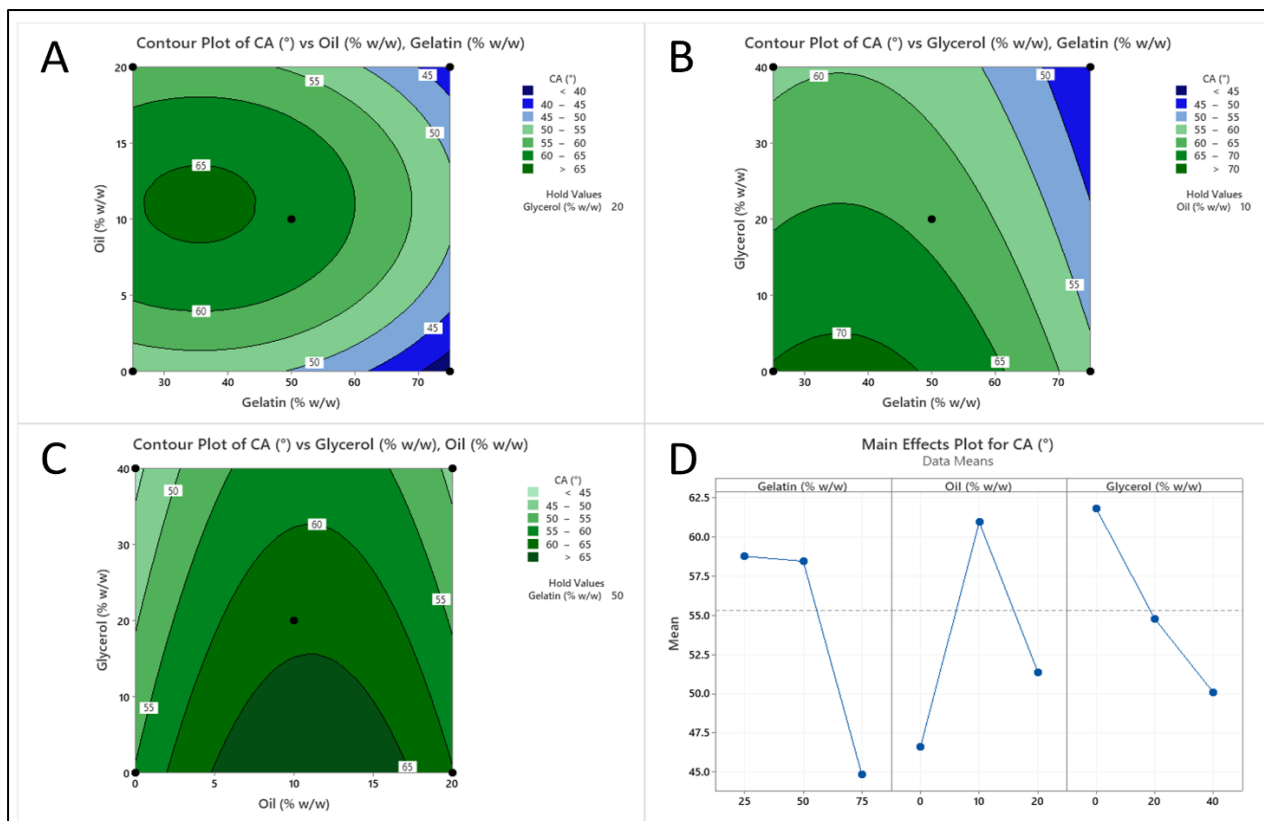
Figure 5.9: Contour plots for A) the effect of gelatin and oil levels on CA; B) the effect of gelatin and glycerol levels on CA; and C) the effect of oil and glycerol levels on CA. D) Main effect plot for CA.

5.3.1.6 Simultaneous optimization and validation of regression models

Based on the intended potential applications of chitosan composite films, three optimized FFS formulations were obtained using simultaneous optimization of response parameters. Table 5.5 shows the provided target values for the responses and obtained optimized formulations along with their desirability function, while Table 5.6 summarizes the intended applicability and functionality of the resultant optimized films in different food product categories. Film thickness and their moisture content (EMC) were not optimized in this study as these properties do not directly influence the applicability of the edible films. On the other hand, set target ranges were provided for mechanical properties of composite films to ensure a reasonable balance between their strength, rigidity and stretchability. Moreover, water vapour permeability (WVP) was targeted to be minimum in all optimized formulations as a low WVP of the packaging material is generally critical for most food packaging applications.

Table 5.5: Target responses and optimized composite film formulations based on desirability function.

Response parameters	Formulation 1	Formulation 2	Formulation 3
	Target	*Target*	*Target*
Film thickness (μm)	NO	NO	NO
Equilibrated moisture content (%)	NO	NO	NO
Degree of swelling (%)	Minimize	NO	Maximize
Water solubility (%)	Minimize	NO	Maximize
Opacity VIS (A.nm/mm)	Minimize	Minimize	NO
Opacity UV (A.nm/mm)	Maximize	Maximize	NO
Tensile strength (MPa)	Range (35 - 45)	Range (35 - 45)	Range (35 - 45)
Elongation at break (%)	Range (35 - 45)	Range (45 - 55)	Range (35 - 45)
Elastic modulus (MPa)	Range (800-1000)	Range (800-1000)	Range (800-1000)
Water vapour permeability (g.mm/kPa.h.m^2)	Minimize	Minimize	Minimize
Contact angle (°)	Maximize	NO	NO
Gelatin (X_1)	59.34	43.76	59.69
Oil (X_2)	11.31	15.42	0
Glycerol (X_3)	14.94	17.41	11.55
Desirability (D)	0.81	0.84	0.77

NO: Not optimized.

Table 5.6: Potential applicability and functionality of optimized composite edible films.

Optimized FFS	Food product category	Applicability	Functionality of edible film
Formulation 1	Medium-moisture processed food products Examples - Cheese, tofu and processed meat products like sausages etc.	Edible films used in direct contact with the moist surface of the food	• Prevention from microbial spoilage • Prevention from dehydration • Prevention from photolytic degradation
Formulation 2	Fresh and cut fruits and vegetables Examples - Strawberries, apples, mushrooms, leafy vegetables etc.	Edible films used in direct or indirect contact with the food surface (comparatively low moisture on product surface)	• Allowing respiration of fruits and vegetables • Prevention from microbial spoilage • Prevention from dehydration • Prevention from photolytic degradation • Basic containment function • Reduction of single-use plastic packaging
Formulation 3	Dry or low-moisture food products Examples - Instant noodles, spice mixes, instant coffee powder etc.	Edible films used to contain the product and can be cooked or consumed along with the product	• Solubility in water • Edible nature of the film • Basic containment function • Reduction of single-use plastic packaging

Composite films intended for wrapping or coating food products with moist surfaces (formulation 1) were optimized for high resistance towards water swelling (DS) and solubility (WS) and high surface hydrophobicity (high CA) in order to ensure their structural integrity after coming in direct contact with product's surface moisture. Alternatively, films intended for packaging fresh or cut fruits and vegetables with relatively dry surfaces (formulation 2) were not required to have high resistance towards surface water to maintain their integrity and thus were not optimized for their DS, WS and CA. However, both formulations (1 and 2) were targeted for high UV resistance to prevent photolytic degradation of products and high transparency to ensure product visibility to the consumer. The target range of EAB for formulation 2 was kept a bit higher to provide extra flexibility and prevention against puncturing from the sharp edges or stalks of fruits and vegetables. Films obtained from the third formulation were intended to contain dry products that can be further packed into outer paper-based packaging to prevent films from contamination and maintain their edibility. Therefore, these films were not optimized for their optical properties but were targeted for maximum DS and WS to ensure product release in water during preparation.

Table 5.7: Predicted and experimental response data for optimized formulations.

Response parameters	Formulation 1		Formulation 2		Formulation 3	
	Predicted value and range at 95% CI*	*Experimental value*	*Predicted value and range at 95% CI**	*Experimental value*	*Predicted value and range at 95% CI**	*Experimental value*
Film thickness (μm)	64.79 (62.75 - 66.84)	66.87 ± 4.61	76.01 (74.14 - 77.87)	74.53 ± 5.37	52.12 (48.89 - 55.34)	51.12 ± 7.69
Equilibrated moisture content (%)	10.01 (8.74-11.25)	12.25 ± 1.36	11.06 (9.65 - 12.48)	13.12 ± 0.92	11.11 (9.42 - 12.79)	11.40 ± 1.45
Degree of swelling (%)	86.53 (75.23 - 97.83)	83.51 ± 5.47	59.14 (46.58 - 71.71)	61.06 ± 2.04	138.18 (121.03 - 155.34)	157.21 ± 4.89
Water solubility (%)	23.74 (22.85 - 24.61)	23.02 ± 1.81	21.61 (20.61 - 22.62)	19.98 ± 1.27	28.59 (27.24 - 29.95)	30.87 ± 3.35
Opacity VIS (A.nm/mm)	480.46 (446.35 - 514.58)	498.80 ± 23.89	436.74 (396.32 - 477.17)	438.59 ± 9.49	333.78 (279.62 - 387.95)	297.00 ± 7.73
Opacity UV (A.nm/mm)	2262.4 (2142.3 - 2382.5)	2176.1 ± 39.2	2656.0 (2543.9 - 2768.2)	2683.9 ± 53.6	679.6 (504.9 - 854.3)	593.9 ± 28.3
Tensile strength (MPa)	34.63 (30.39 - 38.86)	33.08 ± 2.41	39.69 (34.94 - 44.44)	41.01 ± 3.12	44.07 (38.36 - 49.79)	48.79 ± 5.59
Elongation at break (%)	40.94 (36.01 - 45.88)	41.39 ± 10.05	45.77 (41.05 - 50.48)	48.71 ± 13.74	34.32 (28.88 - 39.76)	27.12 ± 6.34
Elastic modulus (MPa)	880.4 (791.1 - 969.7)	863.5 ± 51.2	821.1 (722.0 - 920.1)	798.6 ± 43.5	1187.5 (1062.7 - 1312.4)	1259.6 ± 69.1
Water vapour permeability (g.mm/kPa.h.m^2)	1.06 (0.94 - 1.18)	1.05 ± 0.03	1.09 (0.98 - 1.21)	1.11 ± 0.04	0.86 (0.68 - 1.02)	0.79 ± 0.06
Contact angle (°)	61.8 (58.3 - 65.2)	58.9 ± 2.5	63.6 (60.2 - 66.9)	61.8 ± 1.9	48.5 (43.6 - 53.4)	45.6 ± 1.6

*CI: Confidence interval.

Table 5.7 compares the experimental response data for all three optimized films with their predicted values obtained from the regression models. Minitab 19 Statistical Software was used to obtain the predicted ranges at a confidence interval of 95%. As can be observed from the results, the experimental values for each optimized formulation appeared in their predicted ranges with slight variations. This validates the present optimization study and demonstrates the adequacy and reliability of the regression equations in predicting the response parameters for chitosan-gelatin-oil composite films.

5.3.2 Low MW Lobster-Shell Chitosan Composite Films

5.3.2.1 Characterization of low MW lobster chitosan

The low MW lobster chitosan (LLCh) obtained from the enzymatic hydrolysis of LCh was bright white in appearance in contrast to the pink colour of its substrate (LCh powder), indicating a loss of pigments either during the hydrolysis step or during the removal of minerals from the hydrolysate using membrane dialysis. The utilized procedure for preparing LLCh powder was highly efficient, with a production yield of 84.3 ± 2.7% and provided a reasonably pure product with no available minerals ($\approx$ 0% ash content) and a final moisture content of 2.24 ± 0.07% (w/w db). The observed product loss ($\approx$ 15.7%) can be attributed to the removal of LLCh chains with a molecular weight of less than 100-500 Da (MWCO of dialysis membrane) from the hydrolysate during the purification step. The protein and lipid content of LLCh was not determined in this study as no proteins or lipids were available in the substrate, i.e. LCh powder (refer to Chapter 3, Section 3.3.1.1), and the utilized procedure does not add any lipids or proteins in the hydrolysate except for a small amount of added enzyme.

Table 5.8 lists the average molecular weights and polydispersity index (PDI) of LLCh and LCh (data taken from Chapter 3 for reference) samples. It can be observed from the results that the average MWs of LLCh were approximately half compared to LCh, indicating the efficacy of Viscozyme® L as a non-specific hydrolyzing enzyme for chitosan. Moreover, the PDI of LLCh was significantly higher than LCh, suggesting a broader MW distribution in the hydrolyzed product.

Table 5.8: Average molecular weights (MW) and polydispersity index for lobster-shell chitosan (LCh) and hydrolyzed low MW lobster-shell chitosan (LLCh).

	Peak MW (M$_P$)	Weight average MW (M$_W$)	Number average MW (M$_N$)	Viscosity average MW (M$_V$)	Polydispersity Index (PDI)
LCh	389 ± 22 kDa[A]	341 ± 47 kDa[A]	308 ± 25 kDa[A]	363 ± 23 kDa[A]	1.10 ± 0.06[A]
LLCh	181 ± 21 kDa[B]	154 ± 7 kDa[B]	106 ± 9.0 kDa[B]	159 ± 17 kDa[B]	1.45 ± 0.08[B]

The difference between the two mean values followed by the same letter in the same column is statistically insignificant ($p > 0.05$) as determined by Tukey's HSD test.

5.3.2.2   *Physicochemical characterization of LLCh-based films*

The values of all physicochemical properties obtained from LLCh based neat and composite films (developed from the three previously optimized formulations) and their LCh based counterparts (for comparison) are shown in Table 5.9. From a qualitative perspective, LCh and LLCh films were quite similar in appearance and flexibility; however, significant differences ($p < 0.05$) were found in some of their physicochemical properties due to a difference in the molecular weights (MW) of chitosan. LLCh films showed a slight but insignificant reduction ($p > 0.05$) in their thickness compared to LCh films which can be attributed to a denser packing and low entanglement of LLCh chains owing to their low MW (Alves et al., 2019). A similar slight reduction in film thickness for low MW chitosan composite films can be observed from the data reported by Liu et al. (2012), but the authors did not provide any explanation behind these changes.

The equilibrated moisture content (EMC) of neat LLCh films was significantly lower ($p < 0.05$) than neat LCh films and could again be associated with the denser packing of LLCh chains, leaving less free volume in the film matrix resulting in a lower absorbed and bound moisture (Pereda et al., 2011). These results were in agreement with the previous reports made by Alves et al. (2019) and García et al. (2015). On the other hand, such a decrease in EMC was not observed for composite films, which could be linked with the low concentrations of chitosan in these films and interactions between chitosan and gelatin molecules. No change in the degree of swelling (DS) was observed between neat LCh and LLCh films; however, LLCh composite films showed a significantly lower ($p < 0.05$) DS compared to LCh composite films. These observations suggest

that the degree of intermolecular interactions between chitosan, gelatin and glycerol were significantly higher when the MW of chitosan was lower, thus preventing the excessive swelling of the film matrix when submerged in water. In contrast, the water solubility (WS) for all LLCh films was significantly higher ($p < 0.05$) than the LCh films, which can be explained by the increased solubility of chitosan with a reduction in its MW (Alves et al., 2019). Alves et al. (2019) and Leceta, Guerrero, & de la Caba (2013) have reported similar results when comparing the solubility of low and high MW chitosan-based films.

The opacity of the neat and composite films in the visible spectrum (OP$_{VIS}$) increased with a reduction in the MW of chitosan, which followed the previous reports made by several authors (Alves et al., 2019; García et al., 2015; Leceta, Guerrero, & de la Caba, 2013). Leceta, Guerrero, & de la Caba (2013) reasoned that low MW chitosan was prone to a higher degree of Maillard reaction and oxidation due to their higher content of reducing ends which may have caused an increased yellowness and thus a reduction in the film transparency. A similar increase in the opacity of the LLCh composite films in the ultraviolet spectrum (OP$_{UV}$) was also observed. However, this trend was reversed in the case of neat films, although no suitable explanation could be found to justify this behaviour.

A decrease in the MW of chitosan had a detrimental effect on all mechanical properties of neat and composite films, but the effect was significant ($p < 0.05$) only in the case of the tensile strength (TS) of neat LLCh films. This dependency of chitosan film's tensile properties on the MW of chitosan has been previously observed by various authors and is generally explained by a reduction in the entanglement network of chitosan chains with low MW, which results in lower strength and flexibility for these films (Alves et al., 2019; Fernández-Pan et al., 2010; Liu et al., 2012; Nunthanid et al., 2001; Park et al., 2002). The water vapour permeability (WVP) of the films also reduced with the MW of chitosan ($p < 0.05$ only for neat films), which may have been associated with their low EMC and high film density. On the contrary, no significant effect ($p > 0.05$) of MW was observed on the surface hydrophobicity of the neat or composite films. Leceta, Guerrero, & de la Caba (2013) have reported similar observations regarding the surface contact angle (CA) of low and high MW chitosan films.

Table 5.9: Physicochemical properties of lobster-shell chitosan (LCh) and hydrolyzed low MW lobster-shell chitosan (LLCh) based neat and optimized composite films.

Physcicochemical properties	Neat films		Formulation 1		Formulation 2		Formulation 3	
	LCh	LLCh	LCh	LLCh	LCh	LLCh	LCh	LLCh
FT (µm)	54.1 ± 3.2[A]	50.9 ± 3.7[A]	66.9 ± 4.6[A]	61.0 ± 5.1[A]	74.5 ± 5.4[A]	72.5 ± 4.6[A]	51.1 ± 7.7[A]	47.7 ± 3.3[A]
ECM (%)	23.3 ± 1.3[A]	19.0 ± 1.5[B]	12.3 ± 1.4[A]	12.5 ± 0.5[A]	13.1 ± 0.9[A]	12.7 ± 1.7[A]	11.4 ± 1.5[A]	10.9 ± 1.0[A]
DS (%)	280.4 ± 17.8[A]	288.2 ± 11.5[A]	83.5 ± 5.6[A]	73.0 ± 2.8[B]	61.0 ± 2.0[A]	49.3 ± 3.6[B]	157.2 ± 4.9[A]	119.7 ± 10.7[B]
WS (%)	24.2 ± 1.7[A]	29.5 ± 0.8[B]	23.0 ± 1.8[A]	30.9 ± 1.5[B]	20.0 ± 1.3[A]	27.6 ± 0.7[B]	30.9 ± 3.4[A]	40.6 ± 2.1[B]
OP_{VIS} (A.nm/mm)	402.8 ± 16.8[A]	487.6 ± 15.3[B]	498.8 ± 23.9[A]	550.3 ± 15.3[B]	438.59 ± 9.49[A]	531.0 ± 34.6[B]	297.00 ± 7.73[A]	376.5 ± 23.9[B]
OP_{UV} (A.nm/mm)	817.3 ± 16.7[A]	738.8 ± 26.7[B]	2176.1 ± 39.2[A]	2338.2 ± 5.7[B]	2683.9 ± 53.6[A]	2909.5 ± 43.7[B]	593.9 ± 28.3[A]	744.2 ± 7.9[B]
TS (MPa)	80.1 ± 3.6[A]	71.8 ± 4.3[B]	33.01 ± 2.4[A]	31.4 ± 1.5[A]	41.0 ± 3.1[A]	38.4 ± 4.6[A]	48.8 ± 5.6[A]	46.7 ± 1.9[A]
EAB (%)	54.6 ± 2.9[A]	49.9 ± 2.2[A]	41.4 ± 10.1[A]	39.1 ± 4.5[A]	48.71 ± 13.8[A]	44.3 ± 11.2[A]	27.1 ± 6.3[A]	24.3 ± 3.6[A]
EM (MPa)	2254 ± 178[A]	2197 ± 136[A]	864 ± 51[A]	843 ± 39[A]	799 ± 44[A]	784 ± 70[A]	1260 ± 69[A]	1110 ± 102[A]
WVP (g.mm/kPa.h.m²)	0.89 ± 0.04[A]	0.81 ± 0.01[B]	1.05 ± 0.03[A]	1.01 ± 0.02[A]	1.11 ± 0.04[A]	1.08 ± 0.06[A]	0.79 ± 0.06[A]	0.70 ± 0.04[A]
CA (°)	70.5 ± 1.2[A]	71± 1.7[A]	58.9 ± 2.5[A]	56.6± 0.7[A]	61.8 ± 1.9[A]	61.7 ± 1.7[A]	45.6 ± 1.6[A]	44.1 ± 2.0[A]

FT: film thickness; EMC; equilibrated moisture content; DS: degree of swelling; WS: water solubility; OP_{VIS} and OP_{UV}: film opacity in the visible and UV spectrum; TS: tensile strength; EAB: elongation at break; EM: elastic modulus; WVP: water vapour permeability; CA: surface contact angle. The difference between the mean values of a film type (Neat or optimized formulations) followed by the same letter in the same row is statistically insignificant ($p > 0.05$) as determined by Tukey's HSD test.

5.3.3 Antimicrobial Properties of Lobster-shell Chitosan and Composite Films

In order to estimate the antimicrobial activity of LCh and LLCh-based neat and composite (optimized) films, *E. coli* inoculated growth media suspensions were incubated with film samples ($\approx$ 5 mg/mL) for 24 h and the optical density (OD) of the suspensions was recorded at the 6th, 12th and 24th h of incubation. The OD results are presented in Figure 5.10 in terms of % inhibition of *E. coli* with the values obtained for the low-density polyethylene (LDPE) film samples taken as a reference (0% inhibition). Ampicillin (1 µg/mL) and acetic acid (1 µL/mL) were used as positive controls for comparison. The tested concentration of acetic acid was chosen based on the estimations of free acetic acid present in the chitosan-based films. As evident from the results, neat LCh and LLCh films offered the highest inhibition against *E. coli* (77 – 83%) over the 24 h incubation period, which was statistically similar (p > 0.001) to the 6th h reading and significantly higher (p > 0.001) than the 12th and 24th h reading of both positive controls. The significantly higher activity of neat films compared to acetic acid control suggests that while the free acetic acid in the chitosan films may have contributed to their inhibitory potential, the primary antimicrobial activity of the films was due to their chitosan content.

The biocidal activity of chitosan is often associated with its cationic amino groups that interact with the negatively charged microbial cell membrane components and alter their structure and permeability, leading to the leakage of cytoplasmic contents and the death of microbes (Aider, 2010; Elsabee, 2015; Kingkaew et al., 2014; Rajpal, 2007). Therefore, the availability of free -NH$_2$ groups in the films that can interact with the microbes dictates the antimicrobial potential of chitosan-based films. As composite films have low chitosan content and most of their active -NH$_2$ groups are bound in strong hydrophilic interactions between chitosan, gelatin and glycerol, their antimicrobial activity is significantly lower than the neat films. Similar observations have been previously made by Jridi et al. (2014) while comparing the antimicrobial activity of chitosan, gelatin and chitosan-gelatin composite films against several gram-positive and gram-negative bacteria.
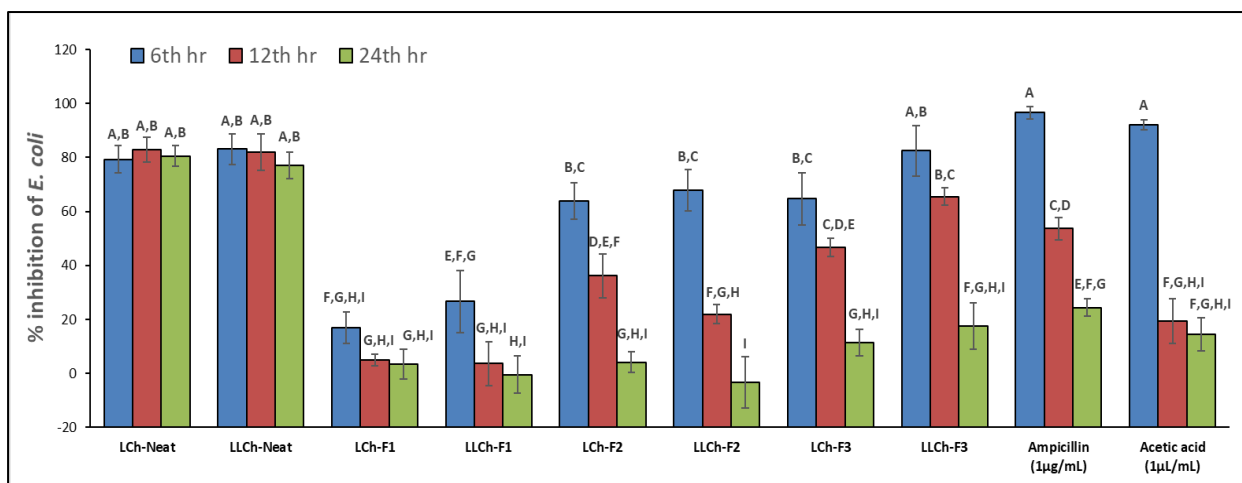
Figure 5.10: Antimicrobial activity (optical density data) of LCh and LLCh based films in terms of % inhibition of E. coli with LDPE control films as a reference (0% inhibition). Columns with different letters indicate significantly different means (p < 0.001) determined by Tukey's HSD test.

The MW of chitosan (LCh vs LLCh) did not significantly affect (p > 0.001) the inhibitory activity of neat and composite films. However, these observations contradict the widely reported increase in the antimicrobial activity of chitosan with a reduction in their molecular weight due to the enhanced mobility of small chitosan chains and their effective binding with the microbial membranes (Goy et al., 2009; Ke et al., 2021; Shin et al., 2001). This contradiction can be explained by the difference in the MW of LCh and LLCh, which might not be sufficient to present a significant difference in their antimicrobial activities. Leceta, Guerrero, Ibarburu, et al. (2013) also reported similar observations while comparing the biocidal activity of low and high MW chitosan films against *E. coli* 0517H.

Among the optimized composites, films obtained from formulation 3 (F3) showed the highest inhibitory activity, followed by the films obtained from formulations 2 (F2) and 1 (F1). This could be explained by the high solubility (WS) of F3 films and their low glycerol content compared to other formulations, which may have allowed for a higher concentration of chitosan to be dissolved in the growth media, thus providing a higher degree of *E. coli* growth inhibition. On the other hand, the higher activity of F2 films compared to F1 films can be associated with their higher content of chitosan (56% w/w in F2 vs 40% w/w in F1). F1 and F2 films also showed a very low or even negative % inhibition at the 24th h reading, which may have been the result of

127

dissolved gelatin in the growth media being used as a nutrient source (protein source) by the bacteria.

In order to validate the antimicrobial activity results based on the OD data, the CFUs in the bacterial suspensions post 24 h incubation were enumerated using subcultivation, the data for which is shown in Table 5.11 in terms of log (CFU/mL). As can be seen, neat LCh and LLCh films had the lowest surviving *E. coli* CFUs ($p < 0.05$), while all other films and positive controls showed no significant difference ($p > 0.05$) in their CFUs, thus supporting the 24th h observations from the OD data (Figure 5.10).

Table 5.10: Colony-forming units (CFUs) of E. coli remaining after 24 hours of incubation with the LCh and LLCh based films (neat and optimized) or control samples.

Samples	Log (CFU/mL)
LDPE	10.11 ± 0.18^{A}
LCh-Neat	6.20 ± 0.19^{D}
LLCh-Neat	6.39 ± 0.09^{D}
LCh-F1	$10.03 \pm 0.11^{A,B}$
LLCh-F1	$10.14 \pm 0.16^{A,B,C}$
LCh-F2	$9.97 \pm 0.15^{A,B,C}$
LLCh-F2	9.94 ± 0.15^{C}
LCh-F3	$9.66 \pm 0.07^{A,B,C}$
LLCh-F3	$9.51 \pm 0.13^{B,C}$
Ampicillin (1 µg/mL)	$9.53 \pm 0.09^{B,C}$
Acetic acid (1 µL/mL)	$9.81 \pm 0.02^{A,B,C}$

LDPE: low-density polyethylene; LCh: lobster-shell chitosan; LLCh: low MW lobster-shell chitosan; F: formulation. The difference between the two mean values followed by the same letter in the same column is statistically insignificant ($p > 0.05$) as determined by Tukey's HSD test.

5.4 SUMMARY AND CONCLUDING REMARKS

This chapter describes the development of response surface models that successfully predicted the physicochemical properties of plasticized lobster-shell chitosan – fish gelatin – sunflower oil composite films based on their FFS formulations. Further, these formulations were simultaneously optimized to produce films suitable for particular applications with specific functionalities. While these optimization models are limited to lobster-shell chitosan – fish gelatin composites, they cover a wide range of response values for several critical parameters (physicochemical properties) that can help in tailoring edible films with specific properties for various food packaging applications.

The observations from the enzymatic hydrolysis of lobster chitosan showed the potential of Viscozyme-L (a commercial non-specific cellulolytic enzyme) as a relatively cheap alternative to costly chitosan-specific hydrolyzing enzymes such as chitosanases (Hamed et al., 2016). Replacing lobster chitosan with its hydrolyzed product in the optimized FFS formulations showed an increased water solubility and opacity (visible and UV) and reduced swelling potential for the resultant composite films without significantly influencing their mechanical and water vapour barrier properties. Neat lobster-shell chitosan films, irrespective of the molecular weight of chitosan, were highly efficient in inhibiting *E. coli* growth, while optimized composite films showed relatively lower inhibition. However, in order to regard these edible films as antimicrobial, evaluation of their activities against several other species of bacteria (gram-positive and gram-negative) and fungi is necessary.

Overall, this study provided a comprehensive understanding of the effects of chitosan molecular weight and incorporation of fish gelatin, sunflower oil and glycerol on the properties of lobster-shell derived chitosan films, which can help devise future strategies to further improve and expand their applicability as a food packaging material.

CHAPTER 6

CONCLUSIONS AND RECOMMENDATIONS

6.1 SUMMARY AND CONCLUSIONS

This thesis presented a methodical approach to developing application-specific blends incorporating chitosan extracted from the shell-waste of Atlantic lobsters as a film-forming biopolymer. The thesis explored the compatibility of lobster-shell chitosan with fish gelatin and sunflower oil to produce antimicrobial edible films for potential food packaging and preservation applications. The present section summarizes the major findings from all experimental Chapters and provides concluding remarks pertaining to the original research objectives of this thesis.

In **Chapter 3**, neat solvent cast films obtained from the lobster shell-waste-derived crude chitosan (LCh) and commercially available chitosan products were characterized and compared based on their physical, optical, mechanical and barrier properties. The procedure implemented for the extraction of chitosan from lobster shells was highly efficient with an extraction yield of 18.4% (w/w dry lobster shells) and provided a reasonably pure high molecular weight product (weight average MW of 341 kDa) with a light pink appearance due to the residual pigments. While preparing chitosan film-forming solutions, ultrasonication treatment was highly effective and superior to vacuum application and magnetic stirring for de-gassing and homogenization, respectively. The prepared solvent cast films of LCh and commercial chitosan showed very similar physicochemical properties, i.e. a high degree of swelling (DS: 228 - 293 %), low water solubility (WS: 17 – 27 %), high tensile strength (TS: 69 - 80 MPa), low % elongation (EAB: 47 – 58 %), poor resistance to water vapour permeability (WVP: 0.8 – 0.9 g.mm/kPa.h.m^2), high resistance to UV (OP$_{UV}$: 742 – 834 A.nm/mm) and high surface hydrophobicity (ethylene glycol CA: 64 – 71°), which are comparable to the values previously reported in the literature. Moreover, the residual pigments in the LCh did not affect its film properties, thereby eliminating the need for a de-pigmentation step and thus potentially reducing the cost of chitosan extraction for edible film applications.

In **Chapter 4**, a comprehensive evaluation of the effects of drying temperature, polymer concentration and incorporation of fish gelatin (Ge) and sunflower oil (O) on the properties of LCh films was performed. Observations from this study indicated a high degree of interaction between chitosan, gelatin, oil and plasticizer (glycerol) on a molecular level; however, an increase in the drying temperature adversely affected these interactions. In general, films dried at 60 or 80 °C showed poor mechanical properties and enhanced DS and WVP compared to the films dried at 37 °C. Moreover, high-temperature dried films also showed poor homogeneity and high variability in their properties. Films obtained from low polymer concentration solutions (1% LCh) had lower DS, EAB and WVP than high-polymer concentration films (2% LCh). The presence of gelatin significantly reduced the rigidity and WVP of the composite films while increasing their DS and thermal stability. On the other hand, oil in the films significantly increased their hydrophobicity and OP_{UV} and decreased their DS, WS, WVP and transparency. Overall, this study demonstrated the ability of Ge and O in altering and modifying the physicochemical properties of LCh films to a great extent and thus established their suitability as blending materials for developing LCh composite films with desired functionality.

In **Chapter 5**, optimization models for the formulations of plasticized LCh-Ge-O film-forming solutions were developed using response surface methodology in order to prepare composite films with customized physicochemical properties suitable for their intended applications. Additionally, the effect of chitosan molecular weight on the physicochemical and antimicrobial properties of neat and optimized LCh films was also studied. The regression equations obtained from this study were highly efficient ($R^2 > 0.87$) and reliable (validated optimizations models) in predicting the physicochemical properties of the composite films. Simultaneous optimization was employed for developing three optimized film formulations with different functionalities specific to their niche packaging applications. Reducing the molecular weight of LCh (weight average MW of 154 kDa) increased the WS and OP_{UV} and decreased the DS and transparency of the optimized composite films without affecting their mechanical, water vapour barrier or antimicrobial properties. Neat LCh films showed a very high inhibition of *E. coli* growth (77 – 83% inhibition); however, the incorporation of gelatin, oil or glycerol in the films significantly reduced their activity. Although based on these observations, the prospects of LCh-Ge-O composite films tailored for specific food packaging applications seem quite promising, a

further improvement in the properties of these films, especially in their RH sensitivity and water vapour barrier properties, is still needed in order to expand their commercial applicability and compete with conventional plastic packaging.

6.2 CONTRIBUTIONS TO THE RESEARCH FIELD

To the best of the author's knowledge, chitosan derived from Atlantic lobster shell-waste has been utilized for the first time in the development of edible films. Moreover, while some previous reports have explored blends of chitosan and gelatin to produce solvent cast films, this is the first time the structural, thermal and physicochemical properties of the composite films of lobster-shell chitosan (LCh), fish gelatin (Ge) and sunflower oil (O), and the effects of drying temperature on the properties of these films have been investigated. The insights provided by this work into the feasibility of Atlantic lobster shell-waste as a sustainable source of low-cost crude chitosan for edible film applications and the applicability of fish gelatin and sunflower oil as blending material to enhance and modify the properties of these films can potentially address some of the issues pertaining to the commercialization of chitosan-based packaging solutions.

Another contribution of this work are the obtained optimization models for LCh-Ge-O composite films that allow for the customization of a wide range of film properties based on their composition. But more importantly, the associated regression equations provide a comprehensive understanding regarding the complex interaction mechanisms between LCh, Ge, O and glycerol in the films. This can assist researchers in predicting and controlling the behaviour of these composite films and help devise future strategies to overcome their limitations as an eco-friendly and functional food packaging alternative to conventional plastic films.

6.3 RECOMMENDATIONS FOR FUTURE WORK

- The present work indicated the potential of neat and composite LCh films in inhibiting *E. coli* growth; however, a comprehensive evaluation of their activity against fungi and other gram-positive and gram-negative bacteria is essential in order to establish these films as

antimicrobial. Additionally, the ability of these films in preventing microbial spoilage in contained food products should also be explored.

- Although this study targeted several key physicochemical properties of edible films critical to food packaging applications, investigation of other important properties such as permeability to O_2, CO_2 and ethylene gas, resistance to the migration of lipids and oils, sensory and organoleptic characteristics, stability during storage/ageing and heat sealability of LCh-composite films is critical for their eventual commercialization.

- Due to the marine origin of film constituents (chitosan and fish gelatin) and the intended edibility of the films, the allergenicity and safety (for human consumption) of these films should be examined.

- Finally, other significant factors like the type and concentration of solvent acids or modification approaches like neutralization, cross-linking and grafting, along with different drying methods such as vacuum drying, should also be explored as potential strategies to further improve the properties and address the commercial production and scalability issues of LCh-based films.

REFERENCES

Aguirre-Joya, J. A., De Leon-Zapata, M. A., Alvarez-Perez, O. B., Torres-León, C., Nieto-Oropeza, D. E., Ventura-Sobrevilla, J. M., Aguilar, M. A., Ruelas-Chacón, X., Rojas, R., Ramos-Aguiñaga, M. E., & Aguilar, C. N. (2018). Basic and Applied Concepts of Edible Packaging for Foods. In *Food Packaging and Preservation* (pp. 1–61). Elsevier. https://doi.org/10.1016/B978-0-12-811516-9.00001-4

Aider, M. (2010). Chitosan application for active bio-based films production and potential in the food industry: Review. *LWT - Food Science and Technology*, *43*(6), 837–842. https://doi.org/10.1016/j.lwt.2010.01.021

Alishahi, A., Mirvaghefi, A., Tehrani, M. R., Farahmand, H., Shojaosadati, S. A., Dorkoosh, F. A., & Elsabee, M. Z. (2011). Enhancement and Characterization of Chitosan Extraction from the Wastes of Shrimp Packaging Plants. *Journal of Polymers and the Environment*, *19*(3), 776–783. https://doi.org/10.1007/s10924-011-0321-5

Almazrouei, M., Elagroudy, S., & Janajreh, I. (2019). Transesterification of waste cooking oil: Quality assessment via thermogravimetric analysis. *Energy Procedia*, *158*, 2070–2076. https://doi.org/10.1016/j.egypro.2019.01.478

Alvarenga, E. S. de. (2011). Characterization and Properties of Chitosan. In M. Elnashar (Ed.), *Biotechnology of Biopolymers* (pp. 92–108). InTech. https://doi.org/10.5772/17020

Alves, A. C. R. S., Lima, A. M. F., Tiera, M. J., & Aparecida de Oliveira Tiera, V. (2019). Biopolymeric Films of Amphiphilic Derivatives of Chitosan: A Physicochemical Characterization and Antifungal Study. *International Journal of Molecular Sciences*, *20*(17), 4173. https://doi.org/10.3390/ijms20174173

Angelo, M., Cerqueira, P. R., Couto Teixeira, J. A., & Augusto Vicente, A. (2017). Edible Packaging Today. In *Edible Food Packaging* (pp. 1–8). CRC Press. https://doi.org/10.1201/b19468-1

Annu, Ahmed, S., & Ikram, S. (2017). Chitin and Chitosan: History, Composition and Properties. In *Chitosan* (pp. 1–24). John Wiley & Sons, Inc. https://doi.org/10.1002/9781119364849.ch1

Ansorena, M. R., Marcovich, N. E., & Pereda, M. (2018). Food Biopackaging Based on Chitosan. In *Handbook of Ecomaterials* (pp. 1–27). Springer International Publishing. https://doi.org/10.1007/978-3-319-48281-1_68-1

AOAC. (1990). *Official methods of analysis of the association of official analytical chemists* (15th ed.). AOAC International Publisher.

Aranaz, I., Mengíbar, M., Harris, R., Miralles, B., Acosta, N., Calderón, L., Sánchez, Á., & Heras, Á. (2014). Role of Physicochemical Properties of Chitin and Chitosan on their Functionality. *Current Chemical Biology*, *8*, 27–42.

Arbia, W., Arbia, L., Adour, L., & Amrane, A. (2013). Chitin Extraction from Crustacean Shells Using Biological Methods-A Review. *Food Technol. Biotechnol.*, *51*(1), 12–25.

Archer, M., & Russel, D. (2008). Crustacea Processing Waste Management. In *Seafish Research & Development*.

Arnold, N. D., Brück, W. M., Garbe, D., & Brück, T. B. (2020). Enzymatic Modification of Native Chitin and Conversion to Specialty Chemical Products. *Marine Drugs*, *18*(2), 93. https://doi.org/10.3390/md18020093

Arvanitoyannis, I. S., Nakayama, A., & Aiba, S. ichi. (1998). Chitosan and gelatin based edible films: State diagrams, mechanical and permeation properties. *Carbohydrate Polymers*, *37*(4), 371–382. https://doi.org/10.1016/S0144-8617(98)00083-6

Arya, S. K., Manohar, M., Singh, G., & Siddiqui, W. A. (2017). Chitin and Chitosan-Complexes and Their Applications. In *Chitosan* (pp. 151–165). John Wiley & Sons, Inc. https://doi.org/10.1002/9781119364849.ch6

ASTM Internation. (2016). *ASTM E96/E96M-16 Standard Test Methods for Water Vapor Transmission of Materials.* https://doi.org/10.1520/E0096_E0096M-16

ASTM Internation. (2018). *ASTM D882-18 Standard Test Method for Tensile Properties of Thin Plastic Sheeting.* https://doi.org/10.1520/D0882-18

Avena-Bustillos, R. J., Olsen, C. W., Olson, D. A., Chiou, B., Yee, E., Bechtel, P. J., & McHugh, T. H. (2006). Water Vapor Permeability of Mammalian and Fish Gelatin Films. *Journal of Food Science*, *71*(4), E202–E207. https://doi.org/10.1111/j.1750-3841.2006.00016.x

Azarifar, M., Ghanbarzadeh, B., Sowti Khiabani, M., Akhondzadeh Basti, A., Abdulkhani, A., Noshirvani, N., & Hosseini, M. (2019). The optimization of gelatin-CMC based active films containing chitin nanofiber and Trachyspermum ammi essential oil by response surface methodology. *Carbohydrate Polymers*, *208*(December 2018), 457–468. https://doi.org/10.1016/j.carbpol.2019.01.005

Azeredo, H. M. C., Mattoso, L. H. C., Wood, D., Williams, T. G., Avena-Bustillos, R. J., & McHugh, T. H. (2009). Nanocomposite Edible Films from Mango Puree Reinforced with Cellulose Nanofibers. *Journal of Food Science*, *74*(5), N31–N35. https://doi.org/10.1111/j.1750-3841.2009.01186.x

Balau, L., Lisa, G., Popa, M., Tura, V., & Melnig, V. (2004). Physico-chemical properties of Chitosan films. *Open Chemistry*, *2*(4), 638–647. https://doi.org/10.2478/BF02482727

Baron, R. D., Pérez, L. L., Salcedo, J. M., Córdoba, L. P., & Sobral, P. J. do A. (2017). Production and characterization of films based on blends of chitosan from blue crab (Callinectes sapidus) waste and pectin from Orange (Citrus sinensis Osbeck) peel. *International Journal of Biological Macromolecules*, *98*, 676–683. https://doi.org/10.1016/j.ijbiomac.2017.02.004

Bégin, A., Calsteren, M.-R. Van, & Van Calsteren, M.-R. (1999). Antimicrobial films produced from chitosan. *International Journal of Biological Macromolecules*, *26*(1), 63–67. https://doi.org/10.1016/S0141-8130(99)00064-1

Bertuzzi, M. A., Castro Vidaurre, E. F., Armada, M., & Gottifredi, J. C. (2007). Water vapor permeability of edible starch based films. *Journal of Food Engineering*, *80*(3), 972–978. https://doi.org/10.1016/j.jfoodeng.2006.07.016

Blanco-Fernandez, B., Rial-Hermida, M. I., Alvarez-Lorenzo, C., & Concheiro, A. (2013). Edible chitosan/acetylated monoglyceride films for prolonged release of vitamin e and antioxidant activity. *Journal of Applied Polymer Science*, *129*(2), 626–635. https://doi.org/10.1002/app.38766

Blanco-Pascual, N., & Gómez-Estaca, J. (2017). Production and Processing of Edible Packaging Stability and Applications. In *Edible Food Packaging* (pp. 153–180). CRC Press. https://doi.org/10.1201/b19468-5

Boßelmann, F., Romano, P., Fabritius, H., Raabe, D., & Epple, M. (2007). The composition of the exoskeleton of two crustacea: The American lobster Homarus americanus and the edible crab Cancer pagurus. *Thermochimica Acta*, *463*(1–2), 65–68. https://doi.org/10.1016/j.tca.2007.07.018

Boy, R., Maness, C., & Kotek, R. (2016). Properties of chitosan/soy protein blended films with added plasticizing agent as a function of solvent type at acidic pH. *International Journal of Polymeric Materials and Polymeric Biomaterials*, *65*(1), 11–17. https://doi.org/10.1080/00914037.2015.1038821

Brugnerotto, J., Lizardi, J., Goycoolea, F. ., Argüelles-Monal, W., Desbrières, J., & Rinaudo, M. (2001). An infrared investigation in relation with chitin and chitosan characterization. *Polymer*, *42*(8), 3569–3580. https://doi.org/10.1016/S0032-3861(00)00713-8

Cazón, P., & Vázquez, M. (2020). Mechanical and barrier properties of chitosan combined with other components as food packaging film. *Environmental Chemistry Letters*, *18*(2), 257–267. https://doi.org/10.1007/s10311-019-00936-3

Cerqueira, M. A., Souza, B. W. S., Teixeira, J. A., & Vicente, A. A. (2012a). Effect of glycerol and corn oil on physicochemical properties of polysaccharide films - A comparative study. *Food Hydrocolloids*, *27*(1), 175–184. https://doi.org/10.1016/j.foodhyd.2011.07.007

Cerqueira, M. A., Souza, B. W. S., Teixeira, J. A., & Vicente, A. A. (2012b). Effects of Interactions between the Constituents of Chitosan-Edible Films on Their Physical Properties. *Food and Bioprocess Technology*, *5*(8), 3181–3192. https://doi.org/10.1007/s11947-011-0663-y

Chen, F. (2015). *Chitosan and chitosan/wheat gluten blends: properties of extrudates, solid films and bio-foams* (Issue September) [KTH Royal Institute of Technology Copyright]. http://www.diva-portal.org/smash/record.jsf?dswid=2646&aq=%5B%5B%5D%5D&aq2=%5B%5B%5D%5D&sf=all&aqe=%5B%5D&af=%5B%5D&searchType=SIMPLE&sortOrder=author_sort_asc&onlyFullText=false&noOfRows=50&language=en&pid=diva2%3A848170&dspwid=2646

Chen, X., Yang, H., & Yan, N. (2016). Shell Biorefinery: Dream or Reality? *Chemistry - A European Journal*, *22*(38), 13402–13421. https://doi.org/10.1002/chem.201602389

Cheng, L. H., Abd Karim, A., & Seow, C. C. (2008). Characterisation of composite films made of konjac glucomannan (KGM), carboxymethyl cellulose (CMC) and lipid. *Food Chemistry*, *107*(1), 411–418. https://doi.org/10.1016/j.foodchem.2007.08.068

Chiou, B. Sen, Avena-Bustillos, R. J., Bechtel, P. J., Imam, S. H., Glenn, G. M., & Orts, W. J. (2009). Effects of drying temperature on barrier and mechanical properties of cold-water fish gelatin films. *Journal of Food Engineering*, *95*(2), 327–331. https://doi.org/10.1016/j.jfoodeng.2009.05.011

Corazzari, I., Nisticò, R., Turci, F., Faga, M. G., Franzoso, F., Tabasso, S., & Magnacca, G. (2015). Advanced physico-chemical characterization of chitosan by means of TGA coupled on-line with FTIR and GCMS: Thermal degradation and water adsorption capacity. *Polymer Degradation and Stability*, *112*, 1–9. https://doi.org/10.1016/j.polymdegradstab.2014.12.006

Córdoba, L. J. P., & Sobral, P. J. A. (2017). Physical and antioxidant properties of films based on gelatin, gelatin-chitosan or gelatin-sodium caseinate blends loaded with nanoemulsified active compounds. *Journal of Food Engineering*, *213*, 47–53. https://doi.org/10.1016/j.jfoodeng.2017.05.023

Cui, L., Gao, S., Song, X., Huang, L., Dong, H., Liu, J., Chen, F., & Yu, S. (2018). Preparation and characterization of chitosan membranes. *RSC Advances*, *8*(50), 28433–28439. https://doi.org/10.1039/c8ra05526b

Danaei, M., Dehghankhold, M., Ataei, S., Hasanzadeh Davarani, F., Javanmard, R., Dokhani, A., Khorasani, S., & Mozafari, M. (2018). Impact of Particle Size and Polydispersity Index on the Clinical Applications of Lipidic Nanocarrier Systems. *Pharmaceutics*, *10*(2), 57. https://doi.org/10.3390/pharmaceutics10020057

Dangaran, K., Tomasula, P. M., & Qi, P. (2009). Structure and Function of Protein-Based Edible Films and Coatings. In *Edible Films and Coatings for Food Applications* (pp. 25–56). Springer New York. https://doi.org/10.1007/978-0-387-92824-1_2

Debeaufort, F., & Voilley, A. (2009). Lipid-Based Edible Films and Coatings. In K. C. Huber & M. E. Embuscado (Eds.), *Edible Films and Coatings for Food Applications* (pp. 135–168). Springer New York. https://doi.org/10.1007/978-0-387-92824-1_5

Derringer, G., & Suich, R. (1980). Simultaneous Optimization of Several Response Variables. *Journal of Quality Technology*, *12*(4), 214–219. https://doi.org/10.1080/00224065.1980.11980968

Díaz-Rojas, E. I., Argüelles-Monal, W. M., Higuera-Ciapara, I., Hernández, J., Lizardi-Mendoza, J., & Goycoolea, F. M. (2006). Determination of Chitin and Protein Contents During the Isolation of Chitin from Shrimp Waste. *Macromolecular Bioscience*, *6*(5), 340–347. https://doi.org/10.1002/mabi.200500233

Dimzon, I. K. D., Ebert, J., & Knepper, T. P. (2013). The interaction of chitosan and olive oil: Effects of degree of deacetylation and degree of polymerization. *Carbohydrate Polymers*, *92*(1), 564–570. https://doi.org/10.1016/j.carbpol.2012.09.035

Dutta, P. K., Tripathi, S., Mehrotra, G. K., & Dutta, J. (2009). Perspectives for chitosan based antimicrobial films in food applications. *Food Chemistry*, *114*(4), 1173–1182. https://doi.org/10.1016/j.foodchem.2008.11.047

Elsabee, M. Z. (2015). Chitosan-Based Edible Films. In K. G. Ramawat & J.-M. Mérillon (Eds.), *Polysaccharides* (pp. 829–870). Springer International Publishing. https://doi.org/10.1007/978-3-319-16298-0_7

Epure, V., Griffon, M., Pollet, E., & Avérous, L. (2011). Structure and properties of glycerol-plasticized chitosan obtained by mechanical kneading. *Carbohydrate Polymers*, *83*(2), 947–952. https://doi.org/10.1016/j.carbpol.2010.09.003

Erkmen, O., & Barazi, A. O. (2018). General Characteristics of Edible Films. *Journal of Food Biotechnology Research*, *2*(1:3). http://www.imedpub.com/journal-food-biotechnology-research/

Falguera, V., Quintero, J. P., Jiménez, A., Muñoz, J. A., & Ibarz, A. (2011). Edible films and coatings: Structures, active functions and trends in their use. *Trends in Food Science & Technology*, *22*(6), 292–303. https://doi.org/10.1016/j.tifs.2011.02.004

FAO. (2020). *FAO Yearbook. Fishery and Aquaculture Statistics 2018/FAO annuaire. Statistiques des pêches et de l'aquaculture 2018/FAO anuario. Estadísticas de pesca y acuicultura 2018*. FAO. https://doi.org/10.4060/cb1213t

FAO. (2021). GLOBEFISH Highlights - A quarterly update on world seafood markets. In *Globefish Highlights No. 1–2021*. FAO. https://doi.org/10.4060/cb4129en

Fernandes, S. C. M., Freire, C. S. R., Silvestre, A. J. D., Pascoal Neto, C., Gandini, A., Berglund, L. A., & Salmén, L. (2010). Transparent chitosan films reinforced with a high content of nanofibrillated cellulose. *Carbohydrate Polymers*, *81*(2), 394–401. https://doi.org/10.1016/j.carbpol.2010.02.037

Fernández-de Castro, L., Mengíbar, M., Sánchez, Á., Arroyo, L., Villarán, M. C., Díaz de Apodaca, E., & Heras, Á. (2016). Films of chitosan and chitosan-oligosaccharide neutralized and thermally treated: Effects on its antibacterial and other activities. *LWT*, *73*, 368–374. https://doi.org/10.1016/j.lwt.2016.06.038

Fernández-Pan, I., Ziani, K., Pedroza-Islas, R., & Maté, & J. I. (2010). Effect of Drying Conditions on the Mechanical and Barrier Properties of Films Based on Chitosan. *Drying Technology*, *28*, 1350–1358. https://doi.org/10.1080/07373937.2010.482692

Fernandez-Saiz, P., Lagarón, J. M., & Ocio, M. J. (2009). Optimization of the film-forming and storage conditions of chitosan as an antimicrobial agent. *Journal of Agricultural and Food Chemistry*, *57*(8), 3298–3307. https://doi.org/10.1021/jf8037709

Fisheries and Oceans Canada. (2018). *Outlook to 2027 for Canadian Fish and Seafood*.

Fisheries and Oceans Canada. (2019a). *Canada's Fisheries Fast Facts 2019*.

Fisheries and Oceans Canada. (2019b). *Value of provincial landings*. https://www.dfo-mpo.gc.ca/stats/commercial/land-debarq/sea-maritimes/s2019pv-eng.htm

Fisheries and Oceans Canada. (2019c). *Volume of provincial landings*. https://www.dfo-mpo.gc.ca/stats/commercial/land-debarq/sea-maritimes/s2019pq-eng.htm

Friedman, M., & Juneja, V. K. (2010). Review of Antimicrobial and Antioxidative Activities of Chitosans in Food. *Journal of Food Protection*, *73*(9), 1737–1761. https://doi.org/10.4315/0362-028X-73.9.1737

García, M. A., Pérez, L., De La Paz, N., González, J., Rapado, M., & Casariego, A. (2015). Effect of molecular weight reduction by gamma irradiation on chitosan film properties. *Materials Science and Engineering C*, *55*, 174–180. https://doi.org/10.1016/j.msec.2015.05.009

Gbenebor, O. P., Adeosun, S. O., Lawal, G. I., Jun, S., & Olaleye, S. A. (2017). Acetylation, crystalline and morphological properties of structural polysaccharide from shrimp exoskeleton. *Engineering Science and Technology, an International Journal*, *20*(3), 1155–1165. https://doi.org/10.1016/j.jestch.2017.05.002

Ghanem, A., & Katalinich, M. (2005). Characterization of chitosan films for tissue engineering applications. *Applied Bionics and Biomechanics*, *2*(1), 9–16. https://doi.org/10.1533/abbi.2004.0004

Gómez-Estaca, J., Gómez-Guillén, M. C., Fernández-Martín, F., & Montero, P. (2011). Effects of gelatin origin, bovine-hide and tuna-skin, on the properties of compound gelatin–chitosan films. *Food Hydrocolloids*, *25*(6), 1461–1469. https://doi.org/10.1016/j.foodhyd.2011.01.007

Goy, R. C., Britto, D. de, & Assis, O. B. G. (2009). A review of the antimicrobial activity of chitosan. *Polímeros*, *19*(3), 241–247. https://doi.org/10.1590/S0104-14282009000300013

Grande, R., Pessan, L. A., & Carvalho, A. J. F. (2018). Thermoplastic blends of chitosan: A method for the preparation of high thermally stable blends with polyesters. *Carbohydrate Polymers*, *191*(December 2017), 44–52. https://doi.org/10.1016/j.carbpol.2018.02.087

Guilbert, S., Gontard, N., & Cuq, B. (1995). Technology and applications of edible protective films. *Packaging Technology and Science*, *8*(6), 339–346. https://doi.org/10.1002/pts.2770080607

Gutiérrez, T. J. (2017). Chitosan Applications for the Food Industry. In *Chitosan* (pp. 183–232). John Wiley & Sons, Inc. https://doi.org/10.1002/9781119364849.ch8

Haghighi, H., Biard, S., Bigi, F., De Leo, R., Bedin, E., Pfeifer, F., Siesler, H. W., Licciardello, F., & Pulvirenti, A. (2019). Comprehensive characterization of active chitosan-gelatin blend films enriched with different essential oils. *Food Hydrocolloids*, *95*, 33–42. https://doi.org/10.1016/j.foodhyd.2019.04.019

Haghighi, H., De Leo, R., Bedin, E., Pfeifer, F., Siesler, H. W., & Pulvirenti, A. (2019). Comparative analysis of blend and bilayer films based on chitosan and gelatin enriched with LAE (lauroyl arginate ethyl) with antimicrobial activity for food packaging applications. *Food Packaging and Shelf Life*, *19*, 31–39. https://doi.org/10.1016/j.fpsl.2018.11.015

Haghighi, H., Licciardello, F., Fava, P., Siesler, H. W., & Pulvirenti, A. (2020). Recent advances on chitosan-based films for sustainable food packaging applications. *Food Packaging and Shelf Life*, *26*, 100551. https://doi.org/10.1016/j.fpsl.2020.100551

Hahn, T., Tafi, E., Paul, A., Salvia, R., Falabella, P., & Zibek, S. (2020). Current state of chitin purification and chitosan production from insects. *Journal of Chemical Technology & Biotechnology*, *95*(11), 2775–2795. https://doi.org/10.1002/jctb.6533

Hahn, T., & Zibek, S. (2018). Sewage Polluted Water Treatment via Chitosan: A Review. In *Chitin-Chitosan - Myriad Functionalities in Science and Technology*. InTech. https://doi.org/10.5772/intechopen.75395

Hamdi, M., Nasri, R., Li, S., & Nasri, M. (2019). Bioactive composite films with chitosan and carotenoproteins extract from blue crab shells: Biological potential and structural, thermal, and mechanical characterization. *Food Hydrocolloids*, *89*(July 2018), 802–812. https://doi.org/10.1016/j.foodhyd.2018.11.062

Hamed, I., Özogul, F., & Regenstein, J. M. (2016). Industrial applications of crustacean by-products (chitin, chitosan, and chitooligosaccharides): A review. *Trends in Food Science and Technology*, *48*, 40–50. https://doi.org/10.1016/j.tifs.2015.11.007

Han, J. H. (2014). Edible Films and Coatings. In *Innovations in Food Packaging* (pp. 213–255). Elsevier. https://doi.org/10.1016/B978-0-12-394601-0.00009-6

Hanani, Z. A. N., O'Mahony, J. A., Roos, Y. H., Oliveira, P. M., & Kerry, J. P. (2014). Extrusion of gelatin-based composite films: Effects of processing temperature and pH of film forming solution on mechanical and barrier properties of manufactured films. *Food Packaging and Shelf Life*, *2*(2), 91–101. https://doi.org/10.1016/j.fpsl.2014.09.001

Healy, M. G., Romo, C. R., & Bustos, R. (1994). Bioconversion of marine crustacean shell waste. *Resources, Conservation and Recycling*, *11*(1–4), 139–147. https://doi.org/10.1016/0921-3449(94)90085-X

Homez-Jara, A., Daza, L. D., Aguirre, D. M., Muñoz, J. A., Solanilla, J. F., & Váquiro, H. A. (2018). Characterization of chitosan edible films obtained with various polymer concentrations and drying temperatures. *International Journal of Biological Macromolecules*, *113*, 1233–1240. https://doi.org/10.1016/j.ijbiomac.2018.03.057

Hosseini, S. F., Rezaei, M., Zandi, M., & Ghavi, F. F. (2013). Preparation and functional properties of fish gelatin-chitosan blend edible films. *Food Chemistry*, *136*(3–4), 1490–1495. https://doi.org/10.1016/j.foodchem.2012.09.081

Hülsey, M. J. (2018). Shell biorefinery: A comprehensive introduction. In *Green Energy and Environment* (Vol. 3, Issue 4, pp. 318–327). KeAi Publishing Communications Ltd. https://doi.org/10.1016/j.gee.2018.07.007

Ilangumaran, G. (2014). *Microbial degradation of lobster shells to extract chitin derivatives for plant disease management* (Issue November). Dalhousie University, Halifax, Canada.

Ilangumaran, G., Stratton, G., Ravichandran, S., Shukla, P. S., Potin, P., Asiedu, S., & Prithiviraj, B. (2017). Microbial Degradation of Lobster Shells to Extract Chitin Derivatives for Plant Disease Management. *Frontiers in Microbiology*, *8*(MAY), 1–14. https://doi.org/10.3389/fmicb.2017.00781

Ioelovich, M. (2017). Nitrogenated Polysaccharides - Chitin and Chitosan, Characterization and Application. In *Chitosan* (pp. 25–70). John Wiley & Sons, Inc. https://doi.org/10.1002/9781119364849.ch2

Ismillayli, N., Andayani, I. G. A. S., Honiar, R., Mariana, B., Sanjaya, R. K., & Hermanto, D. (2020). Polyelectrolyte Complex (PEC) film based on chitosan as potential edible films and their antibacterial activity test. *IOP Conference Series: Materials Science and Engineering*, *959*(1). https://doi.org/10.1088/1757-899X/959/1/012009

Jahit, I. S., Nazmi, N. N. M., Isa, M. I. N., & Sarbon, N. M. (2016). Preparation and physical properties of gelatin/CMC/chitosan composite films as affected by drying temperature. *International Food Research Journal*, *23*(3), 1068–1074.

Jim, F. (2013). *Multiple Regression Analysis: Use Adjusted R-Squared and Predicted R-Squared to Include the Correct Number of Variables*. Minitab Blog. https://blog.minitab.com/en/adventures-in-statistics-2/multiple-regession-analysis-use-adjusted-r-squared-and-predicted-r-squared-to-include-the-correct-number-of-variables

Jridi, M., Hajji, S., Ayed, H. Ben, Lassoued, I., Mbarek, A., Kammoun, M., Souissi, N., & Nasri, M. (2014). Physical, structural, antioxidant and antimicrobial properties of gelatin-chitosan composite edible films. *International Journal of Biological Macromolecules*, *67*, 373–379. https://doi.org/10.1016/j.ijbiomac.2014.03.054

Kakaei, S., & Shahbazi, Y. (2016). *Effect of chitosan-gelatin film incorporated with ethanolic red grape seed extract and Ziziphora clinopodioides essential oil on survival of Listeria monocytogenes and chemical, microbial and sensory properties of minced trout fillet*. https://doi.org/10.1016/j.lwt.2016.05.021

Katalinich, M. (2001). *Characterization of chitosan films for cell culture applications* [The University of Maine]. https://digitalcommons.library.umaine.edu/cgi/viewcontent.cgi?article=1244&context=etd

Kaur, S., & Dhillon, G. S. (2015). Recent trends in biological extraction of chitin from marine shell wastes: a review. *Critical Reviews in Biotechnology*, *35*(1), 44–61. https://doi.org/10.3109/07388551.2013.798256

Kaya, M., Baran, T., Mentes, A., Asaroglu, M., Sezen, G., & Tozak, K. O. (2014). Extraction and Characterization of α-Chitin and Chitosan from Six Different Aquatic Invertebrates. *Food Biophysics*, *9*(2), 145–157. https://doi.org/10.1007/s11483-013-9327-y

Ke, C. L., Deng, F. S., Chuang, C. Y., & Lin, C. H. (2021). Antimicrobial actions and applications of Chitosan. *Polymers*, *13*(6). https://doi.org/10.3390/polym13060904

Kerton, F. M., Liu, Y., Omari, K. W., & Hawboldt, K. (2013). Green chemistry and the ocean-based biorefinery. *Green Chemistry*, *15*(4), 860. https://doi.org/10.1039/c3gc36994c

Khouri, J. (2019). *Chitosan Edible Films Crosslinked by Citric Acid* [University of Waterloo]. https://uwspace.uwaterloo.ca/handle/10012/14877

Kim, K. M., Son, J. H., Kim, S.-K., Weller, C. L., & Hanna, M. A. (2006). Properties of Chitosan Films as a Function of pH and Solvent Type. *Journal of Food Science*, *71*(3), E119–E124. https://doi.org/10.1111/j.1365-2621.2006.tb15624.x

Kingkaew, J., Kirdponpattara, S., Sanchavanakit, N., Pavasant, P., & Phisalaphong, M. (2014). Effect of molecular weight of chitosan on antimicrobial properties and tissue compatibility of chitosan-impregnated bacterial cellulose films. *Biotechnology and Bioprocess Engineering*, *19*(3), 534–544. https://doi.org/10.1007/s12257-014-0081-x

Kishore, R. S. K., Pappenberger, A., Dauphin, I. B., Ross, A., Buergi, B., Staempfli, A., & Mahler, H. C. (2011). Degradation of polysorbates 20 and 80: Studies on thermal autoxidation and hydrolysis. *Journal of Pharmaceutical Sciences*, *100*(2), 721–731. https://doi.org/10.1002/jps.22290

Kittur, F. S., Kumar, K. R., & Tharanathan, R. N. (1998). Functional packaging properties of chitosan films. *Z Lebensm Unters Forsch A*, *206*(1), 44–47. https://doi.org/10.1007/s002170050211

Kocira, A., Kozłowicz, K., Panasiewicz, K., Staniak, M., Szpunar-Krok, E., & Hortyńska, P. (2021). Polysaccharides as Edible Films and Coatings: Characteristics and Influence on Fruit and Vegetable Quality—A Review. In *Agronomy* (Vol. 11, Issue 5). https://doi.org/10.3390/agronomy11050813

Kołodziejska, I., & Piotrowska, B. (2007). The water vapour permeability, mechanical properties and solubility of fish gelatin-chitosan films modified with transglutaminase or 1-ethyl-3-(3-dimethylaminopropyl) carbodiimide (EDC) and plasticized with glycerol. *Food Chemistry*, *103*(2), 295–300. https://doi.org/10.1016/j.foodchem.2006.07.049

Krkić, N., Lazić, V., Petrović, L., Gvozdenović, J., & Pejić, D. (2012). Properties of chitosan-laminated collagen film. *Food Technology and Biotechnology*, *50*(4), 483–489.

Kumari, S., & Kishor, R. (2020). Chitin and chitosan: origin, properties, and applications. In *Handbook of Chitin and Chitosan* (pp. 1–33). Elsevier. https://doi.org/10.1016/B978-0-12-817970-3.00001-8

Kumirska, J., Czerwicka, M., Kaczyński, Z., Bychowska, A., Brzozowski, K., Thöming, J., & Stepnowski, P. (2010). Application of spectroscopic methods for structural analysis of chitin and chitosan. In *Marine Drugs* (Vol. 8, Issue 5, pp. 1567–1636). MDPI AG. https://doi.org/10.3390/md8051567

Leceta, I., Guerrero, P., Cabezudo, S., & de la Caba, K. (2013). Environmental assessment of chitosan-based films. *Journal of Cleaner Production*, *41*, 312–318. https://doi.org/10.1016/j.jclepro.2012.09.049

Leceta, I., Guerrero, P., & de la Caba, K. (2013). Functional properties of chitosan-based films. *Carbohydrate Polymers*, *93*(1), 339–346. https://doi.org/10.1016/j.carbpol.2012.04.031

Leceta, I., Guerrero, P., Ibarburu, I., Dueñas, M. T., & de la Caba, K. (2013). Characterization and antimicrobial analysis of chitosan-based films. *Journal of Food Engineering*, *116*(4), 889–899. https://doi.org/10.1016/j.jfoodeng.2013.01.022

Leceta, I., Peñalba, M., Arana, P., Guerrero, P., & de la Caba, K. (2015). Ageing of chitosan films: Effect of storage time on structure and optical, barrier and mechanical properties. *European Polymer Journal*, *66*, 170–179. https://doi.org/10.1016/j.eurpolymj.2015.02.015

Li, H., Cheng, F., Gao, S., Wu, Z., Dong, L., Lin, S., Luo, Z., & Li, X. (2017). Preparation, characterization, antibacterial properties, and hemostatic evaluation of ibuprofen-loaded chitosan/gelatin composite films. *Journal of Applied Polymer Science*, *134*(42), 1–9. https://doi.org/10.1002/app.45441

Li, M., Liu, P., Zou, W., Yu, L., Xie, F., Pu, H., Liu, H., & Chen, L. (2011). Extrusion processing and characterization of edible starch films with different amylose contents. *Journal of Food Engineering*, *106*(1), 95–101. https://doi.org/10.1016/j.jfoodeng.2011.04.021

Liang, P., Wang, H., Chen, C., Ge, F., Liu, D., Li, S., Han, B., Xiong, X., & Zhao, S. (2013). The use of fourier transform infrared spectroscopy for quantification of adulteration in virgin walnut oil. *Journal of Spectroscopy*, *1*(1). https://doi.org/10.1155/2013/305604

Lima, M. de M., Carneiro, L. C., Bianchini, D., Dias, A. R. G., Zavareze, E. da R., Prentice, C., & Moreira, A. da S. (2017). Structural, Thermal, Physical, Mechanical, and Barrier Properties of Chitosan Films with the Addition of Xanthan Gum. *Journal of Food Science*, *82*(3), 698–705. https://doi.org/10.1111/1750-3841.13653

Liu, B., Wang, D., Yu, G., & Meng, X. (2013). Adsorption of heavy metal ions, dyes and proteins by chitosan composites and derivatives — A review. *Journal of Ocean University of China*, *12*(3), 500–508. https://doi.org/10.1007/s11802-013-2113-0

Liu, F., Chang, W., Chen, M., Xu, F., Ma, J., & Zhong, F. (2019). Tailoring physicochemical properties of chitosan films and their protective effects on meat by varying drying temperature. *Carbohydrate Polymers*, *212*, 150–159. https://doi.org/10.1016/j.carbpol.2019.02.019

Liu, Z., Ge, X., Lu, Y., Dong, S., Zhao, Y., & Zeng, M. (2012). Effects of chitosan molecular weight and degree of deacetylation on the properties of gelatine-based films. *Food Hydrocolloids*, *26*(1), 311–317. https://doi.org/10.1016/j.foodhyd.2011.06.008

Lizardi-Mendoza, J., Argüelles Monal, W. M., & Goycoolea Valencia, F. M. (2016). Chemical Characteristics and Functional Properties of Chitosan. In *Chitosan in the Preservation of Agricultural Commodities* (pp. 3–31). Elsevier. https://doi.org/10.1016/B978-0-12-802735-6.00001-X

Lobster Council of Canada. (2010). *From Trap to Table - A Long Term Value Strategy for the Canadian Lobster Industry* (Issue October).

Lozano-Navarro, J. I., Díaz-Zavala, N. P., Melo-Banda, J. A., Velasco-Santos, C., Paraguay-Delgado, F., Peréz-Sánchez, J. F., Domínguez-Esquivel, J. M., Suárez-Domínguez, E. J., & Sosa-Sevilla, J. E. (2020). Chitosan-starch films modified with natural extracts to remove heavy oil from water. *Water (Switzerland)*, *12*(1), 1–21. https://doi.org/10.3390/w12010017

Majeed, A., Najar, R. A., Choudhary, S., Rehman, W. U., Singh, A., Thakur, S., & Bhardwaj, P. (2017). Practical and Plausible Implications of Chitin- and Chitosan-Based Nanocomposites in Agriculture. In *Chitosan* (pp. 409–430). John Wiley & Sons, Inc. https://doi.org/10.1002/9781119364849.ch15

Malerba, M., & Cerana, R. (2018). Recent advances of chitosan applications in plants. *Polymers*, *10*(2), 1–10. https://doi.org/10.3390/polym10020118

Maria V, D., Bernal, C., & Francois, N. J. (2016). Development of Biodegradable Films Based on Chitosan/Glycerol Blends Suitable for Biomedical Applications. *Journal of Tissue Science & Engineering*, *07*(03). https://doi.org/10.4172/2157-7552.1000187

Marsh, K., & Bugusu, B. (2007). Food packaging - Roles, materials, and environmental issues: Scientific status summary. *Journal of Food Science*, *72*(3). https://doi.org/10.1111/j.1750-3841.2007.00301.x

Martínez-Camacho, A., Cortez-Rocha, M., Ezquerra-Brauer, J., Graciano-Verdugo, A., Rodriguez-Félix, F., Castillo-Ortega, M., Yépiz-Gómez, M., & Plascencia-Jatomea, M. (2010). Chitosan composite films: Thermal, structural, mechanical and antifungal properties. *Carbohydrate Polymers*, *82*, 305–315. https://doi.org/10.1016/j.carbpol.2010.04.069

Matet, M., Heuzey, M. C., Pollet, E., Ajji, A., & Avérous, L. (2013). Innovative thermoplastic chitosan obtained by thermo-mechanical mixing with polyol plasticizers. *Carbohydrate Polymers*, *95*(1), 241–251. https://doi.org/10.1016/j.carbpol.2013.02.052

Mayachiew, P., & Devahastin, S. (2008). Comparative Evaluation of Physical Properties of Edible Chitosan Films Prepared by Different Drying Methods, Drying Technology. *Pornpimon Mayachiew & Sakamon Devahastin*, *26*(2), 176–185. https://doi.org/10.1080/07373930701831309

Mayachiew, P., Devahastin, S., Mackey, B. M., & Niranjan, K. (2010). Effects of drying methods and conditions on antimicrobial activity of edible chitosan films enriched with galangal extract. *Food Research International*, *43*(1), 125–132. https://doi.org/10.1016/j.foodres.2009.09.006

McHugh, T. H., Avena-Bustillos, R., & Krochta, J. M. (1993). Hydrophilic edible films: modified procedure for water vapor permeability and explanation of thickness effects. *Journal of Food Science*, *58*(4), 899–903. https://doi.org/10.1111/j.1365-2621.1993.tb09387.x

McHugh, T. H., & Krochta, J. M. (1994). Dispersed phase particle size effects on water vapor permeability of whey protein-beeswax edible emulsion films. *Journal of Food Processing and Preservation*, *18*(3), 173–188. https://doi.org/10.1111/j.1745-4549.1994.tb00842.x

Mehdizadeh, T., Tajik, H., Langroodi, A. M., Molaei, R., & Mahmoudian, A. (2020). Chitosan-starch film containing pomegranate peel extract and Thymus kotschyanus essential oil can prolong the shelf life of beef. *Meat Science*, *163*, 108073. https://doi.org/10.1016/j.meatsci.2020.108073

Mendes, J. F., Paschoalin, R. T., Carmona, V. B., Sena Neto, A. R., Marques, A. C. P., Marconcini, J. M., Mattoso, L. H. C., Medeiros, E. S., & Oliveira, J. E. (2016). Biodegradable polymer blends based on corn starch and thermoplastic chitosan processed by extrusion. *Carbohydrate Polymers*, *137*, 452–458. https://doi.org/10.1016/j.carbpol.2015.10.093

Miki, W. (1991). Biological functions and activities of animal carotenoids. *Pure and Applied Chemistry*, *63*(1), 141–146. https://doi.org/10.1351/pac199163010141

Miranda, S. P., Garnica, O., Lara-Sagahon, V., & Cárdenas, G. (2004). Water vapor permeability and mechanical properties of chitosan composite films. *Journal of the Chilean Chemical Society*, *49*(2), 173–178. https://doi.org/10.4067/s0717-97072004000200013

Morin-Crini, N., Lichtfouse, E., Torri, G., & Crini, G. (2019). Applications of chitosan in food, pharmaceuticals, medicine, cosmetics, agriculture, textiles, pulp and paper, biotechnology, and environmental chemistry. *Environmental Chemistry Letters*, *17*(4), 1667–1692. https://doi.org/10.1007/s10311-019-00904-x

Mu, S. (2016). *A Real Time Study on Mechano-Optical Properties of Chitosan During Film Formation and Processing* [University of Akron]. https://etd.ohiolink.edu/apexprod/rws_olink/r/1501/10?clear=10&p10_accession_num=akron1462885413

Nadarajah, K. (2005). *Development and characterization of antimicrobial edible films from crawfish chitosan* [LSU Doctoral Dissertations. 1630.]. https://doi.org/https://digitalcommons.lsu.edu/gradschool_dissertations/1630

Nechita, P. (2017). Applications of Chitosan in Wastewater Treatment. In *Biological Activities and Application of Marine Polysaccharides* (pp. 209–228). InTech. https://doi.org/10.5772/65289

Nguyen, T. T., Barber, A. R., Corbin, K., & Zhang, W. (2017). Lobster processing by-products as valuable bioresource of marine functional ingredients, nutraceuticals, and pharmaceuticals. *Bioresources and Bioprocessing*, *4*(1), 1–19. https://doi.org/10.1186/s40643-017-0157-5

Nguyen, T. T., Barber, A. R., Smith, P., Luo, X., & Zhang, W. (2017). Application and optimization of the highly efficient and environmentally-friendly microwave-intensified lactic acid demineralization of deproteinized Rock lobster shells (Jasus edwardsii) for chitin production. *Food and Bioproducts Processing*, *102*, 367–374. https://doi.org/10.1016/j.fbp.2017.02.005

Nieto, M. B. (2009). Structure and Function of Polysaccharide Gum-Based Edible Films and Coatings. In *Edible Films and Coatings for Food Applications* (pp. 57–112). Springer New York. https://doi.org/10.1007/978-0-387-92824-1_3

No, H. K., Meyers, S. P., Prinyawiwatkul, W., & Xu, Z. (2007). Applications of Chitosan for Improvement of Quality and Shelf Life of Foods: A Review. *Journal of Food Science*, *72*(5), R87–R100. https://doi.org/10.1111/j.1750-3841.2007.00383.x

Nunthanid, J., Puttipipatkhachorn, S., Yamamoto, K., & Peck, G. E. (2001). Physical Properties and Molecular Behavior of Chitosan Films. *Drug Development and Industrial Pharmacy*, *27*(2), 143–157. https://doi.org/10.1081/DDC-100000481

Ojagh, S. M., Rezaei, M., Razavi, S. H., & Hosseini, S. M. H. (2010). Development and evaluation of a novel biodegradable film made from chitosan and cinnamon essential oil with low affinity toward water. *Food Chemistry*, *122*(1), 161–166. https://doi.org/10.1016/j.foodchem.2010.02.033

Olivas, G. I. I., & Barbosa-Cánovas, G. (2009). Edible Films and Coatings for Fruits and Vegetables. In *Edible Films and Coatings for Food Applications* (pp. 211–244). Springer New York. https://doi.org/10.1007/978-0-387-92824-1_7

Orzali, L., Corsi, B., Forni, C., & Riccioni, L. (2017). Chitosan in Agriculture: A New Challenge for Managing Plant Disease. In *Biological Activities and Application of Marine Polysaccharides*. InTech. https://doi.org/10.5772/66840

Park, S.-I., Daeschel, M. A., & Zhao, Y. (2004). Functional Properties of Antimicrobial Lysozyme-Chitosan Composite Films. *Journal of Food Science*, *69*(8), M215–M221. https://doi.org/10.1111/j.1365-2621.2004.tb09890.x

Park, S. Y., Lee, B. I., Jung, S. T., & Park, H. J. (2001). Biopolymer composite films based on κ-carrageenan and chitosan. *Materials Research Bulletin*, *36*(3–4), 511–519. https://doi.org/10.1016/S0025-5408(01)00545-1

Park, S. Y., Marsh, K. S., & Rhim, J. W. (2002). Characteristics of Different Molecular Weight Chitosan Films Affected by the Type of Organic Solvents. *Journal of Food Science*, *67*(1), 194–197. https://doi.org/10.1111/j.1365-2621.2002.tb11382.x

Patel, S., Srivastava, S., Singh, M. R., & Singh, D. (2018). Preparation and optimization of chitosan-gelatin films for sustained delivery of lupeol for wound healing. *International Journal of Biological Macromolecules*, *107*, 1888–1897. https://doi.org/10.1016/j.ijbiomac.2017.10.056

Pavlath, A. E., & Orts, W. (2009). Edible Films and Coatings: Why, What, and How? In K. C. Huber & M. E. Embuscado (Eds.), *Edible Films and Coatings for Food Applications* (pp. 1–23). Springer New York. https://doi.org/10.1007/978-0-387-92824-1_1

Pelissari, F. M., Yamashita, F., Garcia, M. A., Martino, M. N., Zaritzky, N. E., & Grossmann, M. V. E. (2012). Constrained mixture design applied to the development of cassava starch-chitosan blown films. *Journal of Food Engineering*, *108*(2), 262–267. https://doi.org/10.1016/j.jfoodeng.2011.09.004

Pelissari, F. M., Yamashita, F., & Grossmann, M. V. E. (2011). Extrusion parameters related to starch/chitosan active films properties. *International Journal of Food Science and Technology*, *46*(4), 702–710. https://doi.org/10.1111/j.1365-2621.2010.02533.x

Pereda, M., Amica, G., & Marcovich, N. . (2012). Development and characterization of edible chitosan/olive oil emulsion films. *Carbohydrate Polymers*, *87*(2), 1318–1325. https://doi.org/10.1016/j.carbpol.2011.09.019

Pereda, M., Aranguren, M. I., & Marcovich, N. E. (2008). Characterization of chitosan/caseinate films. *Journal of Applied Polymer Science*, *107*(2), 1080–1090. https://doi.org/10.1002/app.27052

Pereda, M., Aranguren, M. I., & Marcovich, N. E. (2009). Water vapor absorption and permeability of films based on chitosan and sodium caseinate. *Journal of Applied Polymer Science*, *111*(6), 2777–2784. https://doi.org/10.1002/app.29347

Pereda, M., Ponce, A. G., Marcovich, N. E., Ruseckaite, R. A., & Martucci, J. F. (2011). Chitosan-gelatin composites and bi-layer films with potential antimicrobial activity. *Food Hydrocolloids*, *25*(5), 1372–1381. https://doi.org/10.1016/j.foodhyd.2011.01.001

Prasad, K., Abhay, Kumar, G., Preethi, P., & Pallavi, N. (2018). Edible Coating Technology for Extending Market Life of Horticultural Produce. *Acta Scientific Agriculture*, *2*(5), 55–64.

Prateepchanachai, S., Thakhiew, W., Devahastin, S., & Soponronnarit, S. (2019). Improvement of mechanical and heat-sealing properties of edible chitosan films via addition of gelatin and CO2 treatment of film-forming solutions. *International Journal of Biological Macromolecules*, *131*, 589–600. https://doi.org/10.1016/j.ijbiomac.2019.03.067

Qiao, C., Ma, X., Zhang, J., & Yao, J. (2017). Molecular interactions in gelatin/chitosan composite films. *Food Chemistry*, *235*, 45–50. https://doi.org/10.1016/j.foodchem.2017.05.045

Radovic, M., Adamovic, T., Pavlovic, J., Rusmirovic, J., Tadic, V., Brankovic, Z., & Ivanovic, J. (2019). Supercritical co2 impregnation of gelatin-chitosan films with clove essential oil and characterization thereof. *Chemical Industry and Chemical Engineering Quarterly*, *25*(2), 119–130. https://doi.org/10.2298/CICEQ180323025R

Rajpal, G. (2007). *Color and Mechanical Properties of Chitosan Films during Storage* [University of Tennessee]. https://trace.tennessee.edu/utk_gradthes

Ratner, B. (2009). The correlation coefficient: Its values range between +1/−1, or do they? *Journal of Targeting, Measurement and Analysis for Marketing*, *17*(2), 139–142. https://doi.org/10.1057/jt.2009.5

Repka, M. A., Gutta, K., Prodduturi, S., Munjal, M., & Stodghill, S. P. (2005). Characterization of cellulosic hot-melt extruded films containing lidocaine. *European Journal of Pharmaceutics and Biopharmaceutics*, *59*(1), 189–196. https://doi.org/10.1016/j.ejpb.2004.06.008

Rhodes, C. J. (2018). Plastic Pollution and Potential Solutions. *Science Progress*, *101*(3), 207–260. https://doi.org/10.3184/003685018X15294876706211

Rivero, S., García, M. A., & Pinotti, A. (2009). Composite and bi-layer films based on gelatin and chitosan. *Journal of Food Engineering*, *90*(4), 531–539. https://doi.org/10.1016/j.jfoodeng.2008.07.021

Robert Wall, E. (2020). Regression Analysis and Adjusted R 2. *Journal of Visual Impairment and Blindness*, *114*(4), 332–333. https://doi.org/10.1177/0145482X20939786

Rodrigues, C., de Mello, J. M. M., Dalcanton, F., Macuvele, D. L. P., Padoin, N., Fiori, M. A., Soares, C., & Riella, H. G. (2020). Mechanical, Thermal and Antimicrobial Properties of Chitosan-Based-Nanocomposite with Potential Applications for Food Packaging. *Journal of Polymers and the Environment*, *28*(4), 1216–1236. https://doi.org/10.1007/s10924-020-01678-y

Rodrigues, M. Á. V., Bertolo, M. R. V., Marangon, C. A., Martins, V. da C. A., & Plepis, A. M. de G. (2020). Chitosan and gelatin materials incorporated with phenolic extracts of grape seed and jabuticaba peel: Rheological, physicochemical, antioxidant, antimicrobial and barrier properties. *International Journal of Biological Macromolecules*, *160*, 769–779. https://doi.org/10.1016/j.ijbiomac.2020.05.240

Rodríguez-Núñez, J. R., Madera-Santana, T. J., Sánchez-Machado, D. I., López-Cervantes, J., & Soto Valdez, H. (2014). Chitosan/Hydrophilic Plasticizer-Based Films: Preparation, Physicochemical and Antimicrobial Properties. *Journal of Polymers and the Environment*, *22*(1), 41–51. https://doi.org/10.1007/s10924-013-0621-z

Rossman, J. M. (2009). Commercial Manufacture of Edible Films. In *Edible Films and Coatings for Food Applications* (pp. 367–390). Springer New York. https://doi.org/10.1007/978-0-387-92824-1_14

Rui, L., Xie, M., Hu, B., Zhou, L., Yin, D., & Zeng, X. (2017). A comparative study on chitosan/gelatin composite films with conjugated or incorporated gallic acid. *Carbohydrate Polymers*, *173*, 473–481. https://doi.org/10.1016/j.carbpol.2017.05.072

Santacruz, S., Rivadeneira, C., & Castro, M. (2015). Edible films based on starch and chitosan. Effect of starch source and concentration, plasticizer, surfactant's hydrophobic tail and mechanical treatment. *Food Hydrocolloids*, *49*(May 2021), 89–94. https://doi.org/10.1016/j.foodhyd.2015.03.019

Schaer, L. (2021). Nutrition Research: Lobster shells and poultry rations - Canadian Poultry Magazine. *Canadian Poultry Magazine*, *June*, 23–24. https://www.canadianpoultrymag.com/lobster-shells-and-poultry-rations/

Shen, Z., & Kamdem, D. P. (2015). Development and characterization of biodegradable chitosan films containing two essential oils. *International Journal of Biological Macromolecules*, *74*, 289–296. https://doi.org/10.1016/j.ijbiomac.2014.11.046

Shin, Y., Yoo, D. I., & Jang, J. (2001). Molecular weight effect on antimicrobial activity of chitosan treated cotton fabrics. *Journal of Applied Polymer Science*, *80*(13), 2495–2501. https://doi.org/10.1002/app.1357

Shrivastava, A. (2018). Polymerization. In S. C. Ameta, P. B. Punjabi, R. Ameta, & C. Ameta (Eds.), *Introduction to Plastics Engineering* (pp. 17–48). Elsevier. https://doi.org/10.1016/B978-0-323-39500-7.00002-2

Singh, T. P., Chatli, M. K., & Sahoo, J. (2015). Development of chitosan based edible films: process optimization using response surface methodology. *Journal of Food Science and Technology*, *52*(5), 2530–2543. https://doi.org/10.1007/s13197-014-1318-6

Siriprom, W., Chantarasunthon, K., & Teanchai, K. (2014). Physical and Thermal Properties of Chitosan. *Advanced Materials Research*, *979*, 315–318. https://doi.org/10.4028/www.scientific.net/AMR.979.315

Souza, V. G. L., Pires, J. R. A., Rodrigues, C., Coelhoso, I. M., & Fernando, A. L. (2020). Chitosan Composites in Packaging Industry—Current Trends and Future Challenges. *Polymers*, *12*(2), 417. https://doi.org/10.3390/polym12020417

Srinivasa, P. C., Ramesh, M. N., Kumar, K. R., & Tharanathan, R. N. (2004). Properties of chitosan films prepared under different drying conditions. *Journal of Food Engineering*, *63*(1), 79–85. https://doi.org/10.1016/S0260-8774(03)00285-1

Srinivasa, P. C., Ravi, R., & Tharanathan, R. N. (2007). Effect of storage conditions on the tensile properties of eco-friendly chitosan films by response surface methodology. *Journal of Food Engineering*, *80*(1), 184–189. https://doi.org/10.1016/j.jfoodeng.2006.05.007

Sugumar, S., Mukherjee, A., & Chandrasekaran, N. (2015). Eucalyptus oil nanoemulsion-impregnated chitosan film: Antibacterial effects against a clinical pathogen, Staphylococcus aureus, in vitro. *International Journal of Nanomedicine*, *10*(Supplement 1 Challenges in biomaterials research), 67–75. https://doi.org/10.2147/IJN.S79982

Talón, E., Trifkovic, K. T., Nedovic, V. A., Bugarski, B. M., Vargas, M., Chiralt, A., & González-Martínez, C. (2017). Antioxidant edible films based on chitosan and starch containing polyphenols from thyme extracts. *Carbohydrate Polymers*, *157*, 1153–1161. https://doi.org/10.1016/j.carbpol.2016.10.080

Thakur, R., Saberi, B., Pristijono, P., Stathopoulos, C. E., Golding, J. B., Scarlett, C. J., Bowyer, M., & Vuong, Q. V. (2017). Use of response surface methodology (RSM) to optimize pea starch–chitosan novel edible film formulation. *Journal of Food Science and Technology*, *54*(8), 2270–2278. https://doi.org/10.1007/s13197-017-2664-y

Thériault, G., Hanlon, J., & Creed, L. (2013). *Report of the Maritime Lobster Panel*.

Tomadoni, B., Ponce, A., Pereda, M., & Ansorena, M. R. (2019). Vanillin as a natural cross-linking agent in chitosan-based films: Optimizing formulation by response surface methodology. *Polymer Testing*, *78*, 105935. https://doi.org/10.1016/j.polymertesting.2019.105935

Trung, T. S., Thein-Han, W. W., Qui, N. T., Ng, C.-H., & Stevens, W. F. (2006). Functional characteristics of shrimp chitosan and its membranes as affected by the degree of deacetylation. *Bioresource Technology*, *97*(4), 659–663. https://doi.org/10.1016/j.biortech.2005.03.023

UNEP. (2018). *Plastics: A Roadmap for Sustainability*. http://hdl.handle.net/20.500.11822/25496

Ustunol, Z. (2009). Edible Films and Coatings for Meat and Poultry. In K. C. Huber & M. E. Embuscado (Eds.), *Edible Films and Coatings for Food Applications* (pp. 245–268). Springer New York. https://doi.org/10.1007/978-0-387-92824-1_8

Valenzuela, C., Abugoch, L., & Tapia, C. (2013). Quinoa protein–chitosan–sunflower oil edible film: Mechanical, barrier and structural properties. *LWT - Food Science and Technology*, *50*(2), 531–537. https://doi.org/10.1016/j.lwt.2012.08.010

Varma, A. ., Deshpande, S. ., & Kennedy, J. . (2004). Metal complexation by chitosan and its derivatives: a review. *Carbohydrate Polymers*, *55*(1), 77–93. https://doi.org/10.1016/j.carbpol.2003.08.005

Vieira, M. G. A., Da Silva, M. A., Dos Santos, L. O., & Beppu, M. M. (2011). Natural-based plasticizers and biopolymer films: A review. In *European Polymer Journal* (Vol. 47, Issue 3, pp. 254–263). Pergamon. https://doi.org/10.1016/j.eurpolymj.2010.12.011

Wang, H., Ding, F., Ma, L., & Zhang, Y. (2021). Edible films from chitosan-gelatin: Physical properties and food packaging application. *Food Bioscience*, *40*(January), 100871. https://doi.org/10.1016/j.fbio.2020.100871

Wang, H., Qian, J., & Ding, F. (2017). *Emerging Chitosan-Based Films for Food Packaging Applications*. https://doi.org/10.1021/acs.jafc.7b04528

Wang, P., Fei, P., Zhou, C., & Hong, P. (2021). Stearic acid esterified pectin: Preparation, characterization, and application in edible hydrophobic pectin/chitosan composite films. *International Journal of Biological Macromolecules*. https://doi.org/10.1016/j.ijbiomac.2021.06.030

Wasswa, J., Tang, J., & Gu, X. (2007). Utilization of Fish Processing By-Products in the Gelatin Industry. *Food Reviews International*, *23*(2), 159–174. https://doi.org/10.1080/87559120701225029

Wong, D. W. S., Gastineau, F. A., Gregorski, K. S., Tillin, S. J., & Pavlath, A. E. (1992). Chitosan-Lipid Films: Microstructure and Surface Energy. In *J. Agric. Food Chem* (Vol. 40). https://pubs.acs.org/sharingguidelines

Wydro, P., Krajewska, B., & Hąc-Wydro, K. (2007). Chitosan as a Lipid Binder: A Langmuir Monolayer Study of Chitosan−Lipid Interactions. *Biomacromolecules*, *8*(8), 2611–2617. https://doi.org/10.1021/bm700453x

Xu, J., Wei, R., Jia, Z., & Song, R. (2020). Characteristics and bioactive functions of chitosan/gelatin-based film incorporated with ε-polylysine and astaxanthin extracts derived from by-products of shrimp (Litopenaeus vannamei). *Food Hydrocolloids*, *100*, 105436. https://doi.org/10.1016/j.foodhyd.2019.105436

Xu, W., Mohan, A., Pitts, N. L., Udenigwe, C., & Mason, B. (2020). Bile acid-binding capacity of lobster shell-derived chitin, chitosan and chitooligosaccharides. *Food Bioscience*, *33*, 100476. https://doi.org/10.1016/j.fbio.2019.100476

Xu, Wei. (2017). *Bile acid-binding capacity of lobster shell-derived chitin, chitosan and chitooligosaccharides* [Dalhousie University]. http://hdl.handle.net/10222/73471

Xu, Y. X., Kim, K. M., Hanna, M. A., & Nag, D. (2005). Chitosan–starch composite film: preparation and characterization. *Industrial Crops and Products*, *21*(2), 185–192. https://doi.org/10.1016/j.indcrop.2004.03.002

Yadav, M., Goswami, P., Paritosh, K., Kumar, M., Pareek, N., & Vivekanand, V. (2019). Seafood waste: a source for preparation of commercially employable chitin/chitosan materials. *Bioresources and Bioprocessing*, *6*(1), 8. https://doi.org/10.1186/s40643-019-0243-y

Yan, X.-L., Khor, E., & Lim, L.-Y. (2001). Chitosan-alginate films prepared with chitosans of different molecular weights. *Journal of Biomedical Materials Research*, *58*(4), 358–365. https://doi.org/10.1002/jbm.1029

Yang, T. L. (2011). Chitin-based materials in tissue engineering: Applications in soft tissue and epithelial organ. In *International Journal of Molecular Sciences* (Vol. 12, Issue 3, pp. 1936–1963). Multidisciplinary Digital Publishing Institute (MDPI). https://doi.org/10.3390/ijms12031936

Yao, Y., Ding, D., Shao, H., Peng, Q., & Huang, Y. (2017). Antibacterial Activity and Physical Properties of Fish Gelatin-Chitosan Edible Films Supplemented with D-Limonene. *International Journal of Polymer Science*, *2017*. https://doi.org/10.1155/2017/1837171

Yin, Y., Li, Z., Sun, Y., & Yao, K. (2005). A preliminary study on chitosan/gelatin polyelectrolyte complex formation. *Journal of Materials Science*, *40*(17), 4649–4652. https://doi.org/10.1007/s10853-005-3929-9

Zhang, L., Liu, Z., Wang, X., Dong, S., Sun, Y., & Zhao, Z. (2019). The properties of chitosan/zein blend film and effect of film on quality of mushroom (Agaricus bisporus). *Postharvest Biology and Technology*, *155*, 47–56. https://doi.org/10.1016/j.postharvbio.2019.05.013

Zhang, Y., Rempel, C., & Mclaren, D. (2013). Edible Coating and Film Materials: Carbohydrates. In *Innovations in Food Packaging: Second Edition*. Elsevier Ltd. https://doi.org/10.1016/B978-0-12-394601-0.00012-6

Zhao, D., Yu, S., Sun, B., Gao, S., Guo, S., & Zhao, K. (2018). Biomedical applications of chitosan and its derivative nanoparticles. *Polymers*, *10*(4). https://doi.org/10.3390/polym10040462

Ziani, K., Oses, J., Coma, V., & Maté, J. I. (2008). Effect of the presence of glycerol and Tween 20 on the chemical and physical properties of films based on chitosan with different degree of deacetylation. *LWT - Food Science and Technology*, *41*(10), 2159–2165. https://doi.org/10.1016/j.lwt.2007.11.023